ENSO mechanisms and interactions in a hybrid coupled recharge oscillator model

Dissertation

zur Erlangung des Doktorgrades

der Mathematisch Naturwissenschaftlichen Fakultät

der Christian-Albrechts-Universität zu Kiel

vorgelegt von

Claudia Frauen

Leibniz-Institut für Meereswissenschaften

Forschungsbereich 1

- Maritime Meteorologie -

Kiel, Oktober 2010

Referent: Dr. Dietmar Dommenget

Koreferent: Prof. Dr. Mojib Latif

Tag der mündlichen Prüfung: 01.12.2010

Zum Druck genehmigt: 01.12.2010

gez. Prof. Dr. Lutz Kipp, Dekan

Contents

Parts of this work were published in Geophysical Research Letters:

Frauen, C., and D. Dommenget: El Niño and La Niña amplitude asymmetry caused by atmospheric feedbacks, Geophys. Res. Lett, 37, L18801, doi:10.1029/2010GL044444.

Abstract

The El Niño Southern Oscillation (ENSO) mode is the most important source of interannual climate variability. It has its origin in the interactions of the atmosphere and the tropical Pacific Ocean but the teleconnections of ENSO reach far beyond the tropical Pacific. Although the understanding of ENSO has improved greatly, there are still aspects of ENSO that are not yet well understood. Some of these aspects are the seasonality of ENSO, i.e., the nature of ENSO events to peak in boreal winter, and the asymmetry of ENSO, i.e., the fact that El Niño events are, in general, stronger than La Niña events. Also, the possible effects of a changing climate on ENSO, and the influences of the tropical Indian and the tropical Atlantic Ocean on ENSO are areas of ongoing studies.

For this work, the hybrid coupled model RECHOZ was developed consisting of the ECHAM5 atmospheric general circulation model, the simple recharge oscillator ocean model in the tropical Pacific and a simple mixed layer ocean model outside the tropical Pacific. Despite the simplistic and, by construction, linear representation of ocean dynamics in the RECHOZ model, it is able to simulate the main statistical features of El Niño, including variance, period, seasonality, skewness, and kurtosis.

This model was used to study the seasonality of ENSO and the nonlinearities in the ENSO cycle. Analyses of the model show that atmospheric properties are responsible for the seasonality and nonlinearity of ENSO. A nonlinear relationship between the zonal wind stress and the sea surface temperature (SST) is causing the El Niño-La Niña asymmetry.

With the aid of sensitivity experiments, the effects of changes in the mean state of the tropical Pacific on ENSO due to atmospheric feedbacks were studied and the influences of the

tropical Indian and the tropical Atlantic Ocean on ENSO were analysed. Analyses of the sensitivity experiments show that changes in the mean state of the tropical Pacific have a strong influence on the amplitude and frequency of ENSO. However, the results strongly depend on the pattern of the changes. An El Niño-like warming pattern leads to a strong increase in ENSO variability and shifts the period of ENSO towards longer timescales.
For the tropical Atlantic Ocean no clear influence on ENSO can be detected. In contrast, the tropical Indian Ocean has a strong damping effect on the SST variability in the tropical Pacific and reduces the period of the ENSO cycle.

Zusammenfassung

Der El Niño Southern Oscillation (ENSO) Mode ist die bei weitem wichtigste Ursache zwischenjährlicher Klimavariabilität. ENSO hat seinen Ursprung in den Wechselwirkungen der Atmosphäre und des tropischen Pazifischen Ozeans, aber die Fernwirkungen reichen weit über den tropischen Pazifik hinaus. Obwohl sich das Verständnis des ENSO Phänomens stark verbessert hat, sind einige Aspekte ENSOs noch immer nicht ausreichend verstanden. Einige dieser Aspekte sind die Saisonalität ENSOs, d.h. die Eigenschaft ENSOs im nordhemisphärischen Winter den Höhepunkt zu erreichen, und die Asymmetrie ENSOs, d.h. die Tatsache, dass El Niño Ereignisse für gewöhnlich stärker ausfallen als La Niña Ereignisse. Ebenso sind die möglichen Effekte des Klimawandels auf ENSO und die Einflüsse des tropischen Indischen und des tropischen Atlantischen Ozeans auf ENSO Gegenstand aktueller Forschung.

Im Rahmen dieser Arbeit wurde das hybrid gekoppelte Modell RECHOZ entwickelt, das aus dem allgemeinen atmosphärischen Zirkulationsmodell ECHAM5, dem einfachen Recharge Oscillator Ozeanmodell im tropischen Pazifik und einem einfachen Turbulenzschicht-Ozeanmodell außerhalb des tropischen Pazifiks besteht. Trotz der einfachen und per Konstruktion linearen Darstellung der Ozeandynamik im RECHOZ-Modell ist das Modell in der Lage, die wesentlichen statistischen Eigenschaften ENSOs, wie die Varianz, die Periode, die Saisonalität, die Schiefe und die Kurtosis, zu reproduzieren.

Dieses Modell wurde verwendet, um die Saisonalität ENSOs und die Nichtlinearität im ENSO-Zyklus zu untersuchen. Analysen der Modellergebnisse zeigen, dass atmosphärische Eigenschaften für die Saisonalität und Nichtlinearität ENSOs verantwortlich sind. Ein nicht-

linearer Zusammenhang zwischen der zonalen Windschubspannung und der Meeresoberflächentemperatur (SST) verursacht die El Niño-La Niña Asymmetrie.

Mithilfe von Sensitivitätsexperimenten wurden die Effekte von Veränderungen im mittleren Zustand des tropischen Pazifiks auf ENSO durch atmosphärische Rückkopplungen und die Einflüsse des tropischen Indischen und des tropischen Atlantischen Ozeans auf ENSO analysiert. Untersuchungen der Sensitivitätsexperimente zeigen, dass Veränderungen im mittleren Zustand des tropischen Pazifiks einen starken Einfluss auf die Amplitude und Frequenz von ENSO haben. Allerdings sind die Auswirkungen stark von dem Muster der Veränderungen abhängig. Ein El Niño-artiges Erwärmungsmuster führt zu einem starken Anstieg der ENSO Variabilität und verschiebt die Periode ENSOs zu längeren Zeiträumen.

Für den tropischen Atlantik kann kein deutlicher Einfluss auf ENSO festgestellt werden. Im Gegensatz dazu hat der tropische Indische Ozean einen stark dämpfenden Effekt auf die SST Variabilität im tropischen Pazifik und verringert die Periode des ENSO-Zyklus.

1 Introduction

The El Niño Southern Oscillation (ENSO) phenomenon is the most important source of interannual climate variability. It has its origin in the interactions of the tropical atmosphere and the tropical Pacific Ocean, but the teleconnections of ENSO reach far beyond the tropical Pacific region. Especially the tropical Indian Ocean, the tropical Atlantic Ocean, and the adjacent continents are influenced by ENSO (Latif and Barnett, 1995; Enfield and Mayer, 1997, and many others). Therefore, the predictability of ENSO is of particular importance for global seasonal and long-term climate predictions.

In recent decades the understanding of the ENSO phenomenon has improved greatly. Theoretical explanations for ENSO have been developed, and models have become more advanced and more reliable. Most state-of-the-art coupled general circulation models (GCMs) now simulate a realistic ENSO mode, and El Niño forecasts are reasonably reliable up to about six to twelve months ahead (depending on the season) (Latif et al., 1998). However, there are still aspects of the ENSO phenomenon which are not yet well understood. Although most state-of-the-art climate models now simulate a realistic ENSO mode, they still have systematic errors in the simulated background climate and ENSO variability. Most models have problems simulating the nonlinearities of ENSO correctly (van Oldenborgh et al., 2005) and the tendency of El Niño and La Niña events to peak in early boreal winter is not captured by many models as well (Guilyardi et al., 2009b).

Concerning the behaviour of ENSO in a warming climate, the GCMs show a large spread of results, too. There is no consensus yet in which way the mean state of the tropical Pacific will change. In the fourth assessment report (AR4) of the Intergovernmental Panel on Cli-

mate Change (IPCC) it is stated: "In summary, the multi-model mean projects a weak shift towards conditions which may be described as 'El Niño-like', with sea surface temperatures (SSTs) in the central and eastern equatorial Pacific warming more than those in the west, and with an eastward shift in mean precipitation, associated with weaker tropical circulations (Meehl et al., 2007)." This can also be seen in figure 1.1 where the changes in mean tropical Pacific SST and El Niño variability were calculated for the 1% yr^{-1} CO_2 increase climate change experiments of 16 IPCC AR4 models. Out of these 16 models, 13 show an El Niño-like pattern. In contrast, Collins and CMIP Modeling Groups (2005) again analysed 20 atmosphere-ocean GCMs submitted to the coupled model inter-comparison project (CMIP) where they linked the realism of the simulation of present day ENSO variability in the models to their patterns of future climate change. They found that the most likely scenario is no trend towards either mean El Niño-like or La Niña-like conditions. More recent studies suggest that there is an enhanced equatorial warming rather than an El Niño-like response due to global warming (Liu et al., 2005; Vecchi et al., 2008; DiNezio et al., 2009). It is also still unclear how the ENSO variability will be influenced by global warming. Although most of the models analysed for the IPCC report simulate an El Niño-like warming pattern, they do not agree in the simulated future strength of ENSO (figure 1.1). Half of the models simulating an El Niño-like global warming pattern simulates an increase in ENSO variability. The other half simulates a decrease.

Several studies stress the important role of atmospheric feedbacks in determining the characteristics of the ENSO mode in GCMs (Schneider, 2002; Guilyardi et al., 2004, 2009a). Also future changes in the ENSO properties due to global warming depend strongly on atmospheric feedbacks (Collins et al., 2010).

Another important aspect of ENSO which is not yet fully understood is the influence of the tropical Indian and the tropical Atlantic Ocean on ENSO. These feedbacks are difficult to study in fully coupled GCMs too, because these are just secondary effects dominated by the primary effect of ENSO influencing the tropical Indian and the tropical Atlantic Ocean.

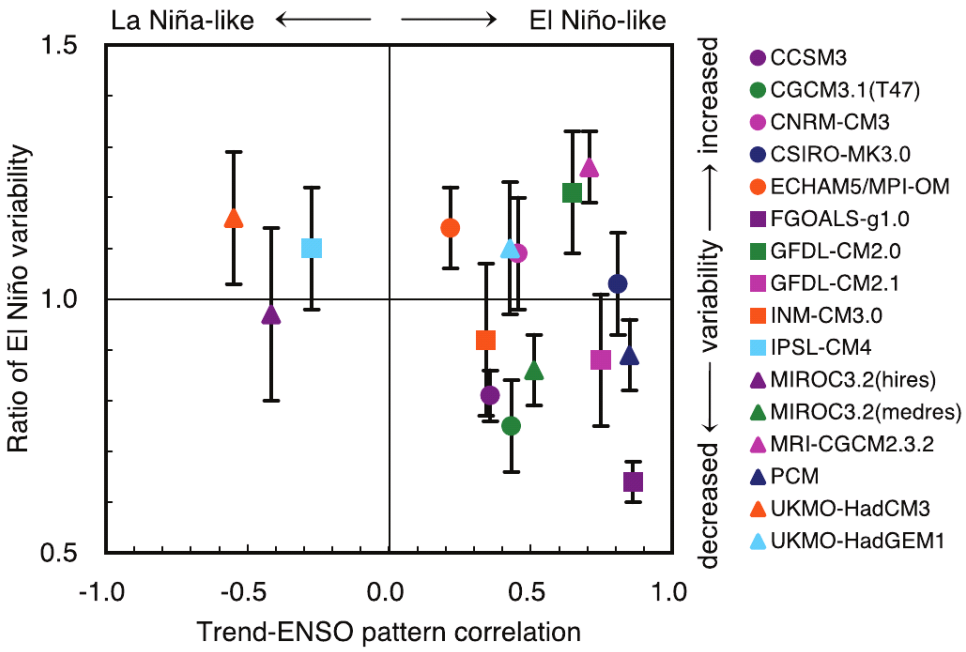

Figure 1.1: Base state change in average tropical Pacific SSTs and change in El Niño variability simulated by atmosphere-ocean GCMs. The base state change (horizontal axis) is denoted by the spatial anomaly pattern correlation coefficient between the linear trend of SST in the 1% yr^{-1} CO_2 increase climate change experiment and the first empirical orthogonal function (EOF) of SST in the control run experiment over the area $10°S$ to $10°N$, $120°E$ to $80°W$ (reproduced from Yamaguchi and Noda (2006)). Positive correlation values indicate that the mean climate change has an El Niño-like pattern, and negative values are La Niña-like. The change in El Niño variability (vertical axis) is denoted by the ratio of the standard deviation of the first EOF of sea level pressure (SLP) between the current climate and a future climate projection. Error bars indicate the 95% confidence interval. The figure is obtained from Meehl et al. (2007) (Figure 10.16).

However, recent studies suggest that the tropical Indian and the Atlantic Ocean might have an important influence on the ENSO cycle (Dommenget et al., 2006; Jansen et al., 2009; Rodriguez-Fonseca et al., 2009).

One alternative to using complex atmosphere-ocean GCMs is to use an hybrid coupeld model (HCM) consisting of a full-complexity atmospheric GCM and a simple linear ocean model to analyse the role of atmospheric feedbacks in the ENSO cycle. Within this work the new HCM RECHOZ was developed, which consists of an atmospheric GCM, the two-dimensional linear recharge oscillator ocean model in the tropical Pacific, and a simple mixed layer ocean

model elsewhere. With this HCM the following key questions will be studied:

- Which atmospheric processes lead to the phase locking of ENSO, with El Niño and La Niña events typically peaking in early boreal winter?
- What are possible atmospheric causes for the amplitude asymmetry between El Niño and La Niña events?
- In which way are changes in the mean state of the tropical Pacific affecting ENSO through atmospheric feedbacks?
- How are the tropical Indian Ocean and the tropical Atlantic Ocean influencing ENSO?

Therefore, in chapter 2, first the climate of the tropical Pacific is described with a particular focus on the ENSO phenomenon. Also the climatic states of the tropical Indian and the tropical Atlantic Ocean are briefly illustrated, and the interactions of the tropical oceans with ENSO are described. Chapter 3 introduces the simple recharge oscillator ocean model and describes the derivation of the new RECHOZ model. How ENSO is simulated in the RECHOZ model is described in chapter 4. Especially the amplitude asymmetry between El Niño and La Niña events and the seasonal phase locking of ENSO are studied with the help of the RECHOZ model. Different sensitivity experiments of the model are analysed to gain a better understanding of the influence of changes in the tropical Pacific mean state on ENSO through atmospheric feedbacks and the interactions of the tropical Indian Ocean and the tropical Atlantic Ocean with ENSO. Finally, chapter 5 provides conclusions and an outlook.

2 The tropical oceans and ENSO

2.1 Observational data sets

Different observational data sets were used to describe the climatic conditions in the tropical oceans and to verify the model results. Observational SST data was taken from the HadISST data set for the period from 1870 to 2003 (Rayner et al., 2003). This is a gridded data set based on an EOF reconstruction of observational data. As thermocline depth data the BMRC data set of the 20° isotherm of Smith (1995) for the period from 1980 to 2002 was used. This is a gridded data set based on an interpolation using data from the Tropical Atmosphere Ocean (TAO) array and ship measurements. Because this time series is very short, also 20° C isotherm depth data obtained from a forced simulation of the Max Planck Institute Ocean Model (MPI-OM) ocean general circulation model (Marsland et al., 2003) was used for the period from 1950 to 2001. The model was forced with zonal wind stress data from the NCEP-NCAR reanalysis (Kalnay and Coauthors, 1996). For the calculation of heat fluxes, standard bulk formulas were used, and a weak relaxation of surface salinity to the Levitus et al. (1994) climatology was applied. This data set was also used for previous studies by Keenlyside and Latif (2007) and Jansen et al. (2009). The results were carefully checked against various observational and reanalysis data sets for the Pacific and the Atlantic Ocean.

2.2 The tropical Pacific Ocean and ENSO

The name 'El Niño' (spanish for the Christ Child) was first given by Peruvian fishermen to a warm ocean current which occured regularly near the coast of Peru around Christmas. Because fish need cool nutrient-rich water, there are much fewer fish during the warm 'El Niño'. Today the term El Niño describes more generally periods with warmer than normal SSTs in the central and eastern equatorial Pacific. The tropical Pacific SST is oscillating on interannual timescales with a positive anomaly during El Niño events and a negative anomaly during La Niña events (Philander, 1985). The peak of these El Niño and La Niña events also occurs around Christmas. These fluctuations in SSTs go along with variations in air pressure difference between the eastern and the western equatorial Pacific regions, which is known as the Southern Oscillation (SO). The SO was first detected by Walker (1924). He described it as a seesaw in the surface pressure between the south-east Pacific high pressure zone and the north Australian-Indonesian low pressure zone that goes along with variations in rainfall and SSTs. Bjerknes (1969) found that the SO is closely linked with the interannual variations in SST in the eastern and central tropical Pacific. Together they form the so-called El Niño Southern Oscillation phenomenon.

2.2.1 The mean state of the tropical Pacific

Although the climate of the tropical Pacific is dominated by the ENSO phenomenon, the background mean state is an interesting system, too. While the eastern part of the equatorial Pacific Ocean is where the coldest SSTs of the whole equatorial area are found, the western part has the warmest SSTs of the whole equatorial region. This leads to a large east-west temperature gradient, which is an important factor for the development of an El Niño event. Thus, for understanding ENSO, it is first essential to understand the mean state in the tropical Pacific.

This mean state arises from the interactions of the atmosphere and the ocean. In the tropical atmosphere two main circulation systems are found: one meridional circulation, the so-called Hadley cell, and one zonal circulation, the so-called Walker circulation. Driven by the high solar altitude warm air rises in a band slightly north of the equator. This band is called the Intertropical Convergence Zone (ITCZ). It is located north of the equator rather than on the equator due to the larger land masses in the Northern Hemisphere. The air rising in the ITCZ is transported poleward, in the subtropics it cools down, and sinks. This produces a circulation towards the ITCZ near the surface and poleward in the upper troposphere: the Hadley cell. Due to the rotation of the earth, the Coriolis force acts on the Hadley cell. Moving air is deflected to the right in the Northern Hemisphere and to the left in the Southern Hemisphere. This causes winds blowing from the northeast north of the ITCZ and from the southeast south of the ITCZ which converge at the ITCZ and result in the easterly trade winds.

These easterly trade winds also influence the ocean surface. Warm water is pushed to the west while there is upwelling of cold subsurface ocean waters in the east. This causes a relatively shallow layer of warm water in the eastern Pacific while in the western Pacific there is a deep layer of warm water. The layer which separates the warm water at the top from the cold deep ocean waters is called the oceanic thermocline. In literature, and also in this thesis, the depth of the thermocline is often defined as the depth of the 20° C isotherm. Usually it is deepest in the west with an upward slope towards the east, where it almost reaches the surface. This leads to strong differences in SST between the eastern and western equatorial Pacific. The warmest temperatures are found in the western equatorial Pacific in the so-called warm pool region while the coldest temperatures are found in the eastern Pacific in an area called the cold tongue. This temperature pattern also leads to the typical pattern of tropical Pacific rainfall with the heaviest rainfall observed across Indonesia and the western tropical Pacific, and the least rainfall found across the eastern tropical Pacific. The east-west SST gradient leads to the second tropical atmospheric circulation, the Walker

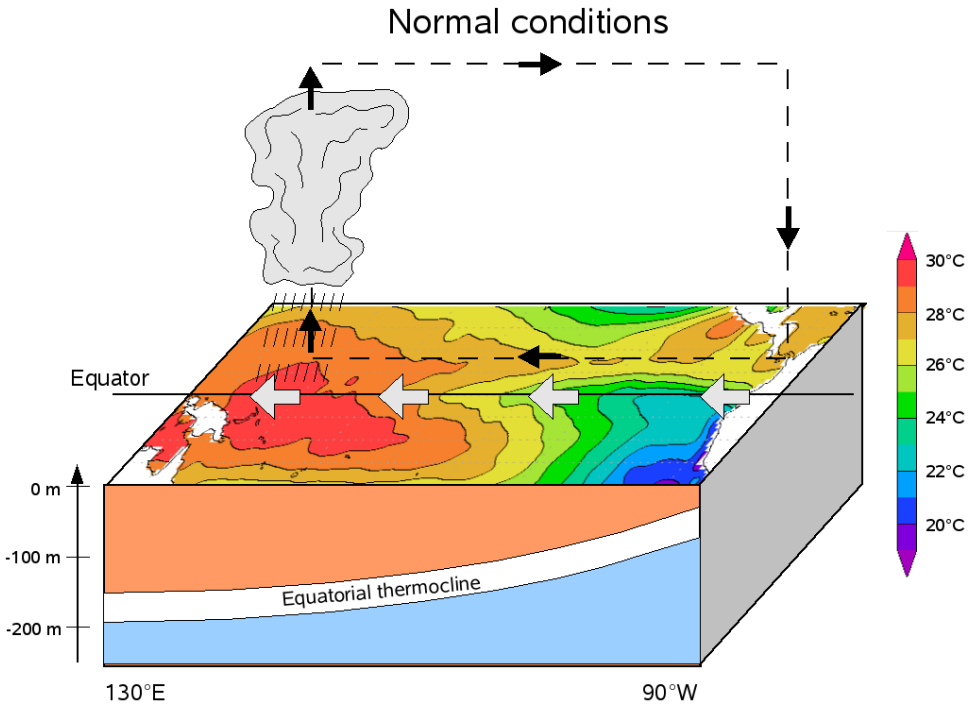

Figure 2.1: Schematic representation of the climatic conditions during the neutral phase of ENSO in the tropical Pacific. The shaded areas above display the composite of observed monthly mean SSTs for neutral conditions. The SSTs are averaged from December to May of the following year for all neutral years ($T_{obs}(December) < |\sigma(T_{obs})|$). The grey arrows are indicating the zonal wind and the black arrows represent the atmospheric circulation.

circulation (see figure 2.1). Above the warm pool the air is rising and transported eastward in the upper troposphere. Accordingly, above the cold tongue region this air sinks and causes an additional westward wind component added to the trade winds at the surface. The rising air in the western Pacific also causes low air pressure above the warm pool while the descending air above the cold tongue results in high air pressure. The pressure difference between Darwin in the west and Tahiti in the east is a common measure for the strength of the SO. Figure 2.1 schematically displays the climatic conditions of the tropical Pacific during the neutral phase of ENSO. For the SST patterns here and in the following schematics of the El Niño and La Niña conditions (figures 2.2 and 2.3), composites of the observed SST in the tropical Pacific were calculated. Therefore, the averages of the SSTs from December to

May of the following year for all neutral ENSO years, El Niño years and La Niña years were calculated. (For a definition of El Niño and La Niña years see section 2.2.3.)

Although the sun "crosses" the equator twice a year, the seasonal cycle of SSTs and surface winds in the eastern equatorial Pacific is dominated by an annual component (Li and Philander, 1996). Along the coast of South America the lowest mean monthly SSTs occur during August and September, and the maximum values of SST are found in March and April (Rasmusson and Carpenter, 1982). In the warm pool region in the western Pacific, only a very weak bi-annual seasonal cycle in SSTs and surface winds exists.

2.2.2 El Niño and La Niña events

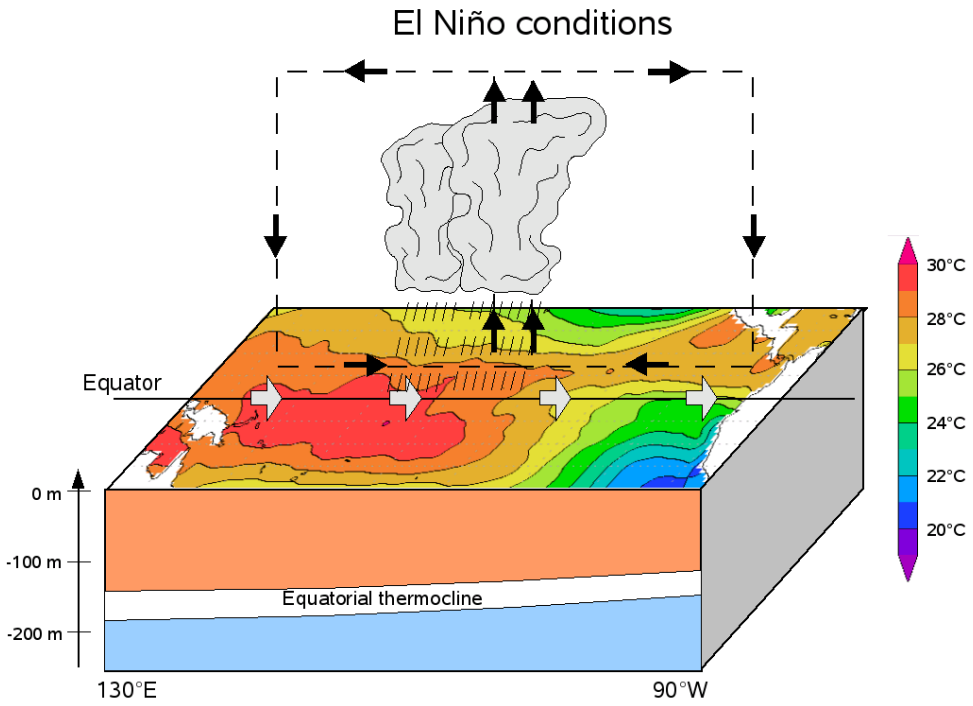

Figure 2.2: Schematic representation of the climatic conditions during the El Niño phase of ENSO in the tropical Pacific. The shaded areas above display the composite of observed monthly mean SSTs for El Niño conditions. The SSTs are averaged from December to May of the following year for all El Niño years ($T_{obs}(December) > \sigma(T_{obs})$). The grey arrows are indicating the zonal wind and the black arrows represent the atmospheric circulation.

During an El Niño event the mean state of the tropical Pacific is disturbed. The origin of this disturbance is still a matter of ongoing discussions. However, to describe the evolution of an El Niño event one can start with an initial positive SST anomaly in the eastern tropical Pacific. This positive SST anomaly reduces the SST gradient and thus the strength of the atmospheric Walker circulation. This results in weaker easterly trade winds at the equator. Weaker trade winds lead to less upwelling and a deeper thermocline in the eastern equatorial Pacific which causes higher SSTs. These reduce the SST gradient along the equator even further. This positive feedback is known as the Bjerknes feedback. In figure 2.2 the conditions in the tropical Pacific during El Niño events are displayed.

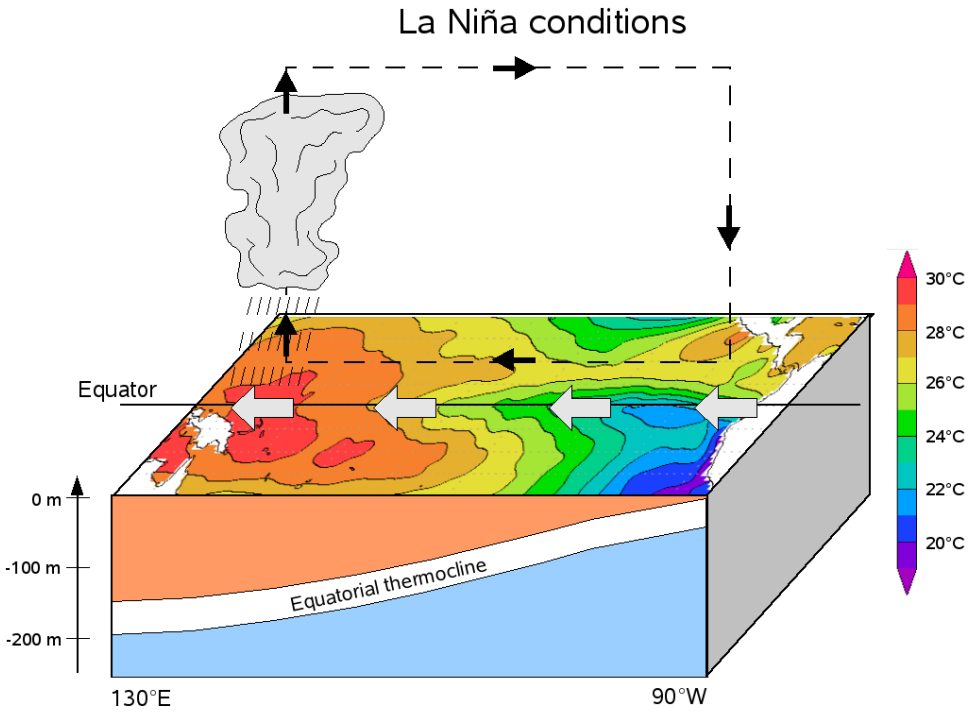

Figure 2.3: Schematic representation of the climatic conditions during the La Niña phase of ENSO in the tropical Pacific. The shaded areas above display the composite of observed monthly mean SSTs for La Niña conditions. The SSTs are averaged from December to May of the following year for all La Niña years ($T_{obs}(December) < -\sigma(T_{obs})$). The grey arrows are indicating the zonal wind and the black arrows represent the atmospheric circulation.

In contrast to El Niño events, where the strength of the equatorial Walker circulation is weakened, during La Niña events the strength of the Walker circulation is even enhanced. Colder than normal SSTs are found in the eastern tropical Pacific which lead to increased easterly trade winds. These increased easterlies also increase the upwelling in the eastern Pacific and thus reduce the depth of the thermocline in this area. The conditions in the tropical Pacific during La Niña events are displayed in figure 2.3.

2.2.3 ENSO variability

Different indices are used to describe the strength of ENSO. One of the most common is the NINO3 index. It denotes the average SST anomaly in a region in the eastern equatorial Pacific ($5°S - 5°N, 90°W - 150°W$). Other common indices are the NINO4 index for an area further to the west or the NINO3.4 index which includes parts of both areas. The SO index which measures the difference in surface air pressure between Darwin and Tahiti is a well known index too, that has been measured for a long time already. In this study the NINO3 index will be used. An El Niño event is defined as an event with a NINO3 index greater than the standard deviation of the NINO3 index. A La Niña event in turn is defined with a NINO3 index smaller than the negative of its standard deviation. The observed standard deviation of the NINO3 index for the period from 1870 to 2003 is $\sigma(T_{obs}) = 0.8\,K$. Figure 2.4 shows the time series of the observed NINO3 index and NINO3 thermocline depth anomalies from the forced MPI-OM simulation for the period from 1950 to 2001. Because in the later model studies only the thermocline depth anomalies averaged over the whole equatorial Pacific ($5°S - 5°N, 130°E - 150°W$) are available, these are shown for comparison in figure 2.5. El Niño and La Niña events occur every couple of years. Especially the very strong El Niños of 1982/83 and 1997/98 are striking. Obviously, there is a strong relationship between the SST anomalies and the thermocline depth anomalies especially in the NINO3 region. The NINO3 thermocline depth anomalies seem to be slightly leading the SST anomalies, while

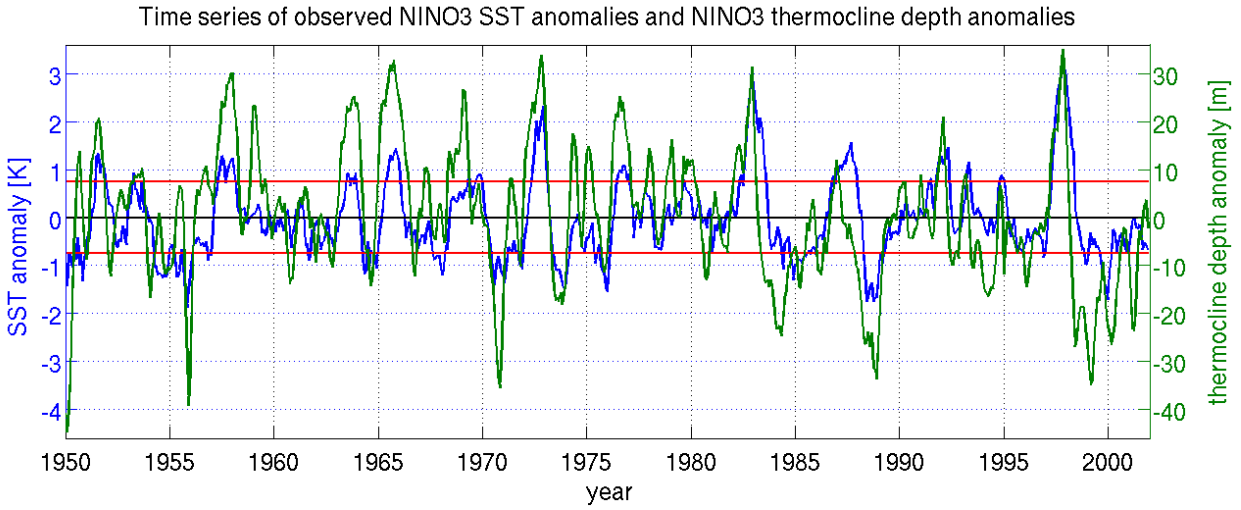

Figure 2.4: Timeseries of observed monthly mean NINO3 SST anomalies and NINO3 thermocline depth anomalies from the forced MPI-OM simulation for the period from 1950 to 2001. The red lines indicate the standard deviation of the SST anomalies.

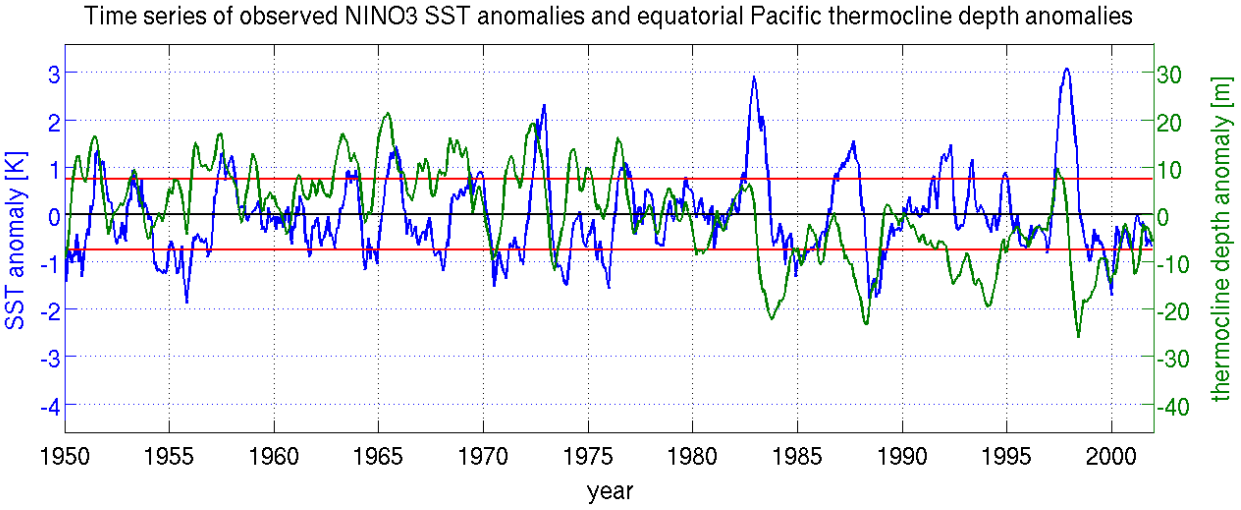

Figure 2.5: Timeseries of observed monthly mean NINO3 SST anomalies and equatorial Pacific thermocline depth anomalies from the forced MPI-OM simulation for the period from 1950 to 2001. The red lines indicate the standard deviation of the SST anomalies.

for the equatorial Pacific thermocline depth anomalies and the NINO3 SST anomalies no clear lag-lead-relationship can be identified from the time series. This lag-lead-relationship becomes clear if one calculates the cross correlation between the thermocline depth anomalies and the SST anomalies (figure 2.6). For the NINO3 thermocline depth anomalies, the cross correlation is maximum when the thermocline depth leads the SST by 1-2 months and stays positive for about 1 year. Positive correlation at positive lag indicates the thermocline depth forces the SST and vice versa for negative lags. For the equatorial Pacific thermocline depth anomalies, one finds the strongest anti-correlation when the SST is leading the thermocline depth for approximately 9 months.

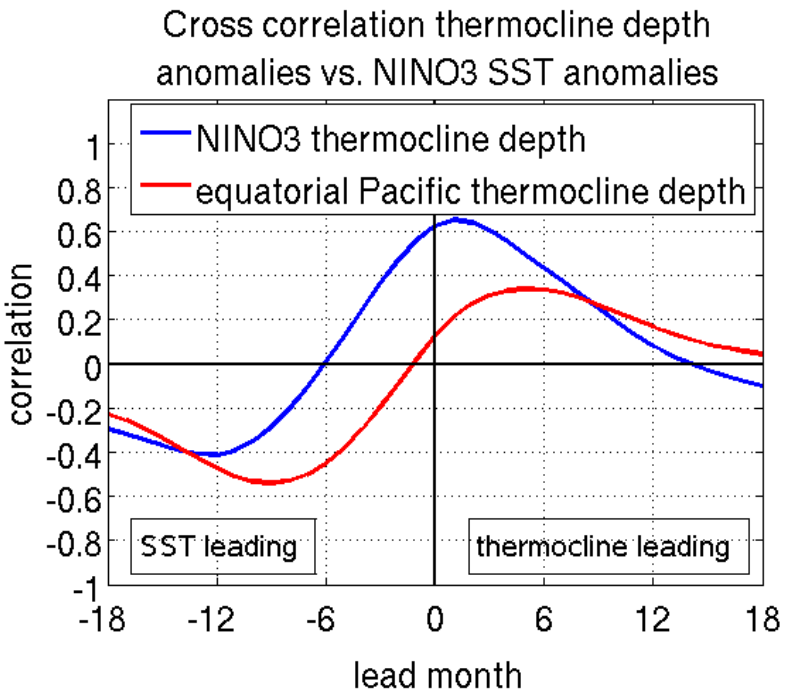

Figure 2.6: Cross correlation between NINO3 thermocline depth anomalies from the forced MPI-OM run and observed NINO3 SST anomalies (blue) and between equatorial Pacific thermocline depth anomalies from the forced MPI-OM run and observed NINO3 SST anomalies (red).

To determine the period of ENSO more precisely one can examine the power spectrum of NINO3 SST anomalies (figure 2.7). For comparison, the spectrum of a first order autoregressive process (AR(1)) fitted to the time series is shown with 90% confidence interval. An AR(1) process represents a red noise process. The peak of the NINO3 SST spectrum is found at periods around 3 1/2 years and is clearly outside the range of the red noise process.

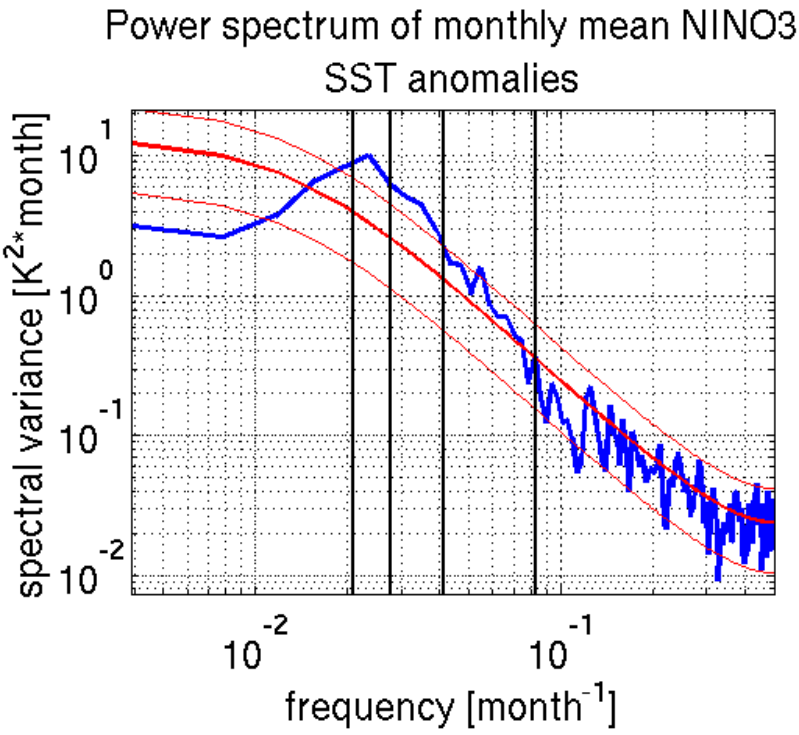

Figure 2.7: Spectrum of observed monthly mean NINO3 SST anomalies (blue). For comparison also the spectrum of a fitted AR(1) process with 90% confidence interval is plotted (red). The vertical black lines indicate periods of 1, 2, 3 and 4 years.

Another characteristic of ENSO is its spatial pattern. One way to describe the pattern of ENSO is to compute composites like was done for the schematic representations of neutral ENSO conditions, El Niño, and La Niña events (figures 2.1, 2.2, and 2.3). Another way is to calculate the pattern of the first EOF of the tropical Pacific SST anomalies (figure 2.8). This is the pattern of maximum variability of the multi-year SST field. Since the SST variability in the tropical Pacific is mostly caused by ENSO, the pattern of the first EOF describes the ENSO pattern very well.

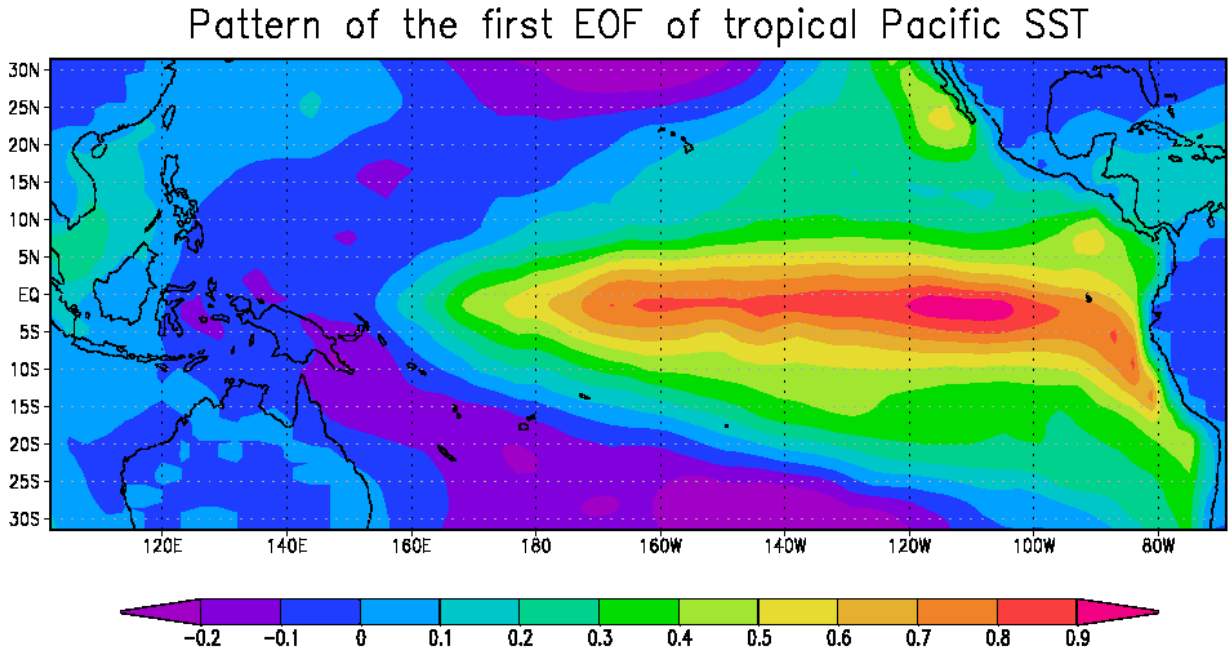

Figure 2.8: Pattern of the first EOF of tropical Pacific SST anomalies. In units of K.

The probability distribution of the NINO3 SST anomalies is shown in figure 2.9. In the NINO3 region, in general, positive SST anomalies are stronger than negative anomalies. This is also underlined by a positive skewness of NINO3 SST anomalies of $\gamma_1(T_{obs}) = 0.7$. Skewness is a measure for the asymmetry of a distribution. The distribution of the NINO3

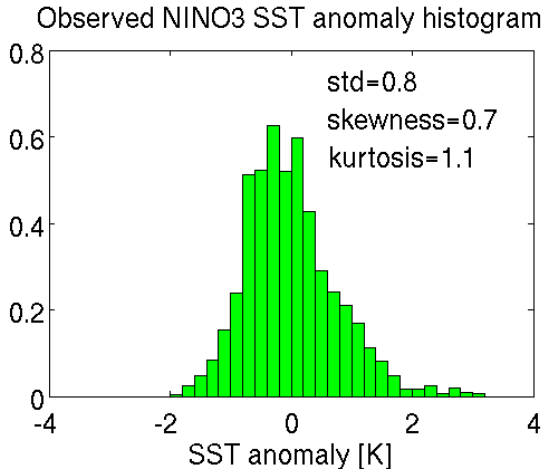

Figure 2.9: Histogram of observed monthly mean NINO3 SST anomalies for the period 1870-2003.

SST anomalies also shows a positive kurtosis of $\gamma_2(T_{obs}) = 1.1$. A positive kurtosis indicates that a distribution has a sharper peak than a normal distribution of equal standard deviation, which means extreme events are more likely than for a normal distribution.
Although great improvements have been made in understanding and predicting ENSO, there are still aspects of the ENSO phenomenon which are not yet understood, like the fact that the El Niño and La Niña events tend to follow a seasonal evolution or the amplitude asymmetry between El Niño and La Niña events.

2.3 The tropical Atlantic Ocean and the tropical Indian Ocean

The tropical Atlantic Ocean and the tropical Indian Ocean are the regions most influenced by ENSO. But to answer the question of whether they also have an influence on ENSO themselves, it is first necessary to understand the climatic states in the tropical Atlantic and the tropical Indian Ocean.
Although the Atlantic Ocean has a different basin size and a different distribution of land masses than the Pacific Ocean and there is no permanent warm pool in the tropical Atlantic, the two tropical oceans have many similarities in their mean climate. Similar to the tropical Pacific there are easterly surface winds, an equatorial cold tongue and a thermocline with an upward slope towards the east in the tropical Atlantic. Also the annual cycles of winds and SSTs show strong similarities between the two tropical oceans. This suggests that there also might be a coupled atmosphere-ocean mode similar to ENSO.
Keenlyside and Latif (2007) showed that the three elements of the Bjerknes feedback, surface winds, heat capacity, and SST, are present in the equatorial Atlantic and show spatial structure and cross correlation functions similar to the tropical Pacific. However, the strength of these feedbacks in the Atlantic is weaker and also other mechanisms seem to influence the SST variability. Another difference to the Pacific ENSO is the tendency of these so-called Atlantic Niño events to peak in boreal summer while ENSO events peak in boreal winter.

The tropical Indian Ocean differs from the other oceans in a number of ways (Schott et al., 2009). First, the Indian Ocean has a very different geometry. It is bounded to the north by the Asian continent which prevents heat export to the north. Additionally, the Asian continent drives the strongest monsoon on Earth and the resulting winds produce a large seasonal variability in the ocean currents. Many currents even show an annual reversal. Another difference to the other tropical oceans is the absence of steady equatorial easterlies, which implies that there also is no climatological equatorial upwelling in the eastern ocean. This is due to the rising branch of the Indian Ocean Walker circulation being located over the maritime continent. Finally, the Indian Ocean has a low-latitude exchange route with the Pacific in the form of the Indonesian Throughflow.

Despite these large differences to the other tropical oceans, some studies suggest that there might be a dynamical climate mode similar to the ENSO mode in the tropical Pacific but intrinsic to the Indian Ocean, the so-called Indian Ocean dipole (IOD). Fischer et al. (2005) and Behera et al. (2006) argue that the IOD could be forced by both ocean dynamics in the Indian Ocean itself and remote forcings from ENSO. On the other hand, Baquero-Bernal et al. (2002), Dommenget (2007), and Jansen et al. (2009) argue that the IOD index might just be a statistical index that has little indication to represent something like a coupled climate mode.

2.4 Interactions of the tropical oceans with ENSO

Although the ENSO mode is mainly a phenomenon of the tropical Pacific Ocean, the teleconnections of ENSO reach far beyond the tropical Pacific. ENSO has a strong influence on global interannual climate variability. SST anomalies in the whole Pacific region, the tropical Indian Ocean and parts of the tropical Atlantic Ocean are correlated with the NINO3 SST anomalies (see figure 2.10). Precipitation anomalies in large parts of the world, for example parts of the Australian continent, India, southeast Africa, and parts of the North and South

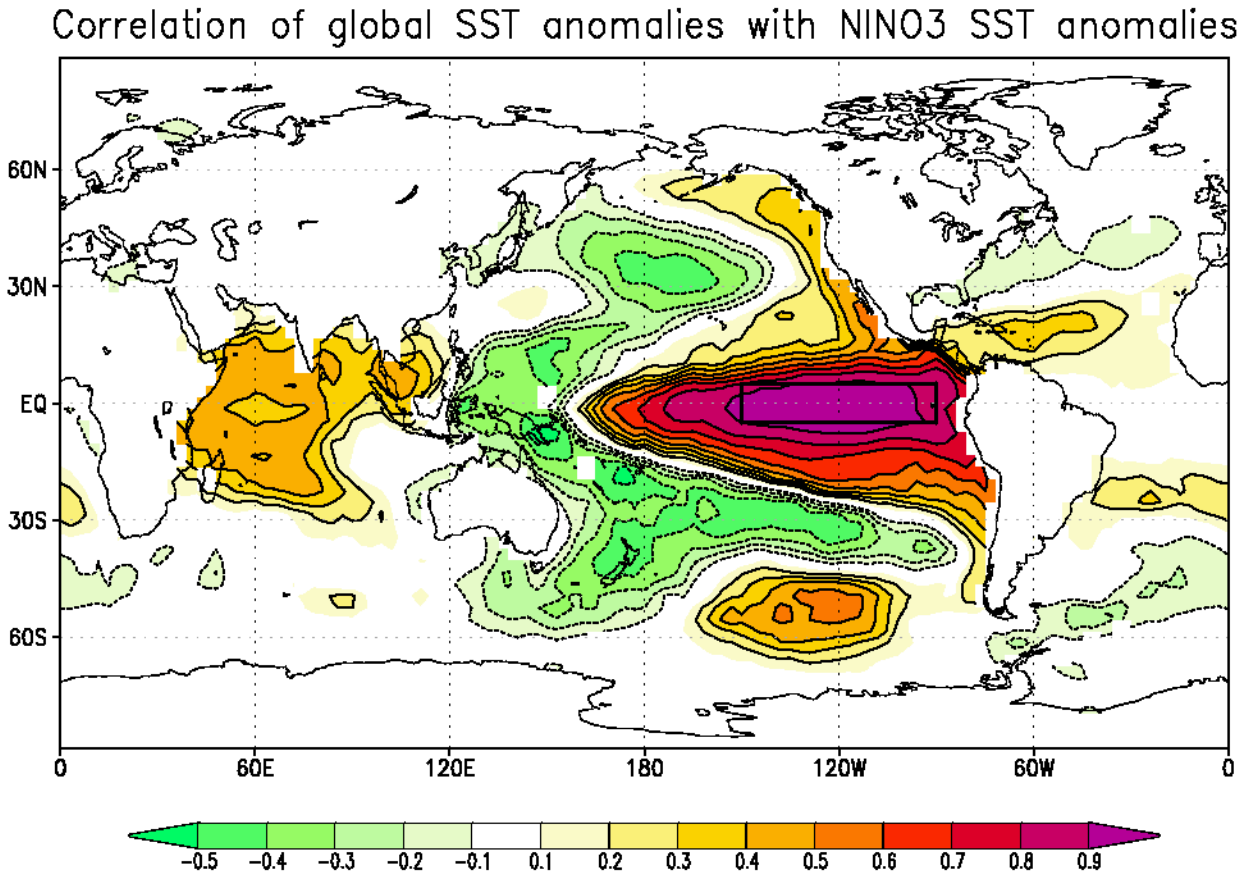

Figure 2.10: Observed correlation of global SST anomalies with NINO3 SST anomalies. The black box indicates the NINO3 region.

American continents, are related to ENSO (Ropelewski and Halpert, 1987). The regions most influenced by ENSO are the tropical Indian Ocean (Latif and Barnett, 1995; Venzke et al., 2000), the tropical Atlantic Ocean (Hastenrath et al., 1987; Enfield and Mayer, 1997; Mo and Häkkinen, 2001; Huang, 2004), and the adjacent continents. However, recent studies also suggest that the other tropical oceans may not only react to the ENSO mode but are influencing ENSO themselves. A first indication for this hypothesis can be found if one examines the cross correlation between the NINO3 SST anomalies and the SST anomalies in the eastern equatorial Atlantic (ATL3) region ($3°S - 3°N, 20°W - 0°E$) and in the tropical western Indian Ocean (WIO) region ($10°S - 10°N, 50° - 70°E$) respectively (figure 2.11). The cross correlation between the NINO3 and the WIO region is strongest when the NINO3

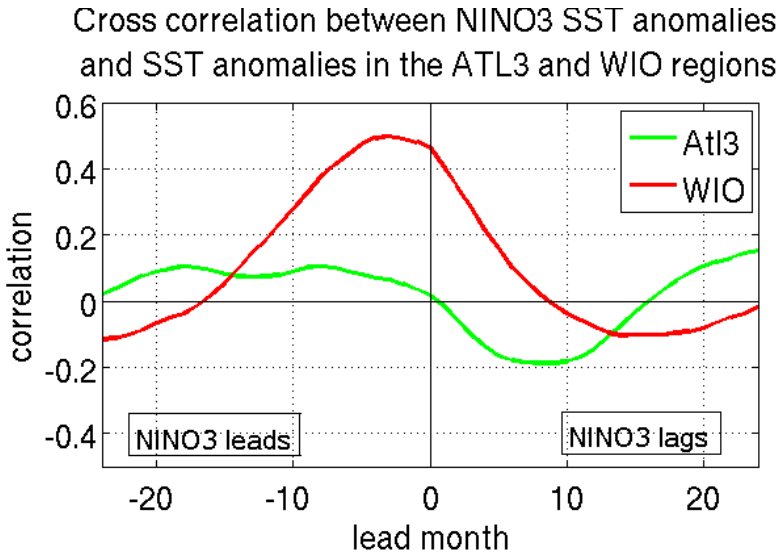

Figure 2.11: Observed cross correlation between the NINO3 SST anomalies and the ATL3 SST anomalies (green) and the NINO3 SST anomalies and the WIO SST anomalies (red).

region is leading by approximately 5 months while the correlation is weak when the WIO is leading. The cross correlation between the NINO3 and the ATL3 region is always weak. However, it is interesting to note the relatively strong correlation when the ATL3 region is leading by approximately 7 - 8 months. This could be a first indication for an influence of the Atlantic ocean on ENSO.

3 The RECHOZ model

3.1 The recharge oscillator

A very useful way to study the basic mechanisms responsible for ENSO is with simple conceptual models, which condense the dynamics of ENSO to ordinary or delay differential equations. The first of these simple conceptual models for ENSO was the delayed action oscillator by Suarez and Schopf (1988). In this model the oscillation is explained by equatorial wave transport processes. An initial westerly wind stress anomaly in the central Pacific generates a downwelling Kelvin wave propagating to the east and an upwelling Rossby wave travelling to the west. The Kelvin wave travels quite rapidly to the east and deepens the thermocline which leads to a warming of the SST. When the slower travelling Rossby wave reaches the western boundary it is reflected back to the east as an upwelling Kelvin wave that reverses the earlier warming in the east. Battisti and Hirst (1989) followed a different derivation and ended up with the same equation. Another approach is the recharge oscillator model, which was first proposed by Jin (1997). In this model the oscillation is explained by discharging (recharging) of equatorial heat content during an El Niño (La Niña) event, and equatorial wave travel times are not explicitely considered. The model consists of four equations for the western Pacific thermocline depth anomaly h_W, the eastern Pacific thermocline depth anomaly h_E, the central Pacific zonal wind stress anomaly τ, and the NINO3 SST anomaly T:

$$\frac{dh_W}{dt} = -r\, h_W - \alpha\, \tau \tag{3.1}$$

$$\frac{dT}{dt} = -c\, T + \gamma\, h_E \tag{3.2}$$

$$\tau = b\, T \tag{3.3}$$

$$h_E = h_W + \tau \tag{3.4}$$

Units are chosen such that the coefficient of τ in equation 3.4 equals one. The first term on the right-hand side in equation 3.1 represents the damping of the upper ocean system through mixing and the equatorial energy loss to the boundary layer currents. The second term represents the Sverdrup transport across the basin, i.e., the transport of heat content to or from the equatorial region depending on the wind forcing, leading to a deepening or flattening of the thermocline. In equation 3.2, the first term on the right-hand side describes the damping of the SST anomaly due to the mean climatological upwelling and heat exchange between the atmosphere and the ocean. The second term is the thermocline upwelling feedback. Equation 3.3 is a simple approximate relation of the wind stress and SST anomalies. Finally, equation 3.4 states that the tilt of the thermocline reacts quasi-instantaneously to wind stress. The equations 3.1 to 3.4 can be combined to a system of two ordinary differential equations:

$$\frac{dh_W}{dt} = -r\, h_W - \alpha\, b\, T \tag{3.5}$$

$$\frac{dT}{dt} = (\gamma\, b - c)\, T + \gamma\, h_W \tag{3.6}$$

Figure 3.1 displays a schematical representation of the physics of the recharge oscillator (equations 3.5 and 3.6). In panel (a) an initial positive SST anomaly induces a westerly wind anomaly over the central to western Pacific. This promptly leads to an anomalous slope of the thermocline. In the east the thermocline deepens which leads to a further

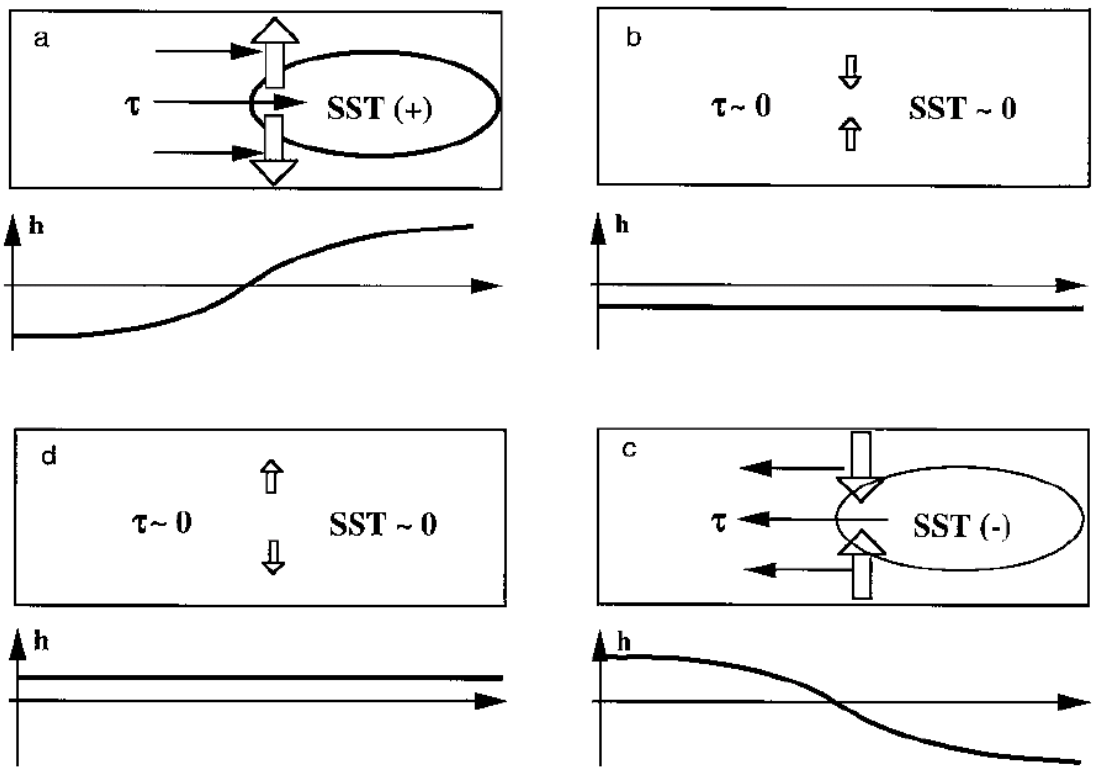

Figure 3.1: Schematic panels of the four phases of the recharge oscillator: (a) the warm phase, (b) the warm to cold transition phase, (c) the cold phase, and (d) the cold to warm transition phase. The rectangular box represents the equatorial Pacific basin, the elliptical circle represents the SST anomaly, the thin and filled arrows represent wind stress anomaly associated with the SST anomaly, and the thick unfilled arrows represent the recharge/discharge of equatorial heat content. Each panel also shows the distribution of the thermocline depth anomaly (h) along the equator. The figure is obtained from Jin (1997).

amplification of the initial SST anomaly and the oscillation reaches a mature phase. In the west the wind stress anomaly gradually reduces the depth of the thermocline and leads to a negative zonal mean thermocline depth anomaly across the Pacific. This deepening of the mean thermocline can also be considered as the discharge of zonal mean equatorial heat content. This discharge of heat content also gradually flattens the thermocline in the east and the oscillation evolves from the warm phase to a transition phase (see figure 3.1 panel (b)). Now the SST anomaly cools to zero and the zonal wind stress anomaly disappears. Together with the wind stress, the anomalous slope of the thermocline diminishes but the entire equatorial thermocline depth stays anomalously shallow due to the discharge of the

heat content during the warm phase. Due to this anomalously shallow thermocline there is an upwelling of cold water in the east, which causes the SST anomaly to become negative. This leads to an easterly wind stress anomaly, which causes a deepening of the thermocline in the west and a further flattening of the thermocline in the east accompanied by a further cooling of the SST. The oscillation reaches its mature cold phase (figure 3.1 panel (c)). Now the enhanced easterlies induce a deepening of the zonal mean thermocline depth or a recharging of the equatorial heat content. The oscillation reaches another transition phase (figure 3.1 panel (d)). The SST anomaly warms to zero again and the anomalously deep zonal mean thermocline leads to a development of a warm phase again.

One way to excite the recharge oscillator is to include a stochastic forcing. Thus the linear conceptual model can be extended as follows:

$$\frac{dh_W}{dt} = -r\,h_W - \alpha\,b\,T - \alpha\,\xi_1 \tag{3.7}$$

$$\frac{dT}{dt} = (\gamma\,b - c)\,T + \gamma\,h_W + \gamma\,\xi_1 + \xi_2 \tag{3.8}$$

where ξ_1 represents a random wind stress forcing added to τ in equations 3.1 and 3.4 and ξ_2 is a random heating added into equation 3.2.

Burgers et al. (2005) derived a more general form of the recharge oscillator by making the assumption $h \approx 0.5\,(h_W + h_E)$ where h is the zonally averaged central Pacific thermocline depth anomaly. So the general recharge oscillator excited by stochastic forcing can be expressed as follows:

$$\frac{dT}{dt} = a_{11}T + a_{12}h + s_1 \tag{3.9}$$

$$\frac{dh}{dt} = a_{21}T + a_{22}h + s_2 \tag{3.10}$$

with s_1 and s_2 representing the combined stochastic forcings.

3.2 Model development

The simple conceptual ENSO models by Suarez and Schopf (1988) and Jin (1997) accounted for big improvements in the understanding of the ENSO phenomenon. Since the time these models were developed, there has been a steady progress in the simulation and prediction of ENSO using coupled GCMs (Latif and Coauthors, 2001; Guilyardi et al., 2009b). Many state-of-the-art coupled GCMs now simulate an ENSO mode that is qualitatively similar to the real-world behaviour. However, recent multimodel analyses show that the models still produce systematic errors in the simulated background climate and in the simulated variability (van Oldenborgh et al., 2005; Capotondi et al., 2006; Guilyardi et al., 2009b). For example van Oldenborgh et al. (2005) studied the ENSO-like model variability in the tropical Pacific in 19 climate models of the IPCC AR4 report. The models show a wide range of behaviour. Two models do not show ENSO-like variability at all. Other models show too regular oscillations or a shorter period than observed. Also the modeled amplitude of ENSO events ranges from less than half to more than double of the observed amplitude. Many models are also not able to capture the the observed seasonality of ENSO. They show only little seasonal modulation or a phase locking to the wrong part of the annual cycle. Most models also cannot reproduce the observed positive skewness of ENSO. They simulate no skewness or even a negative skewness. This indicates that some aspects of ENSO are not yet fully understood and thus it is difficult to make any reliable predictions of how ENSO will behave in future warmer climate.

Several studies point out the important role of atmospheric feedbacks in determining ENSO characteristics in GCMs (Schneider, 2002; Guilyardi et al., 2004, 2009a). To improve the understanding of the influences of atmospheric feedbacks on ENSO properties like the skewness and the nonlinearity, a new HCM RECHOZ was developed which consists of a complex atmospheric GCM coupled to a simple conceptual linear two-dimensional ocean model in the tropical Pacific. This model can also be used to study the effects of changes in the mean

state of the tropical Pacific on ENSO through atmospheric feedbacks and the influences of the tropical Indian and the tropical Atlantic Ocean on ENSO.

The new RECHOZ model is based on the simplified global climate model ECHAM5-OZ (Dommenget and Latif, 2008). As the atmospheric component the GCM ECHAM5 is used, which is described in Roeckner et al. (2003). The mean climatology of the model is described in Roeckner et al. (2004). The model has a horizontal spectral resolution of T31, approximately equivalent to 3.75° by 3.75°, with 19 vertical levels up to 10 hPa and a temporal resolution of 40 minutes. The oceanic component of the model is the simple mixed layer ocean model OZ, which is similar to the model of Alexander and Penland (1996). In this model the ocean consists of 19 vertical layers that are connected through vertical diffusion only. That means that ocean grid points do not communicate with neighbouring points. The density depends on temperature and salinity, but the density variations are only driven by the temperature. At the surface the ocean is forced by heat flux and mechanical wind mixing (Niiler and Kraus, 1977). The temperature of the lowest layer, at a depth of 500 m, is restored to the observed climatology. Effects of the time-mean ocean currents are included by a so-called Q-flux scheme, that ensures a realistic mean state. However, changes in ocean currents are not taken into account. The model realistically simulates monthly mean SST standard deviations and seasonal differences. It also has a realistic SST spectrum in the mid- and higher latitudes (Dommenget and Latif, 2008). Because ocean dynamics are not considered in the model, the SST variability in the tropics is much weaker than observed and has unrealistic spatial structures.

Therefore, in the tropical Pacific ($20°S - 20°N, 130°E$-Pacific eastern boundary) the ocean grid is replaced with the low-order two-dimensional recharge oscillator model based on Burgers et al. (2005) (equations 3.9 and 3.10). The values of the parameters a_{11}, a_{12}, a_{21} and a_{22} were chosen in accordance to the observational estimate of Burgers et al. (2005) (see table 3.1). The stochastic forcings can be assumed to be the central Pacific ($6°S - 6°N, 160°E - 140°W$) zonal wind stress anomaly τ and the NINO3 heat flux anomaly

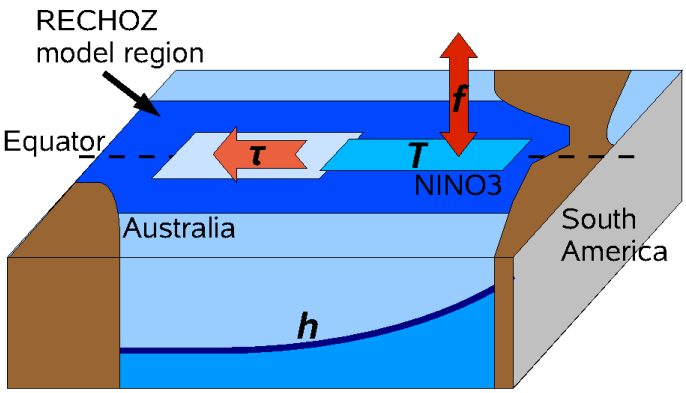

Figure 3.2: Schematic representation of the model variables.

f. A schematic representation of the model variables can be seen in figure 3.2.

It further has to be considered that the couplings to T (a_{11} and a_{21}) are partly caused by oceanic and atmospheric processes:

$$a_{11} = a_{11O} + a_{11A} \tag{3.11}$$

$$a_{21} = a_{21O} + a_{21A} \tag{3.12}$$

It is assumed that the atmospheric coupling to T ($a_{11A}T$ and $a_{21A}T$) is actually a coupling to τ and f:

$$a_{11A} = c_{\tau A}\, r_{T\tau} + c_{fA}\, r_{Tf} \tag{3.13}$$

$$a_{21A} = c_{\tau O}\, r_{T\tau} + c_{fO}\, r_{Tf} \tag{3.14}$$

The linear regressions of τ on T, $r_{T\tau}$, and f on T, r_{Tf}, were estimated from a reference run in which in the tropical Pacific the ocean model was replaced by a harmonic oscillating SST anomaly with the pattern of the first EOF of the tropical Pacific SST anomalies (see figure 2.8), a period of 4 years and an amplitude of $\sqrt{2}$ K. Thus τ and f both have a part proportional to T and an independent part representing the stochastic forcings ξ_1 and ξ_2.

The parameters $c_{\tau A}$, c_{fA}, $c_{\tau O}$ and c_{fO} need to be constrained further. Following Jin (1997)

no heat flux forcing for h is assumed, thus $c_{fO} = 0$. Furthermore, it is assumed that the atmospheric heat flux is integrated by the heat capacity of the mixed layer, mc, with an estimated depth of 80 m, which defines c_{fA}. The parameters $c_{\tau A}$ and $c_{\tau O}$ are not well constrained by neither Jin (1997) nor Burgers et al. (2005). To estimate these parameters for the ECHAM5 atmosphere model the RECHOZ model was tested with a range of parameter values for $c_{\tau A}$, $c_{\tau O}$, and mc. For the values in table 3.1 the statistics of T and h in the RECHOZ model are closest to those observed.

Param.	**Value**	**Param.**	**Value**
a_{11}	$-0.076\ \frac{1}{month}$	a_{11O}	$-0.488\ \frac{1}{month}$
		a_{11A}	$0.412\ \frac{1}{month}$
a_{12}	$0.021\ \frac{K}{month\, m}$		
a_{21}	$-1.400\ \frac{m}{K\, month}$	a_{21O}	$-1.322\ \frac{m}{K\, month}$
		a_{21A}	$-0.078\ \frac{m}{K\, month}$
a_{22}	$-0.008\ \frac{1}{month}$		
$r_{T\tau}$	$7.32 \cdot 10^{10}\ \frac{kg}{m\, month^2\, K}$		
r_{Tf}	$1.51 \cdot 10^{20}\ \frac{kg}{month^3\, K}$		
mc	$1025 \frac{kg}{m^3} \cdot 3994\ \frac{J}{kg\, K} \cdot 80m$		
$c_{\tau A}$	$5.63 \cdot 10^{-12}\ \frac{K\, m\, month}{kg}$		
$c_{\tau O}$	$1.07 \cdot 10^{-13}\ \frac{m^2\, month}{kg}$		

Table 3.1: Parameter values for the RECHOZ model.

So the resulting RECHOZ model equations are:

$$\frac{dT}{dt} = a_{11O}T + a_{12}h + c_{\tau A}\tau + \frac{1}{mc}f \tag{3.15}$$

$$\frac{dh}{dt} = a_{21O}T + a_{22}h + c_{\tau O}\tau \tag{3.16}$$

Note that here the tendencies of h are depending on T, while following Jin (1997) one could replace the T-term with a term proportional to τ because physically the depth of the thermocline is only influenced by the wind stress and not directly by the SST. In this case equation 3.16 would look like:

$$\frac{dh}{dt} = a_{22}h + \frac{1}{r_{T\tau}}a_{21}\tau \tag{3.17}$$

I tested such a model coupled to ECHAM5, but could not find a parameter space in which realistic amplitude and oscillation of T variability would occur. With a parameter a_{21} in the range of the observational estimates of Burgers et al. (2005) the ENSO variability in the model was strongly reduced.

The resulting model temperature anomaly T in equation 3.15 is just one value for the whole tropical Pacific. To get from this one-dimensional model temperature anomaly to basinwide temperature anomalies, the resulting temperature anomaly is multiplied with the pattern of the first EOF of the observed SST anomalies over the tropical Pacific domain (for the EOF pattern see again figure 2.8). The atmosphere model, however, needs absolute temperature values and not temperature anomalies. Therefore, observed tropical Pacific seasonal mean SST values are added when coupled to the ECHAM5 atmosphere model. This means also that the mean state of the tropical Pacific in the model could only change if the mean of the SST anomalies was not equal zero, what is not the case in the RECHOZ model.

In summary, the RECHOZ model is a HCM with a full complexity atmospheric GCM coupled to a ocean model in the tropical Pacific which has by construction linear and seasonally non-varying ocean dynamics. Thus, this model can be used to study the influences of atmos-

pheric feedbacks on the seasonality and nonlinearity of ENSO. By changing the prescribed SST climatology in the tropical Pacific, it can be analysed, how changes in the mean state influence the properties of ENSO through atmospheric feedbacks. It is also easily possible to replace the mixed layer ocean model in different regions by prescribed climatologies to study the influence of climate variability in this regions on the ENSO mode.

3.3 The REOSC-MC model

For comparisons also a simple Monte Carlo reference model (REOSC-MC) is constructed in which the recharge oscillator ocean model in equations 3.15 and 3.16 is taken and the atmospheric GCM forcings τ and f are expressed in terms of T and some white noise forcings:

$$\tau = r_{T\tau}T + \xi_1 \tag{3.18}$$

$$f = r_{Tf}T + \xi_2 \tag{3.19}$$

with $r_{T\tau}$ and r_{Tf} the regression coefficients mentioned above. The standard deviations of the noise terms ξ_1 and ξ_2 were chosen to be identical to the standard deviations of the residuals of the linear regression between T and τ and T and f. The REOSC-MC model was integrated for 10000 years with a timestep of 40 minutes.

4 ENSO in the RECHOZ model

4.1 Main ENSO statistics

First it is analysed how the main properties of ENSO are simulated in the 500-year-long CTRL experiment of the RECHOZ model. The mean values of tropical Pacific SST and zonal wind stress are simulated realistically in the model (figure 4.1 (a) and (b)). The recharge oscillator ocean model only calculates the SST anomaly averaged over the NINO3 region. The SST anomaly is then multiplied with the pattern of the first EOF of the observed tropical Pacific SSTs and added to a monthly varying climatology obtained from observations. Thus, the pattern of the SSTs is fixed and the mean state could only change if the mean of the SST anomalies is not zero, what is not the case for the RECHOZ model. In contrast to many current GCMs which simulate a mean zonal equatorial wind stress that is too strong (Guilyardi et al., 2009b), the RECHOZ model simulates a very realistic zonal wind stress in the tropical Pacific (see for comparison Wittenberg (2004)). The mean zonal wind stress is easterly except for the far western and eastern equatorial Pacific and is strongest in the central Pacific around 15° north of the equator. The mean net heat flux is too strong in the far western Pacific and too weak in the equatorial eastern Pacific (figure 4.1 (c)). In the far eastern Pacific south of the equator is also an area of too strong net heat flux (see for comparison Large and Yeager (2008)). For a more detailed view the single heat flux components are displayed in figure 4.2. The net flux is mainly determined through the latent heat flux (figure 4.2 (b)) and the surface solar radiation (figure 4.2 (c)). The sensible heat flux (figure 4.2 (a)) and the surface thermal radiation (figure 4.2 (d)) are of less importance.

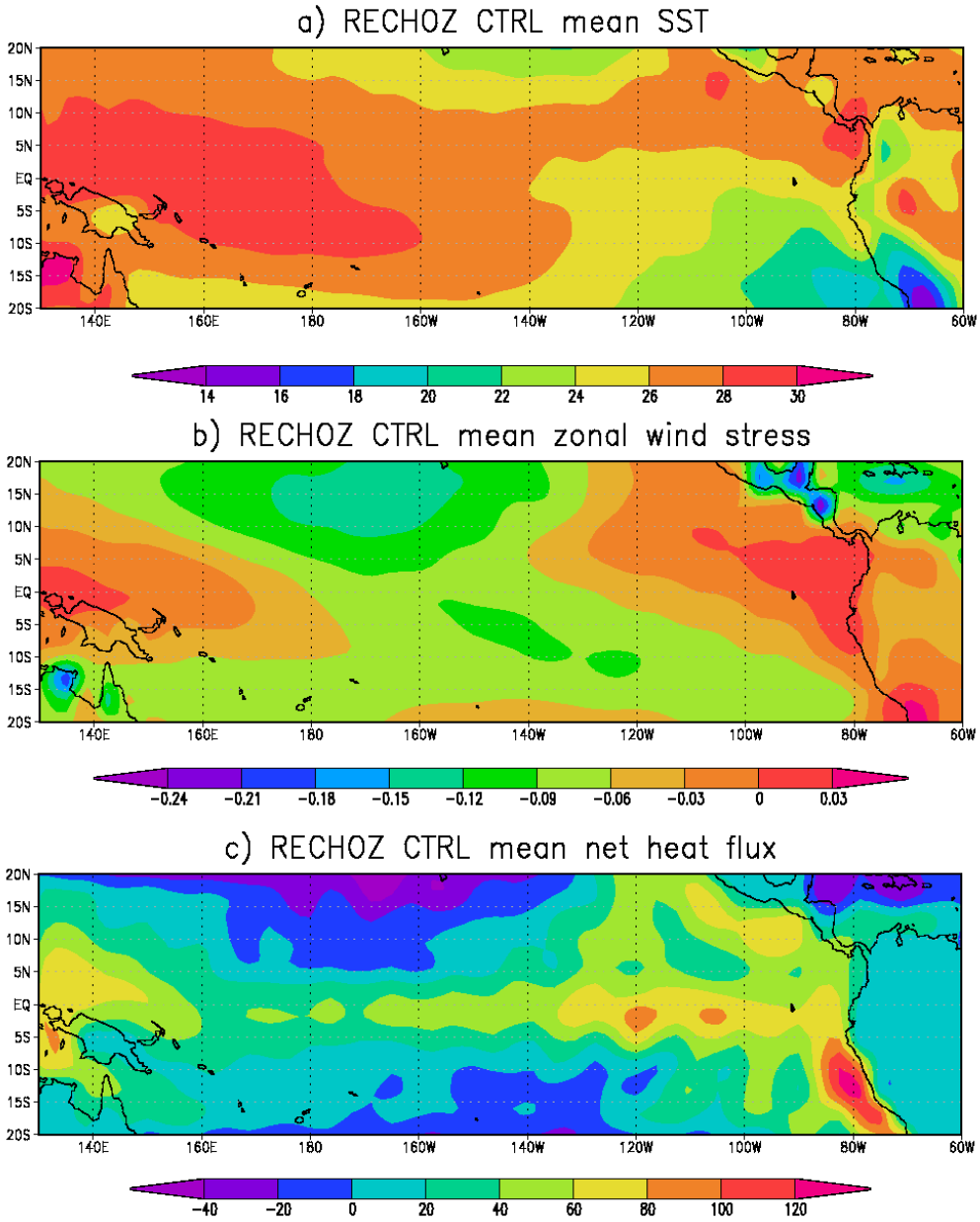

Figure 4.1: Mean values of a) SST [°C], b) zonal wind stress [Pa], and c) net heat flux [W/m^2] for the RECHOZ CTRL run.

The latent heat flux is too strong in the equatorial eastern Pacific which is a common bias in many atmospheric GCMs due to excessive sensitivity of surface air humidity to SST (Lin, 2007). The surface solar radiation is too strong in the eastern Pacific south of the equator and too weak in the equatorial Pacific which are also common atmospheric GCM biases.

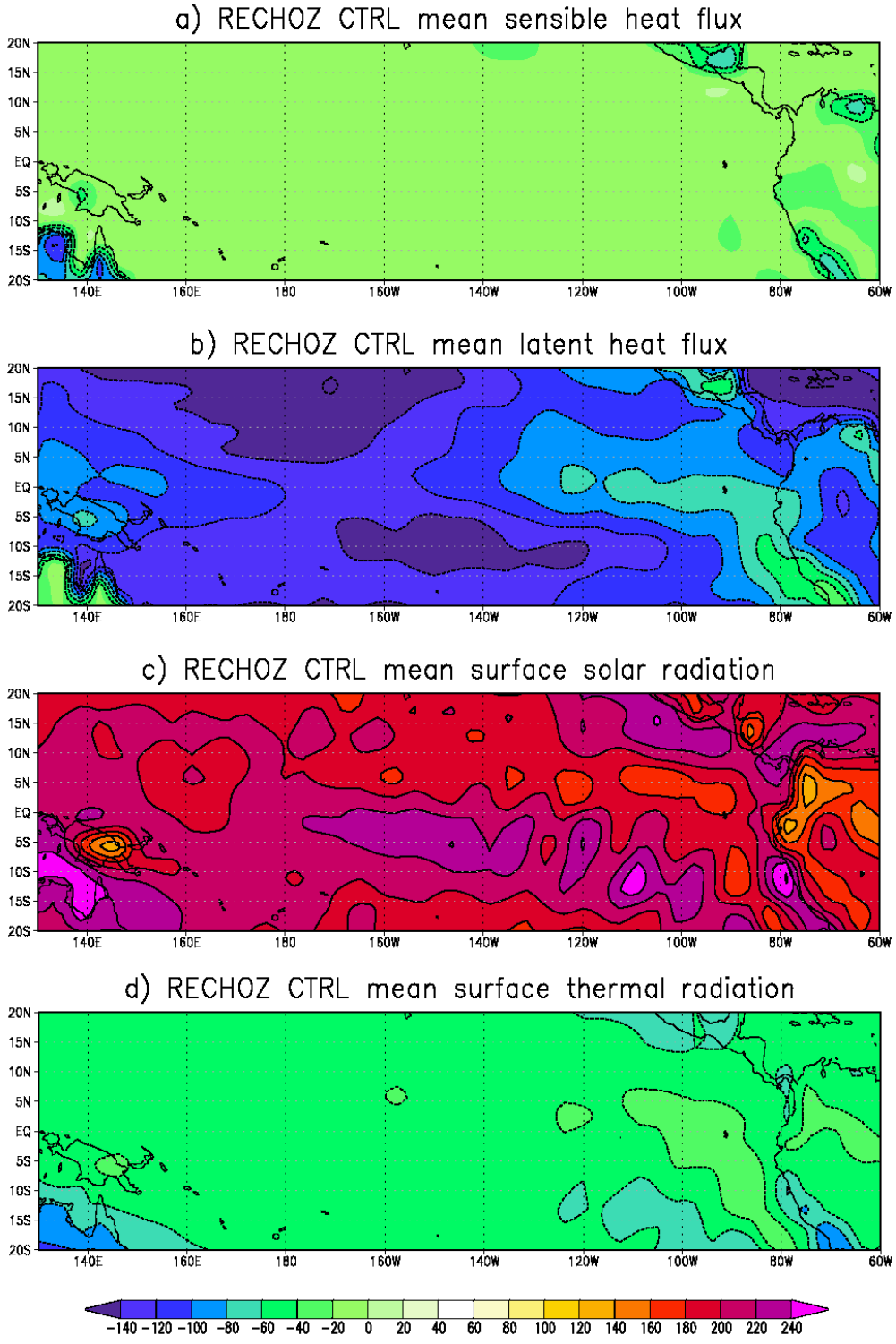

Figure 4.2: Mean values of a) sensible heat flux, b) latent heat flux, c) surface solar radiation, and d) surface thermal radiation for the RECHOZ CTRL run. Units are in W/m^2.

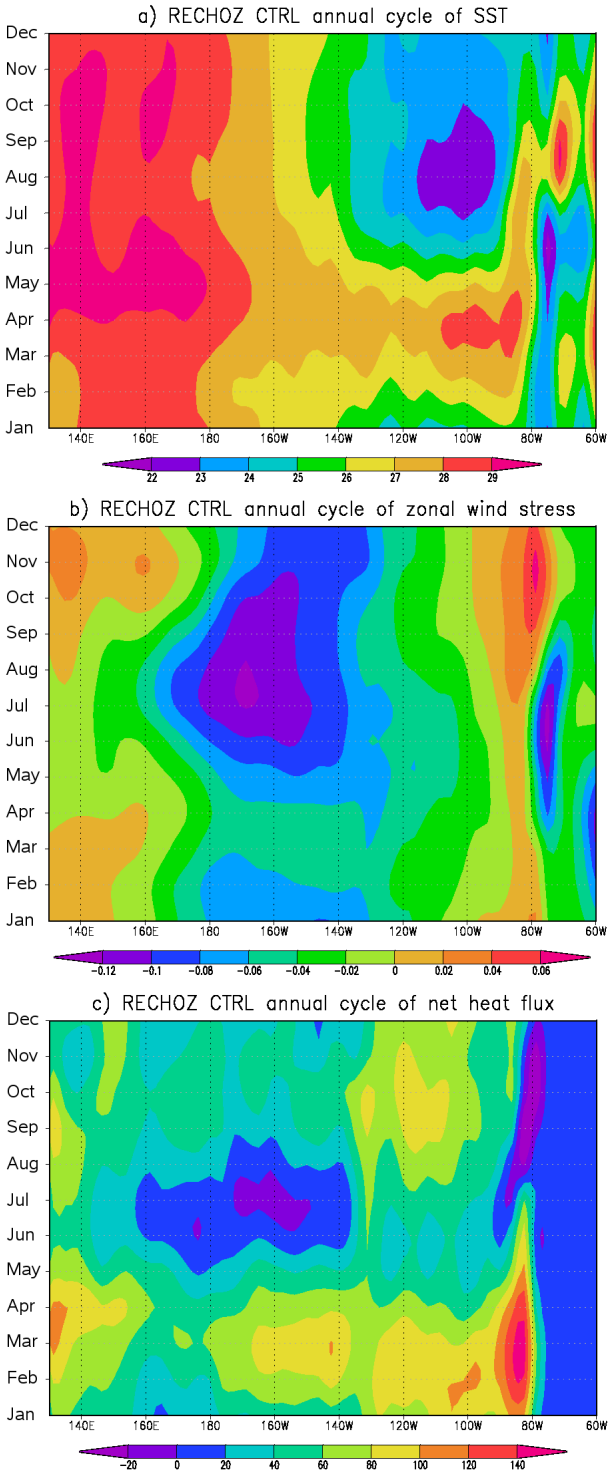

Figure 4.3: Annual cycle of a) SST [°C], b) zonal wind stress [Pa], and c) net heat flux [W/m^2] along the equator (averaged between 5° N and 5° S) for the RECHOZ CTRL run.

The seasonal cycle of SST and zonal wind stress is also simulated realistically in the RECHOZ model (figure 4.3 (a) and (b)). The zonal wind stress is strongest in the Northern Hemisphere summer and autumn and is associated with strong upwelling of cold SST in the eastern Pacific. In the Northern Hemisphere spring the trade winds are weak and the SST in the east Pacific is warm. The SST in the western Pacific shows almost no seasonal evolution. The net heat flux is strongest in Northern Hemisphere spring and autumn and weak in Northern Hemisphere summer (figure 4.3 (c)).

In the following, only the anomalies of the NINO3 SST and the equatorial Pacific thermocline depth are examined as the recharge oscillator ocean model only computes these anomalies. Accordingly, only the central Pacific zonal wind stress anomalies and the NINO3 heat flux anomalies are considered as they are used to force the recharge oscillator ocean model. For comparison, the results of the 10000-year-long REOSC-MC simulation are shown. One has to keep in mind that for the thermocline depth anomalies, comparisons with observations are difficult because the observational time series of thermocline depth data are very short and thus of limited significance.

A first indication of the simulated ENSO behaviour is given by the time series of NINO3 SST anomalies (figure 4.4). The time series of the SST anomalies is comparable with observations and also the standard deviation of the RECHOZ model's NINO3 SST anomalies $\sigma(T) = 0.8\,K$ is in good agreement with observations ($\sigma(T_{obs}) = 0.8\,K$). For a more detailed view the time series of NINO3 SST anomalies and equatorial Pacific thermocline depth anomalies are shown only for the last 50 years of the RECHOZ CTRL simulation in figure 4.5. The time series of the thermocline depth anomalies seems to be more regular than observed, and of smaller amplitude (see for comparison figure 2.5). The standard deviation of the model's thermocline depth anomalies $\sigma(h) = 5.4\,m$ is smaller than in observations ($\sigma(h_{obs}) = 7.5\,m$) as is indicated by the time series.

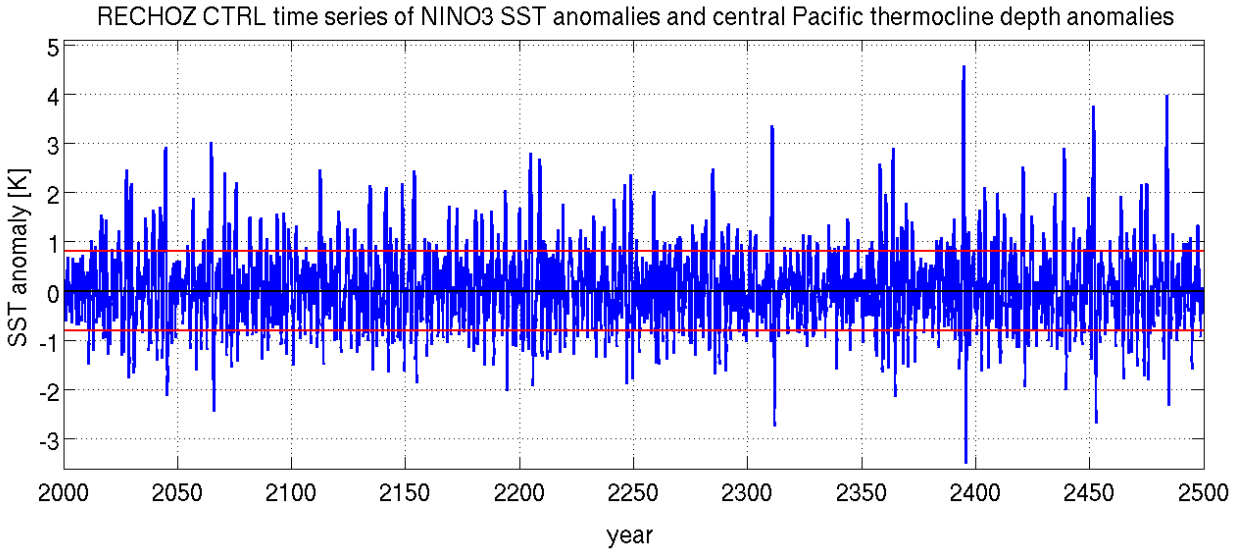

Figure 4.4: Time series of NINO3 SST anomalies (blue) for the period 2000-2500 of the RECHOZ CTRL run. The red lines indicate the standard deviation of the SST anomalies.

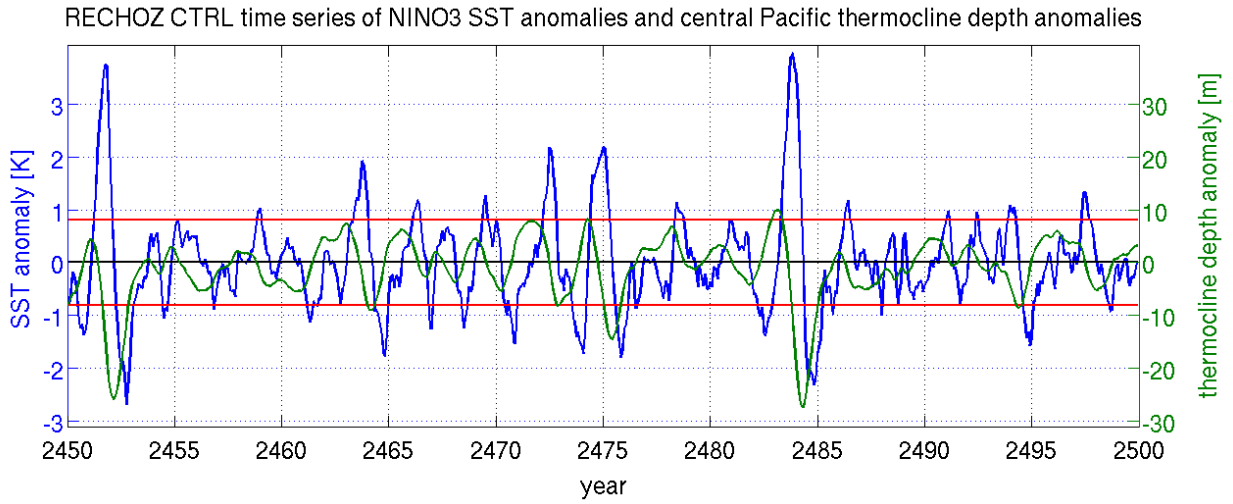

Figure 4.5: Time series of NINO3 SST anomalies (blue) and equatorial Pacific thermocline depth anomalies (green) for the last 50 years of the RECHOZ CTRL run (2450-2500). The red lines indicate the standard deviation of the SST anomalies.

More detailed information of the simulated ENSO in the RECHOZ model can be gained from the power spectrum of NINO3 SST anomalies (figure 4.6). The oscillation in the model is more regular than observed, which may be due to the simple character of the model, and has a peak between periods of about 1.5 and 4 years, which is slightly shorter than in observations but in good agreement with other coupled GCMs (Guilyardi et al., 2009b). The REOSC-MC model has an even more regular oscillation and a peak at slightly longer periods than the RECHOZ model.

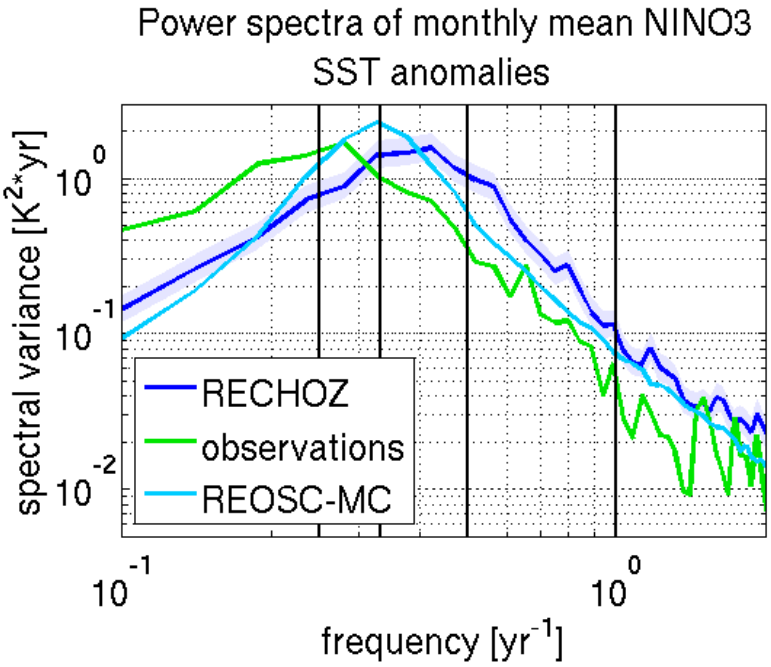

Figure 4.6: Spectra of monthly mean NINO3 SST anomalies for the RECHOZ model (blue) compared to observations (green) and the REOSC-MC model (cyan). The violet shading indicates the 80% confidence level of the RECHOZ model spectrum.

Many state-of-the-art GCMs have problems simulating the seasonal variations in the ENSO cycle. They either show little seasonality or a phase locking to the wrong part of the annual cycle (Guilyardi et al., 2009b). The RECHOZ model simulates a seasonal cycle of NINO3 SST anonalies comparable with observations (figure 4.7). Especially in winter and spring the monthly standard deviations of the NINO3 SST anomalies are very close to observa-

tions, while in summer the variability in the model is too strong. The peak in the seasonal variability is already in autumn, not in early winter like in observations. By definition the REOSC-MC model shows no seasonality.

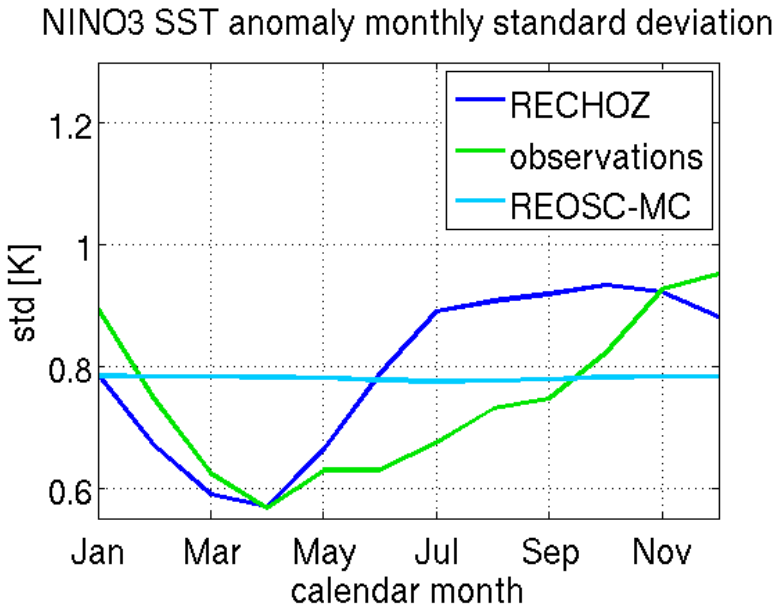

Figure 4.7: Standard deviation of monthly mean NINO3 SST anomalies for each calendar month for the RECHOZ model (blue) compared to observations (green) and the REOSC-MC model (cyan).

Another feature of ENSO which many current GCMs do not capture is its nonlinearity. GCMs often simulate no skewness of NINO3 SST anomalies or even a negative skewness (van Oldenborgh et al., 2005). The histogram of monthly mean NINO3 SST anomalies (figure 4.8 (a)) for the RECHOZ model clearly shows that it is able to simulate a distribution of the SST anomalies comparable with observations (figure 4.8 (b)). The model's skewness $\gamma_1(T) = 0.6$ is in good agreement with the observed ($\gamma_1(T_{obs}) = 0.7$) while the model's kurtosis $\gamma_2(T) = 1.9$ is slightly larger than observed ($\gamma_2(T_{obs}) = 1.1$). The REOSC-MC model is not able to simulate skewness or kurtosis (figure 4.8 (c)).

The 99% confidence level of the Kolmogorov-Smirnov test (Massey (1951)) for a normal distribution is clearly passed (by a factor of two) for the RECHOZ SST anomaly distribution, quantifying the non-normality of the model. In contrast, the REOSC-MC model statistic is

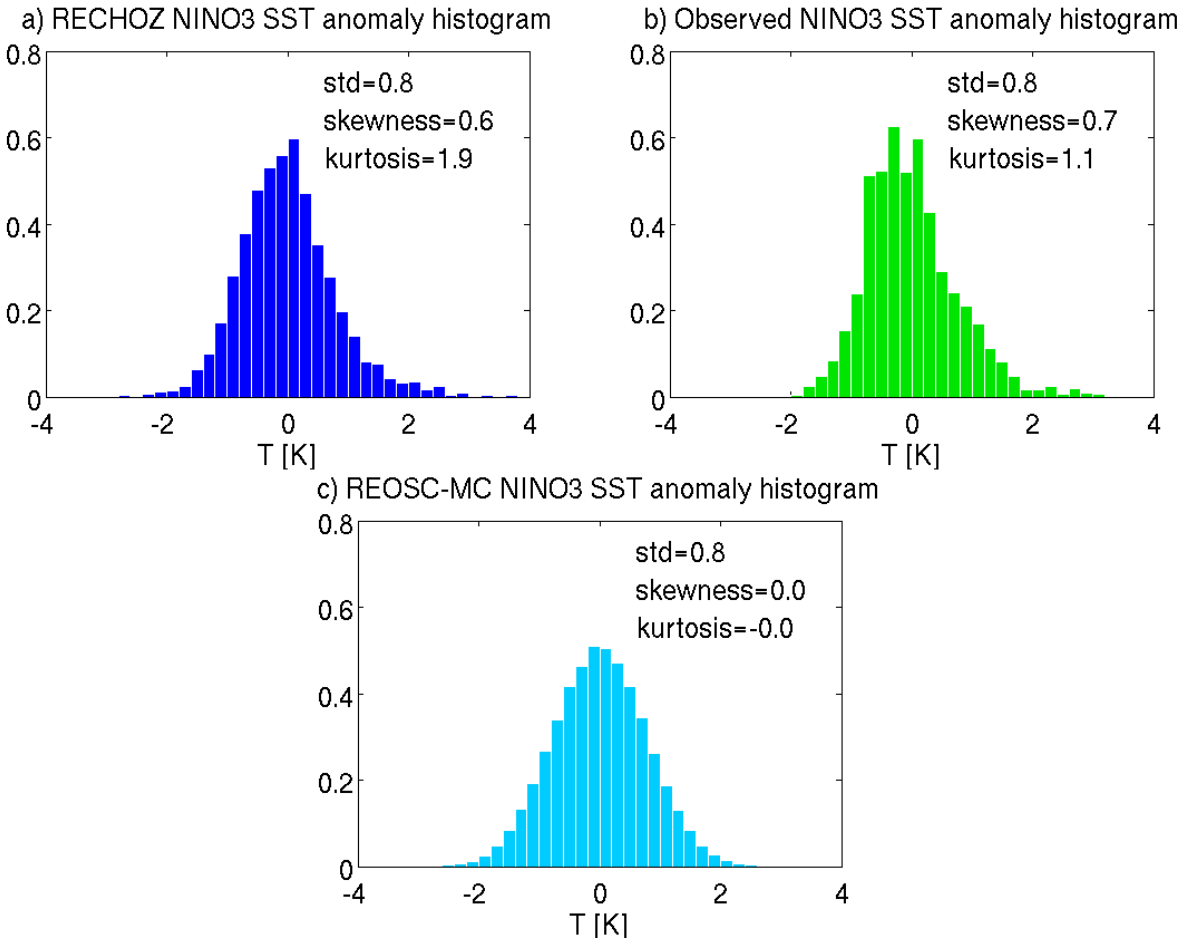

Figure 4.8: Histograms of monthly mean NINO3 SST anomalies for (a) the RECHOZ model, (b) observations and (c) the REOSC-MC model.

well within the Kolmogorov-Smirnov test distribution for a normal distribution, highlighting that the positive skewness and kurtosis in the RECHOZ model have to be caused by the atmospheric forcings. This result holds also if the analysis is repeated for each season individually, to avoid effects of seasonality (see figure 4.9). The skewness of the NINO3 SST anomalies follows a strong seasonal cycle too, with the skewness being strongest in autumn when also the variability is strongest. However, even when the variability is weakest in spring there exists still a positive skewness.

The skewness of the model's thermocline depth anomalies $\gamma_1(h) = -1.2$ is comparable with observations, too ($\gamma_1(h_{obs}) = -0.7$), but the kurtosis $\gamma_2(h) = 2.9$ is much larger than in ob-

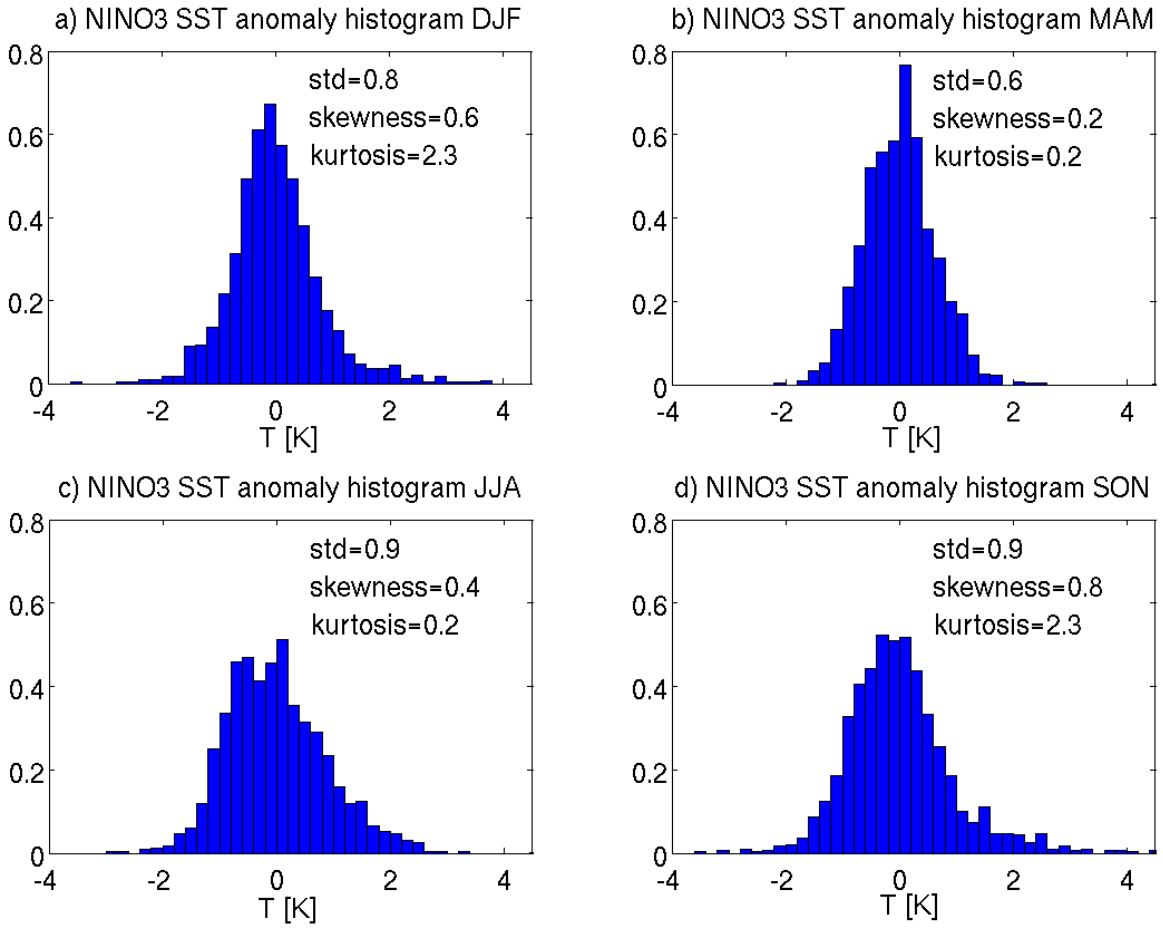

Figure 4.9: Seasonal histograms of monthly mean NINO3 SST anomalies for the RECHOZ model for (a) December - February (DJF), (b) March - May (MAM), (c) June - August (JJA), and (d) September - November (SON).

servations ($\gamma_2(h_{obs}) = 0.6$) (figure 4.10). However, one still has to keep in mind the limited significance of observed thermocline depth data.

Analyses of the cross correlations between the NINO3 SST anomalies, the central Pacific zonal wind stress anomalies and the equatorial Pacific thermocline depth anomalies show that the RECHOZ model produces realistic relationships between the different elements of the Bjerknes feedback. The cross correlation between the NINO3 SST anomalies and the equatorial Pacific thermocline depth anomalies is in good agreement with observations (figure 4.11). However, the correlations are stronger and the SST is leading by only about 7 months in the RECHOZ model, compared to 9 months in the observations. The model's

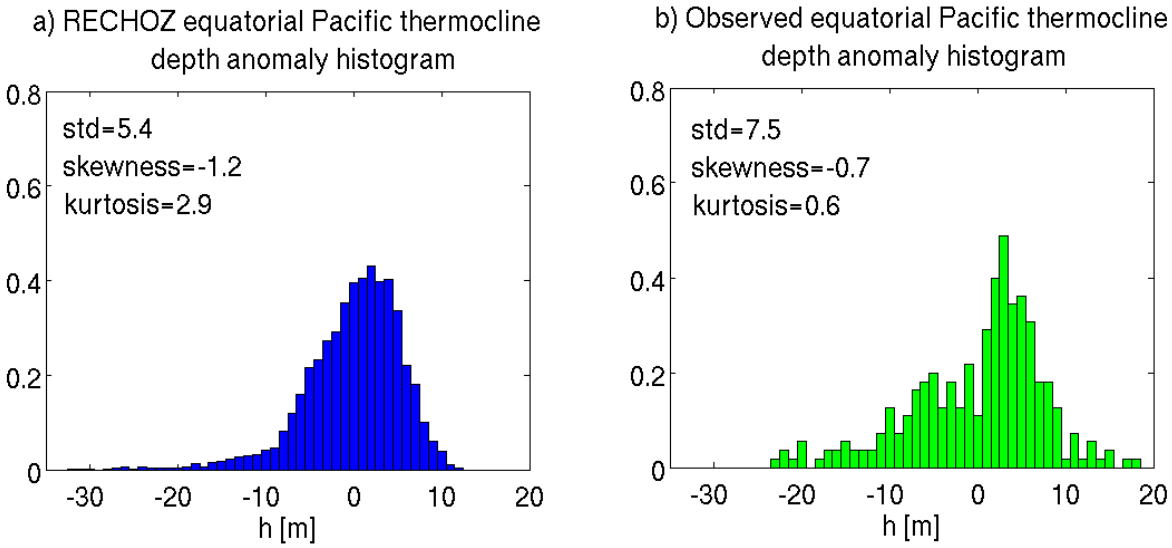

Figure 4.10: Histograms of monthly mean equatorial Pacific thermocline depth anomalies for (a) the RECHOZ model and (b) observations.

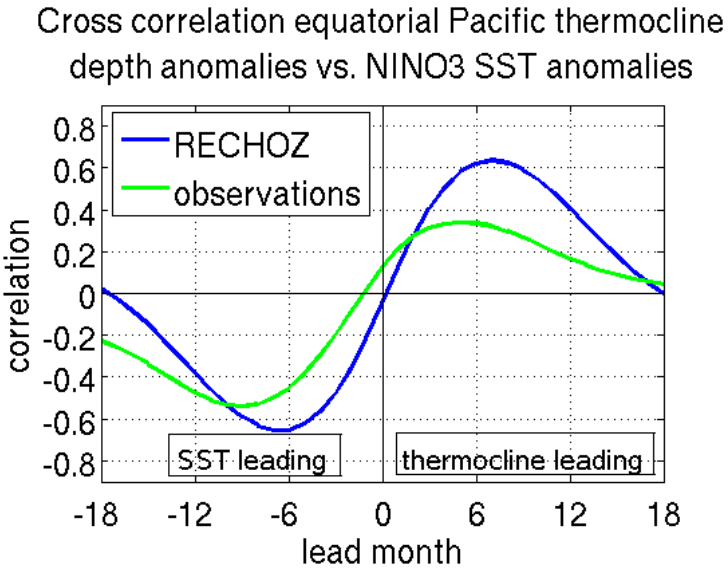

Figure 4.11: Cross correlation between the equatorial Pacific thermocline depth anomalies and NINO3 SST anomalies for the RECHOZ model (blue) and observations (green). Instead of observational thermocline depth data the thermocline depth data obtained from the forced MPI-OM experiment was used.

correlation curve is also more symmetric than in observations, with a strong correlation for the thermocline leading the SST at 6 months, too.

The seasonal cross correlation between the NINO3 SST anomalies and the central Pacific thermocline depth anomalies (figure 4.12) is comparable with the observations. Again the correlations are stronger in the model and the seasonal cycle is less pronounced. Also the seasonal cycle seems to be shifted by approximately 2 months between the model and the observations.

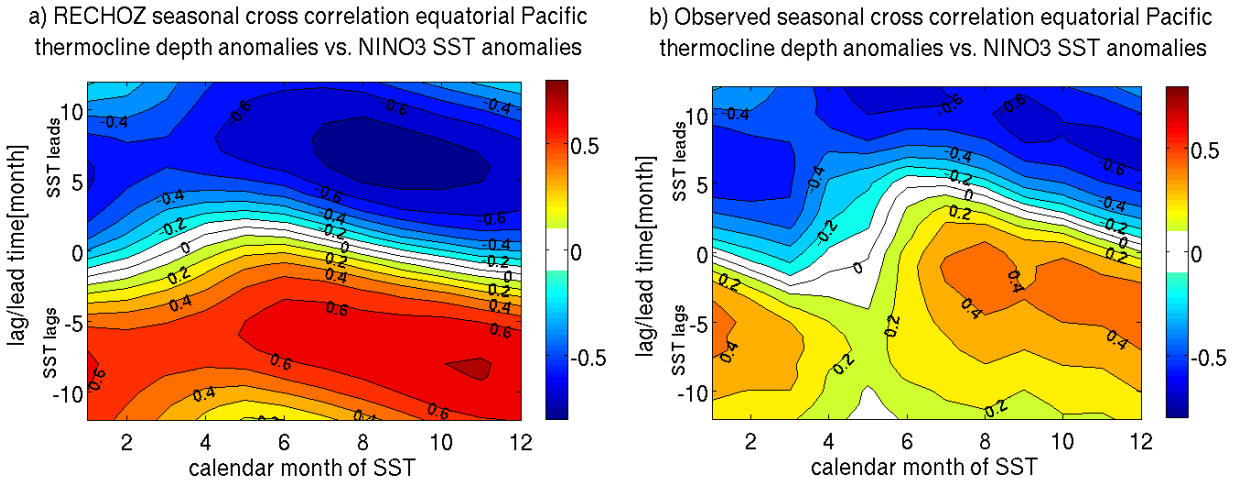

Figure 4.12: Seasonally resolved cross correlation between NINO3 SST anomalies and equatorial Pacific thermocline depth anomalies for (a) the RECHOZ model and (b) observations. Instead of observational thermocline depth data the thermocline depth data obtained from the forced MPI-OM experiment was used.

If one has a look at the relationship between the central Pacific zonal wind stress anomalies and the NINO3 SST anomalies, one can see that both are very strongly correlated (figure 4.13). The wind stress anomalies are slightly leading the SST anomalies by approximately one month.

For the central Pacific zonal wind stress anomalies and the equatorial thermocline depth anomalies one finds that both are strongly anticorrelated (figure 4.14). The cross correlation is strongest when the wind is leading the thermocline by approximately 7 months. That means a positive wind stress anomaly, i.e., weaker easterlies, leads to a negative thermocline

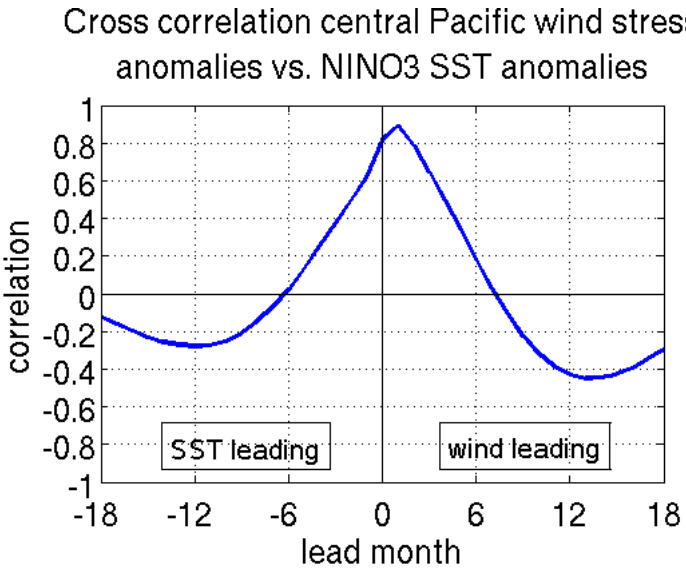

Figure 4.13: Cross correlation between the central Pacific zonal wind stress anomalies and the NINO3 SST anomalies for the RECHOZ CTRL run.

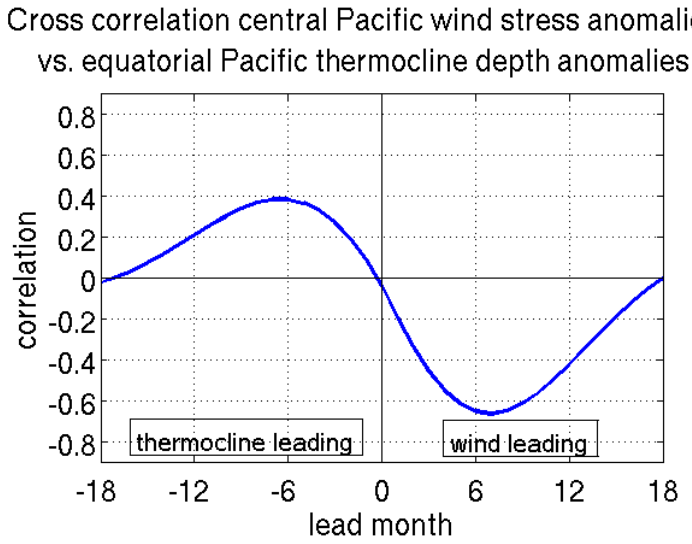

Figure 4.14: Cross correlation between the central Pacific zonal wind stress anomalies and the equatorial Pacific thermocline depth anomalies for the RECHOZ CTRL run.

depth anomaly, i.e., a flatter thermocline, and vice versa.

Interesting is also a look at the cross correlations between the SST anomalies in the NINO3 region in the tropical Pacific and the ATL3 region in the tropical Atlantic and the WIO region in the tropical Indian Ocean (figure 4.15). Between the NINO3 and the ATL3 SST

anomalies there is very little correlation as in the observations (figure 2.11) but also a comparably strong correlation when the thermocline is leading by approximately 7 - 8 months. For the WIO region the correlations are smaller than in the observations.

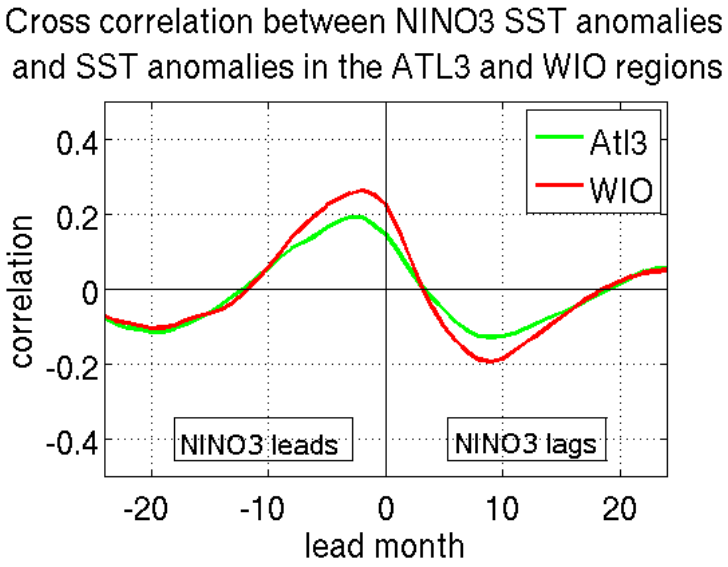

Figure 4.15: RECHOZ CTRL cross correlation between the NINO3 SST anomalies and the ATL3 SST anomalies (green) and the NINO3 SST anomalies and the WIO SST anomalies (red).

One of the advantages of using the simple recharge oscillator ocean model is the possibility to directly analyse the role of the different parameters of the model regarding the ENSO mechanisms and the influences of different feedbacks on this parameters. Therefore, first the resulting model parameters have to be estimated. This can be done by using a linear regression method to fit the parameters of the recharge oscillator model (equations 3.9 and 3.10) to the RECHOZ model output. The parameters resulting from this fit and the standard deviation of the residuals corresponding to the noise terms in the equations can be seen in table 4.1. The resulting parameters differ sligthly from the initial parameters (see table 3.1) but are still within the range of the observational parameter estimates by Burgers et al. (2005).

In conclusion, one can say that despite the very simplistic representaion of ENSO in the model, the RECHOZ model is able to simulate ENSO with very realistic statistical proper-

parameter	value
a_{11}	$-0.065 \pm 0.009 \frac{1}{month}$
a_{12}	$0.025 \pm 0.001 \frac{K}{month\,m}$
a_{21}	$-1.126 \pm 0.006 \frac{m}{K\,month}$
a_{22}	$-0.023 \pm 0.001 \frac{1}{month}$
$\sigma(s_1)$	$0.272 \frac{K}{month}$
$\sigma(s_2)$	$0.207 \frac{m}{month}$

Table 4.1: Resulting model parameters from the RECHOZ CTRL run with 95% confident intervals.

ties. The standard deviation, skewness, and kurtosis of the model's NINO3 SST anomalies agree very well with observations. Also the seasonality of the model's NINO3 SST anomalies can be reproduced by the model. The statistics of the equatorial Pacific thermocline depth anomalies differ slightly from observations, but one has to keep in mind the limited statistical significance of observed thermocline depth data due to the short time series. Thus, in summary, the RECHOZ model proved to be a very useful tool to analyse different aspects of ENSO.

4.2 Seasonality

The tendency of El Niño and La Niña events to peak at the end of the calendar year is one of the main features of ENSO (Rasmusson and Carpenter, 1982). Seasonal factors that could cause this phase locking of El Niño are, for example, atmospheric heating (Philander, 1983), zonal gradients of mean SST, shallow thermocline, strong zonal winds, high SST (Hirst, 1986), and strong upwelling (Battisti, 1988). But the exact physical mechanism

which causes ENSO events to peak at the end of the year is still a point of discussion. Tziperman et al. (1998) suggested that a seasonal amplification of Kelvin and Rossby waves by wind stress anomalies in the central Pacific basin could explain this seasonal evolution of El Niño and La Niña events. In the previous section it was shown that the RECHOZ model is able to reproduce the seasonal cycle of NINO3 SST anomalies. However, not only the SST anomalies follow a seasonal cycle but also the thermocline depth, wind stress, and heat flux anomalies (figure 4.16).

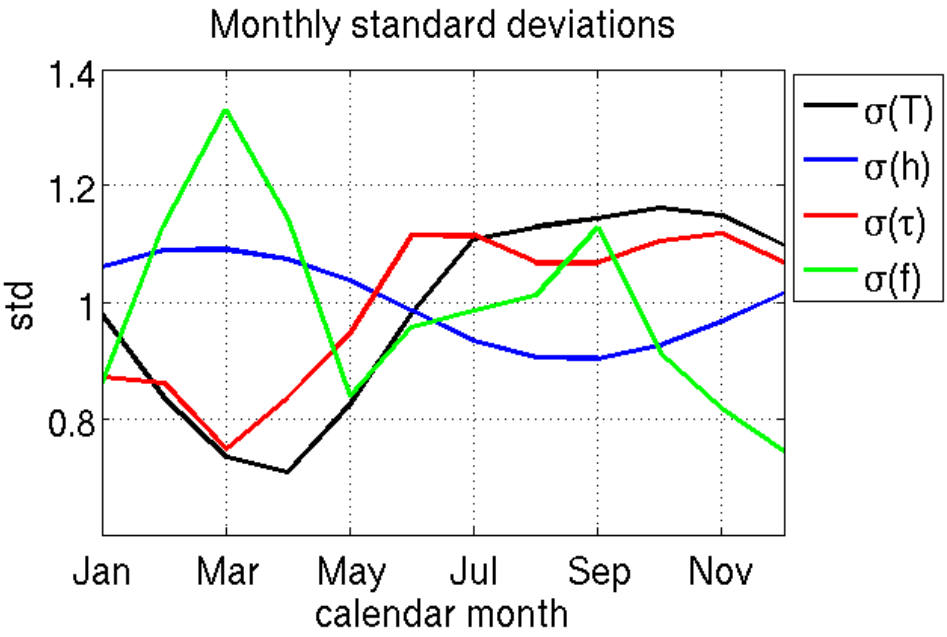

Figure 4.16: Standard deviation of monthly mean NINO3 SST anomalies (black), equatorial Pacific thermocline depth anomalies (blue), central Pacific zonal wind stress anomalies (red), and NINO3 heat flux anomalies (green) for each calendar month for the RECHOZ model. The monthly values are divided by the total standard deviation.

The equatorial Pacific thermocline depth anomalies have an opposite evolution compared to the NINO3 SST anomalies with strongest variability in spring when the SST variability is weak, and weak variability in summer and autumn when the SST variability is strong. The central Pacific zonal wind stress anomalies follow an evolution similar to the NINO3 SST anomalies, with weak variability in spring and strong variability in summer and autumn. In contrast, the NINO3 heat flux anomalies show a different evolution, with two peaks in the

seasonal cycle, one around March and a second around September.

To better understand the seasonality of the RECHOZ model, the seasonal parameter values as they result from the model statistics can be analysed. Thus, for each calendar month a separate parameter fit to the RECHOZ simulation output was performed by using a 3 month moving data block. In figure 4.17 the results of this seasonal parameter fits are displayed.

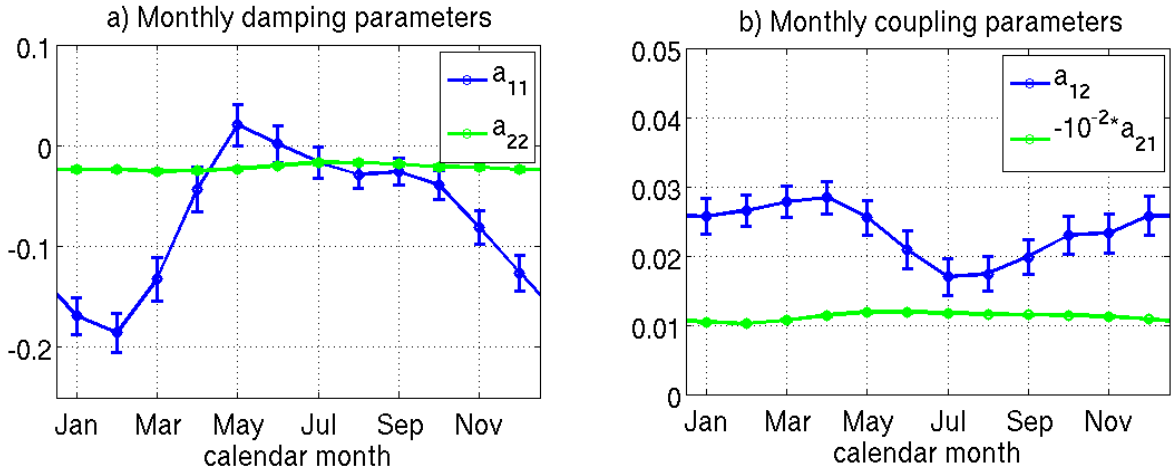

Figure 4.17: (a) Seasonality of the fitted damping parameters a_{11} and a_{22} of the RECHOZ model with 95% confident intervals. (b) Seasonality of the fitted coupling parameters a_{12} and a_{21} of the RECHOZ model with 95% confident intervals.

It can be seen that while the damping of the temperature a_{11} shows a strong seasonality, the damping of the thermocline a_{22} shows almost no seasonal cycle. Also the coupling parameter a_{21} shows only little seasonality while the coupling parameter a_{12} shows a stronger seasonal cycle. Figure 4.18 shows the standard deviations of the residuals resulting from the parameter fits, which correspond to the noise terms s_1 and s_2 in equations [3.9 and 3.10]. In summary, the most significant seasonality is found in the damping of the temperature a_{11}. This seasonality in the RECHOZ model can only be caused by the atmospheric forcings τ and f.

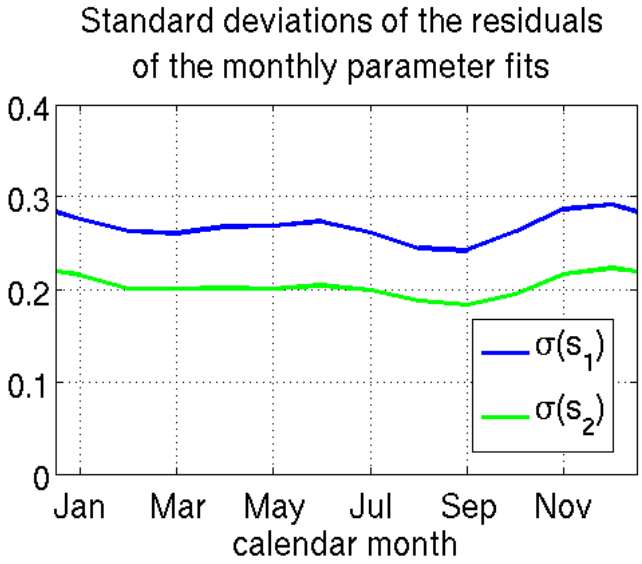

Figure 4.18: Standard deviations of the residuals resulting from the seasonal parameter fits $\sigma(s_1)$ (blue) and $\sigma(s_2)$ (green).

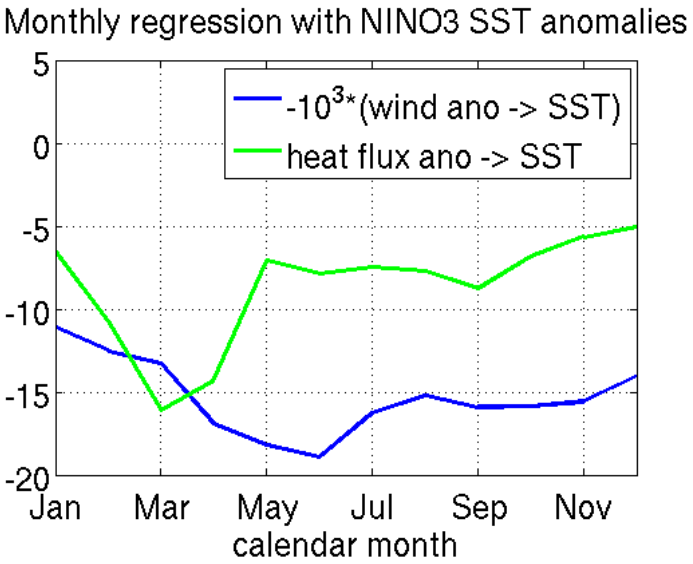

Figure 4.19: Regression of central Pacific zonal wind stress anomalies and NINO3 SST anomalies (blue) and of NINO3 heat flux anomalies and NINO3 SST anomalies (green).

The monthly regressions of the forcings to the NINO3 SST anomalies (figure 4.19) show that the coupling of the zonal wind stress is strongest from April to July when the damping a_{11} is weakest, and the damping a_{11} is strongest from November to March when the coupling to the zonal wind stress is relatively weak. The strong coupling to the heat flux anomalies in

March and April has little influence on the damping of the SST. This is in agreement with Galanti and Tziperman (2000), who calculated the ocean-atmosphere coupling strength in a delayed-oscillator model.

The seasonal varying parameters were included in the REOSC-MC model and the model was again integrated for 10000 years. In figure 4.20 again the seasonal dependence of NINO3 SST anomalies is displayed. With the seasonal varying parameters included the REOSC-MC model is able to produce seasonality similar to the RECHOZ model. A large part of this seasonal cycle can be explained by the seasonality of the damping parameter a_{11} only.

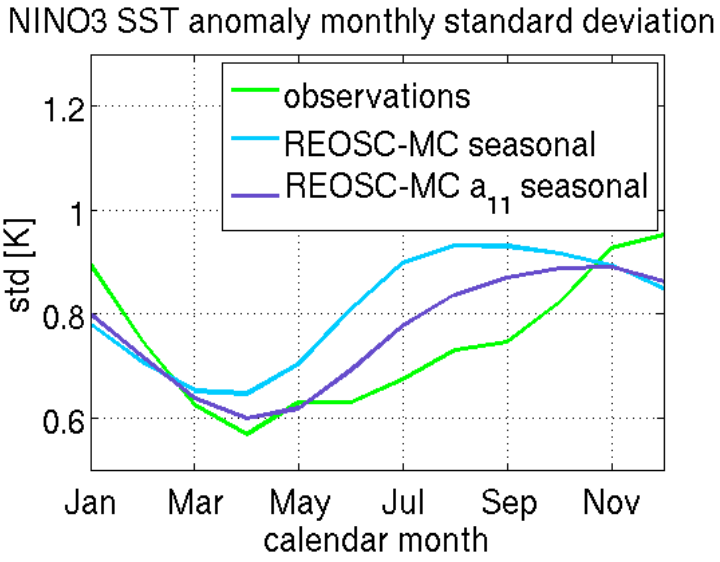

Figure 4.20: Standard deviation of monthly mean NINO3 SST anomalies for each calendar month for observations (green), the REOSC-MC model with seasonal varying parameters (cyan) and the REOSC-MC model with only a_{11} varying (purple).

So, a seasonal variation in the sensitivity of the atmosphere to the SST anomalies is the origin of the seasonal cycle in the strength of the ENSO amplitudes. While in spring and summer there is a reduced damping of the SST due to a stronger coupling of the zonal wind stress to the SST, there is increased damping of the SST in winter and early spring due to a weaker coupling of zonal wind stress.

4.3 Atmospheric nonlinearity

Another interesting feature of ENSO is the fact that the amplitude of El Niño events is significantly larger than the amplitude of La Niña events (Burgers and Stephenson, 1999). What is causing this asymmetric aspect of ENSO is still an open question, but most studies addressing this aspect were focusing on nonlinear oceanic processes (Jin et al., 2003; An and Jin, 2004; Su et al., 2010). Jin et al. (2003) found that during the development phase of El Niño, easterlies in the eastern Pacific intensify the vertical advection of anomalous warm water, which leads to an acceleration of surface warming, while during the transition to La Niña, westerlies in the eastern Pacific reduce the upwelling, which leads to a slowdown of the surface cooling.

Another alternative is that nonlinear processes of the tropical atmosphere could cause the ENSO amplitude asymmetry (Hoerling et al., 1997; Kang and Kug, 2002). Kang and Kug (2002) found indications from observations that the weaker SST anomalies during La Niña events compared to El Niño events may be caused by a westward shift of wind stress anomalies by 10° to 15° which is related to a westward shift of convection anomalies. Philip and van Oldenborgh (2009) used an initially linear intermediate complexity model of the equatorial Pacific in which they introduced extra terms in the atmospheric component. Thereby they showed that the nonlinear response of mean wind stress to SST in the ENSO region has a dominant influence on the nonlinearities in SST in the ENSO cycle.

Although in the RECHOZ model the ocean dynamics are only parameterized and by construction linear, it is able to simulate the skewness and the kurtosis of the NINO3 SST anomalies. So the origin of the nonlinearity of the ENSO cycle in the RECHOZ model has to lie in the atmospheric components. In the model the tropical Pacific Ocean is coupled to the atmosphere via the NINO3 net heat flux anomalies and the central Pacific zonal wind stress anomalies. Figure 4.21 shows the composites of the net heat flux anomalies for El Niño and La Niña events.

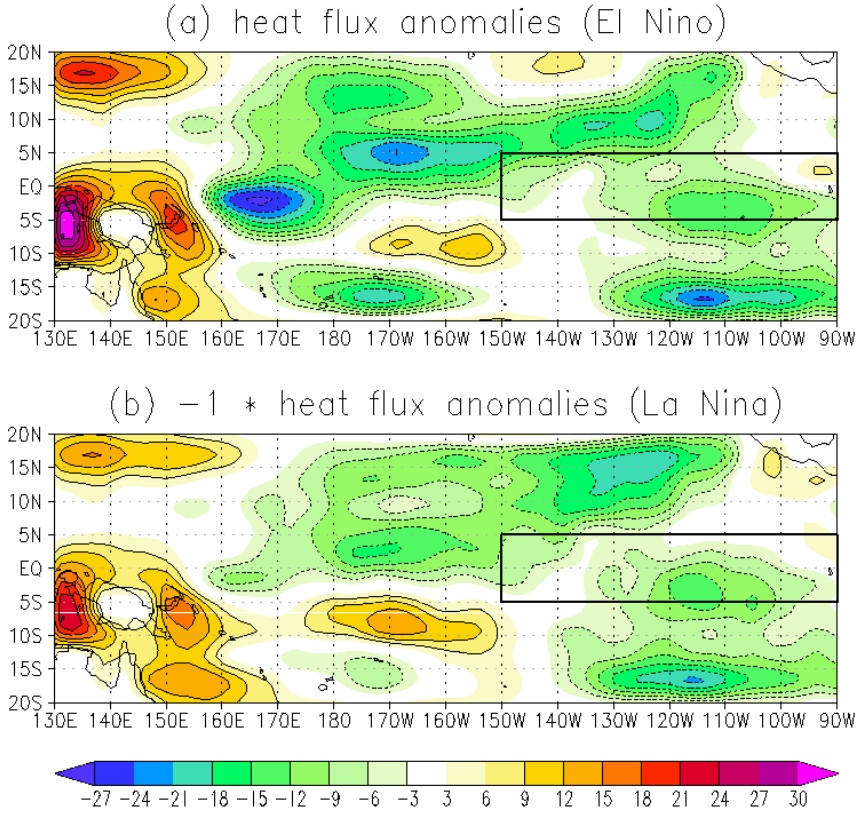

Figure 4.21: (a) Model composite mean values of net heat flux anomalies for all El Niño years ($T(December) > \sigma(T)$) averaged from December to April of the following year. The black box indicates the NINO3 area over which the heat flux anomalies are averaged. (b) The same as (a) but for all La Niña years ($T(December) < -\sigma(T)$) multiplied by -1. Units are in W/m^2.

Especially in the NINO3 region over which the heat flux anomalies are averaged the pattern of the heat flux anomalies look very similar for El Niño and La Niña years. So, the heat flux anomalies cannot be responsible for the nonlinearity of the ENSO amplitudes. Figure 4.22 shows the composites of the zonal wind stress anomalies for El Niño and La Niña events. During the El Niño events, as well as during the La Niña events, strong wind stress anomalies are found in the central Pacific, the area over which the zonal wind stress anomalies are averaged. However, while during El Niño events the area of maximum wind stress spans from 170°E to 165°W, the area of maximum wind stress during La Niña events spans over a much smaller area and is centered more to the west. This is in good agreement with the

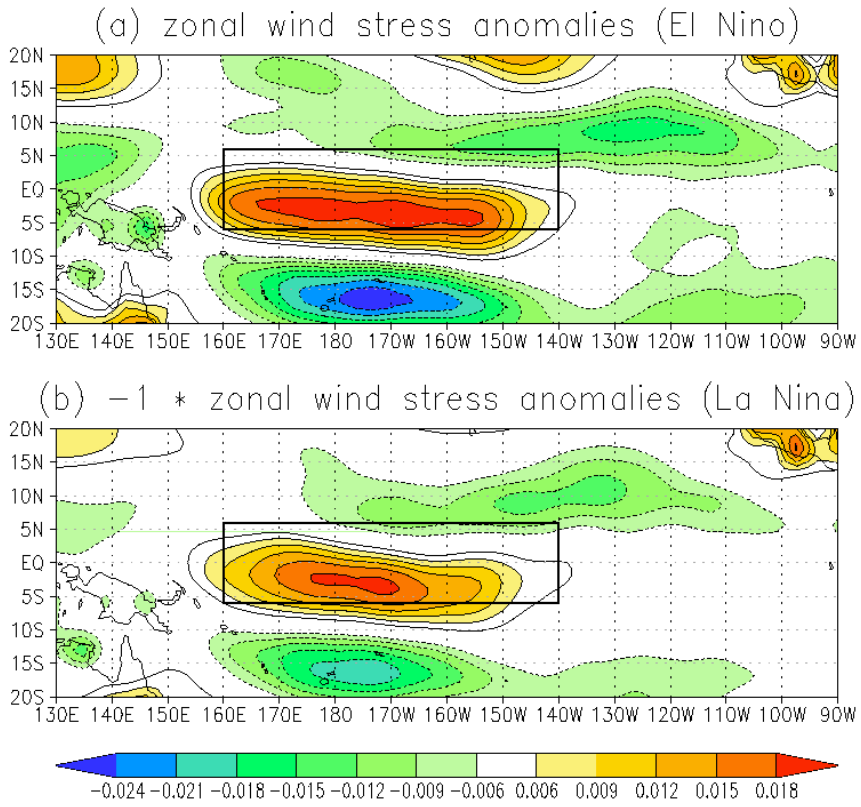

Figure 4.22: (a) Model composite mean values of zonal wind stress anomalies for all El Niño years ($T(december) > \sigma(T)$) averaged from December to April of the following year. The black box indicates the area over which the zonal wind stress anomalies are averaged. (b) The same as (a) but for all La Niña years ($T(december) < -\sigma(T)$) multiplied by -1. Units are in Pa.

results of Kang and Kug (2002), who showed that the relatively weak SST anomalies during La Niña events compared to those of El Niño events are related to a westward shift of the zonal wind stress anomalies. This shift in the wind stress pattern leads to smaller values of the area averaged zonal wind stress anomalies during La Niña events. The shift cannot be due to a shift in the SST pattern because the pattern of the first EOF of tropical Pacific SST anomalies is used as a fixed pattern in the model. So, the shift in the zonal wind stress pattern has to be caused by different convection patterns for warm and cold SST anomalies. The different relationships between NINO3 heat flux anomalies and NINO3 SST anomalies and between central Pacific zonal wind stress anomalies and NINO3 SST anomalies can also

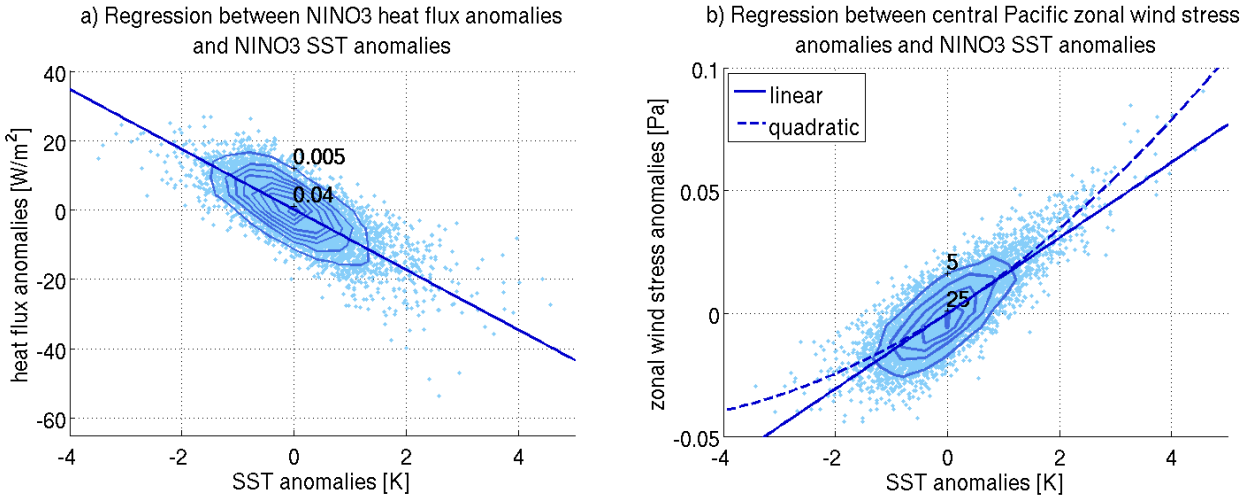

Figure 4.23: (a) Scatter plot of NINO3 heat flux anomalies and NINO3 SST anomalies with linear regression line. The contour interval is $0.005\,K/(W/m^2)$. (b) Scatter plot of central Pacific zonal wind stress anomalies and NINO3 SST anomalies with linear regression line (solid) and the quadratic regression curve (dashed). The contour interval is $5.0\,K/Pa$.

be seen if one has a look at the distribution of heat flux and wind stress anomalies over SST anomalies (figure 4.23). For the heat flux anomalies a linear regression fits very well to the data, pointing out the linear relationship between the NINO3 heat flux anomalies and the NINO3 SST anomalies (figure 4.23 (a)). For the zonal wind stress anomalies a linear regression does not fit to the data especially for large SST anomalies (figure 4.23 (b)). For comparison also the regression curve resulting from a quadratic fit (dashed line) is shown here. Especially for the large SST anomalies the quadratic fit is more suitable.

To test whether this quadratic relationship between the central Pacific zonal wind stress anomalies and the NINO3 SST anomalies could cause the nonlinearities in the RECHOZ model, this quadratic relationship was included in the REOSC-MC model (replacing the linear relationship) and the model was integrated for 1000 years. Figure 4.24 shows the histogram of monthly mean NINO3 SST anomalies resulting from this simulation. With replacing the linear with a nonlinear relationship between the central Pacific zonal wind stress anomalies and the NINO3 SST anomalies, the REOSC-MC model is able to simulate the skewness and kurtosis of ENSO.

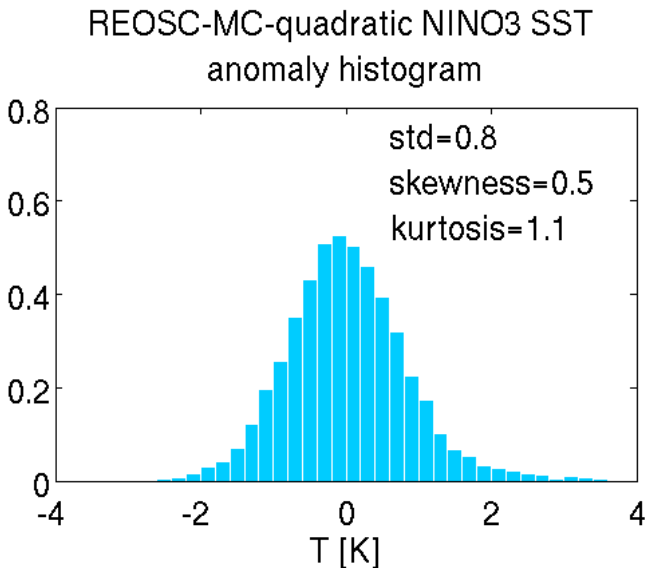

Figure 4.24: Histogram of monthly mean NINO3 SST anomalies for the REOSC-MC model with the quadratic relationship included.

The results of this section show that atmospheric nonlinearities have an important influence on the nonlinearity of ENSO. A nonlinear response of the zonal wind stress to equal-strength but opposite sign SST anomalies can explain the asymmetry between eastern Pacific SST anomalies during El Niño and La Niña events.

4.4 Influence of the tropical Pacific mean state on ENSO

Because of its large socio-economic impacts, the behaviour of ENSO in a changing climate is also of great interest. To analyse the influence of increasing greenhouse gases on the ENSO properties one depends strongly on global coupled atmosphere-ocean GCMs. Most state-of-the-art climate models are able to simulate ENSO-like oscillations in the tropical Pacific. For the current climate the properties of the modeled time series are comparable with observations. However, many of these models still show biases in the simulated background climate and in the ENSO variability.

Recently, many studies analysed long-term simulations of coupled ocean-atmosphere GCMs

using different climate change scenarios to determine the response of the tropical Pacific to global warming. Most of the early studies found an El Niño-like response of the tropical Pacific (Knutson and Manabe, 1995, 1998; Meehl and Washington, 1996; Yu and Boer, 2002; Vavrus and Liu, 2002; Boer and Yu, 2003). Also in the IPCC AR4 report a weak shift towards 'El Niño-like' conditions was found for the multi-model mean (Meehl et al., 2007) (see also figure 1.1).

In contrast, already Cane et al. (1997) pointed out that the El Niño-like behaviour simulated by most GCMs is not in agreement with the observed development of the 20th century, where an increase in the zonal gradient across the equatorial Pacific can be found. Collins and CMIP Modeling Groups (2005) again analysed 20 atmosphere-ocean GCMs submitted to the coupled model inter-comparison project (CMIP). In contrast to the previous model studies they linked the realism of the simulation of present day ENSO variability in the models to their patterns of future climate change. They found that the most likely scenario (p=0.59) in a model-skill-weighted histogram of the CMIP models is no trend towards either mean El Niño-like or La Niña-like conditions. However, there is also a small probability (p=0.16) for a change to El Niño-like conditions in the 1% per year CO_2 increase scenario. More recent studies suggest that there is an enhanced equatorial warming rather than an El Niño-like response due to global warming (Liu et al., 2005; Vecchi et al., 2008; DiNezio et al., 2009). Different mechanisms have been suggested which determine the response of the tropical Pacific to global warming. For example Clement et al. (1996) showed that changes in ocean vertical heat transport could lead to an increase in the zonal SST gradient. Changes in evaporation and cloud feedbacks could lead to a reduction of the zonal SST gradient (Knutson and Manabe, 1995). Recently, Vecchi and Soden (2007) found a weakening of the tropical atmospheric circulation due to global warming as a robust feature in 22 state-of-the-art climate models. Global thermodynamic constraints on the response of the hydrological cycle to global warming lead to a slowing down of the Walker circulation (Held and Soden, 2006). However, there is still large uncertainty in which way the mean state of the tropical

Pacific will change under global warming.

Although there is no consensus yet in which way the mean state of the tropical Pacific will change under global warming, it is clear that changes in the mean state will have an influence on the properties of ENSO. This would also lead to a reduction of the zonal SST gradient. However, it is not clear in which way changes in the mean state alter the ENSO cycle. Although most of the models analysed for the IPCC report simulate an El Niño-like warming pattern, they do not agree in the simulated future strength of ENSO (figure 1.1). Half of the models simulating an El Niño-like global warming pattern simulate an increase in ENSO variability.

Different studies have focused on the relationship between the mean state of the tropical Pacific and the properties of ENSO. Fedorov and Philander (2001) proposed, in a theoretical study, that El Niño frequency and growth rate are related to the mean wind and mean thermocline depth in the tropical Pacific. They distinguished between two modes of oscillation. One is the so-called SST-mode resulting from local SST-wind interactions in the central-east Pacific with a surface east to west propagation of SST anomalies and low amplitude events with a period of 2 - 3 years. The second is the so-called thermocline mode which results from remote wind-thermocline interactions involving the west Pacific with a subsurface west to east propagation and large amplitude events with a period of 4 - 5 years. The thermocline mode requires weaker trade winds and a deeper thermocline compared to the SST mode. The SST mode was observed for the period before the 1976 climate shift while the thermocline mode was evidenced in observations for the post-1976 period with the extreme El Niño events in 1982/83 and 1997/98. Wang and An (2001) attributed the changes in ENSO properties after the mid-1970s to changes in the mean wind. More recently, Guilyardi (2006) analysed the relationship between the mean state and ENSO in 23 coupled ocean-atmosphere models including the IPCC AR4 models under the aspect of global warming, and found no clear relationship between mean NINO3 SST and El Niño characteristics. Thus, at the current state of understanding, no clear statement can be made on how global warming will influence

the tropical Pacific climate system and ENSO. Thus, further investigation is necessary.

To study the influence of changes in the mean state on ENSO through atmospheric feedbacks different sensitivity experiments were performed. In two experiments the mean SST in the tropical Pacific was cooled by 1K (TP-1K) and warmed by 1K (TP+1K) respectively. This was done by subtracting or adding 1K to the prescribed background climatology in the tropical Pacific. Thus, these changes in the mean SST only influence the atmospheric quantities. The ocean can only be influenced via atmospheric feedbacks. Because a uniform cooling or warming of the tropical Pacific is no likely scenario, an additional experiment was performed in which an El Niño-like warming pattern was added to the mean SST in the tropical Pacific (ENPAT). Therefore, the pattern of the first EOF of observed tropical Pacific SST (see figure 2.8) was added to the presribed SST climatology. Again, these changes in the mean SST are only visible for the atmospheric GCM and not for the ocean model. An overview of the sensitivity experiments performed to study the influence of different mean states on the atmospheric feedbacks in the ENSO cycle can be seen in table 4.2.

In the following first the sensitivity experiments with a uniform cooling (TP-1K) or a uniform warming (TP+1K) of the tropical Pacific are analysed. In figure 4.25 the changes in

Exp. ID	**Years**	**Modifications with respect to the CTRL experiment**
CTRL	500	Control run of the RECHOZ model
TP-1K	500	Experiment with the mean SST in the tropical Pacific cooled by 1K
TP+1K	500	Experiment with the mean SST in the tropical Pacific warmed by 1K
ENPAT	500	Experiment with an El Niño-like warming pattern in the tropical Pacific.

Table 4.2: RECHOZ model sensitivity experiments used to study the influences of the tropical Pacific mean state on ENSO through atmospheric feedbacks.

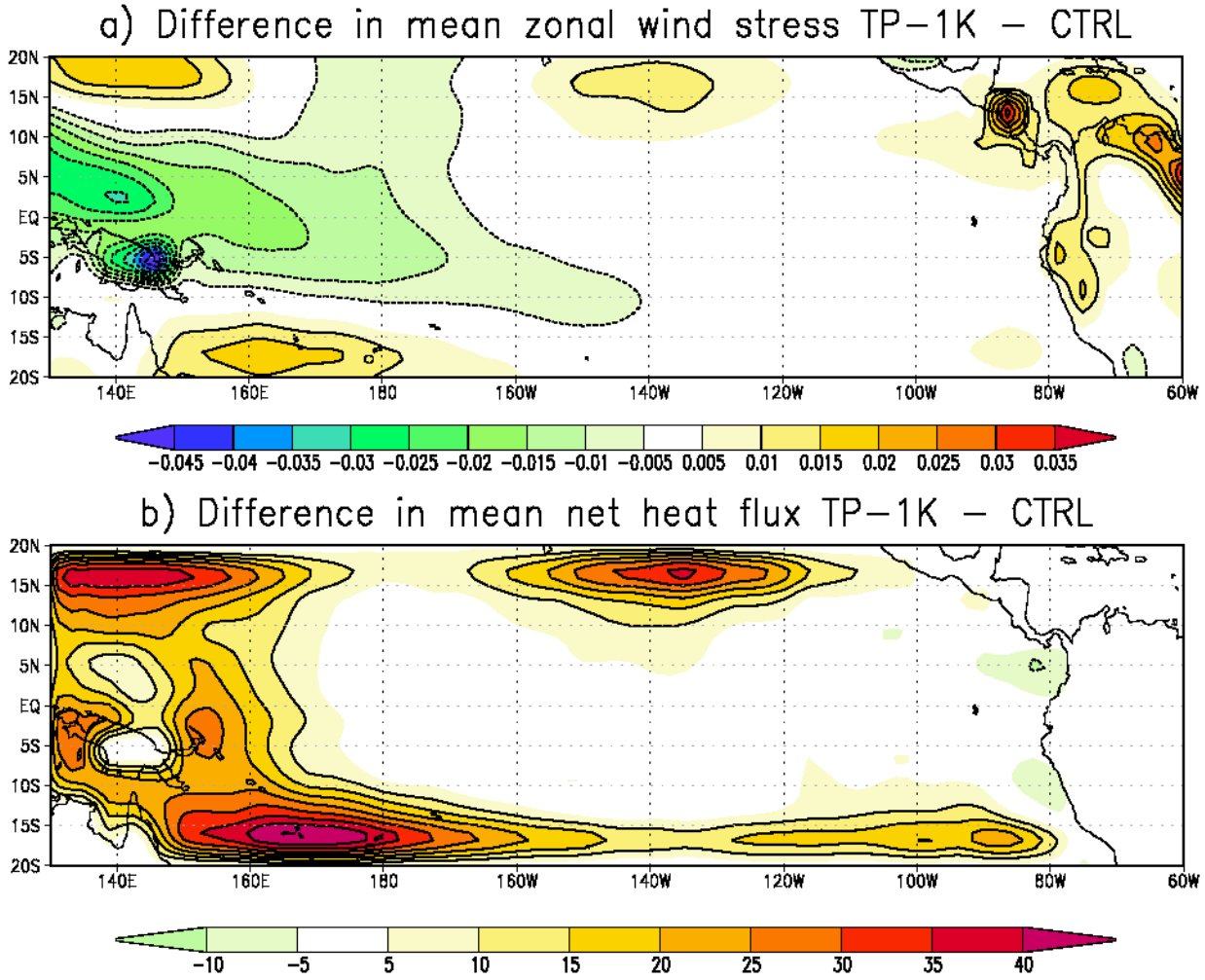

Figure 4.25: Differences in a) mean zonal wind stress [Pa] and b) mean net heat flux [W/m^2] between the TP-1K experiment and the CTRL run.

mean zonal wind stress and mean net heat flux in the TP-1K experiment compared to the CTRL run are displayed. The easterly zonal wind stress in strongly increased in the western and central tropical Pacific. This could be due to a stronger atmospheric circulation, but especially the large increase in the far western Pacific could be an artificial effect because the SST is only reduced in the tropical Pacific. The net heat fluxes in the western Pacific and around 15 ° N and 15 ° S is strongly increased which could be partly due to changes in the cloud feedbacks and partly again an artificial effect.

In figure 4.26 the differences in mean zonal wind stress and mean net heat flux between the

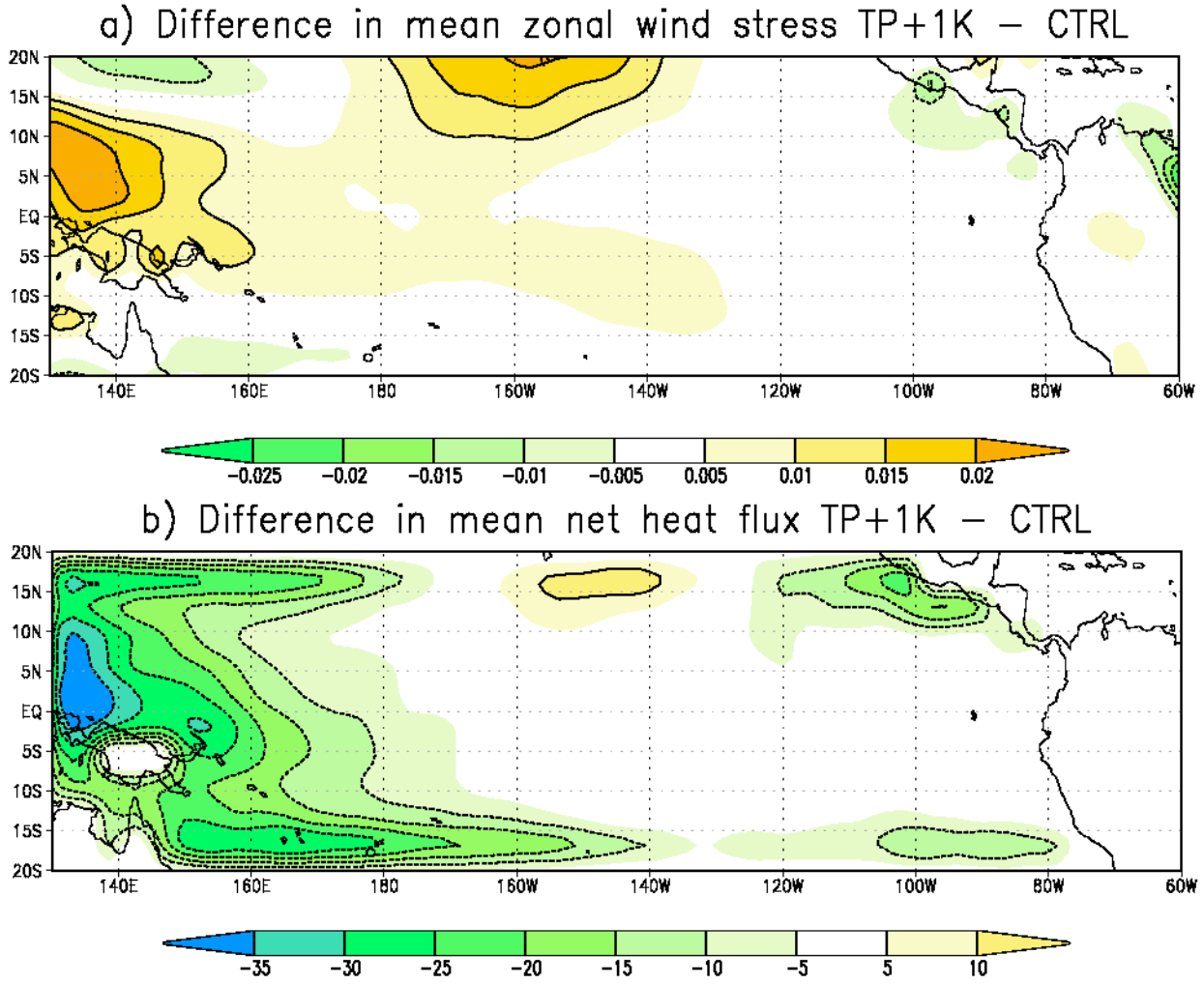

Figure 4.26: Differences in a) mean zonal wind stress [Pa] and b) mean net heat flux [W/m^2] between the TP+1K experiment and the CTRL run.

TP+1K and the CTRL experiment are shown. In the western and central Pacific the easterly zonal wind stress is strongly reduced. Again this could be due to a reduced atmospheric circulation and especially in the far western Pacific also artificial. For the net heat flux in the western Pacific and around 15 ° N and 15 ° S the mean net heat flux is reduced. Again this might be due to changes in the cloud feedbacks in agreement with (DiNezio et al., 2009) and partly artificial. In both exepriments no changes of the mean net heat flux are found in the NINO3 region.

In the following again only the anomalies of the SST, thermocline depth, zonal wind stress

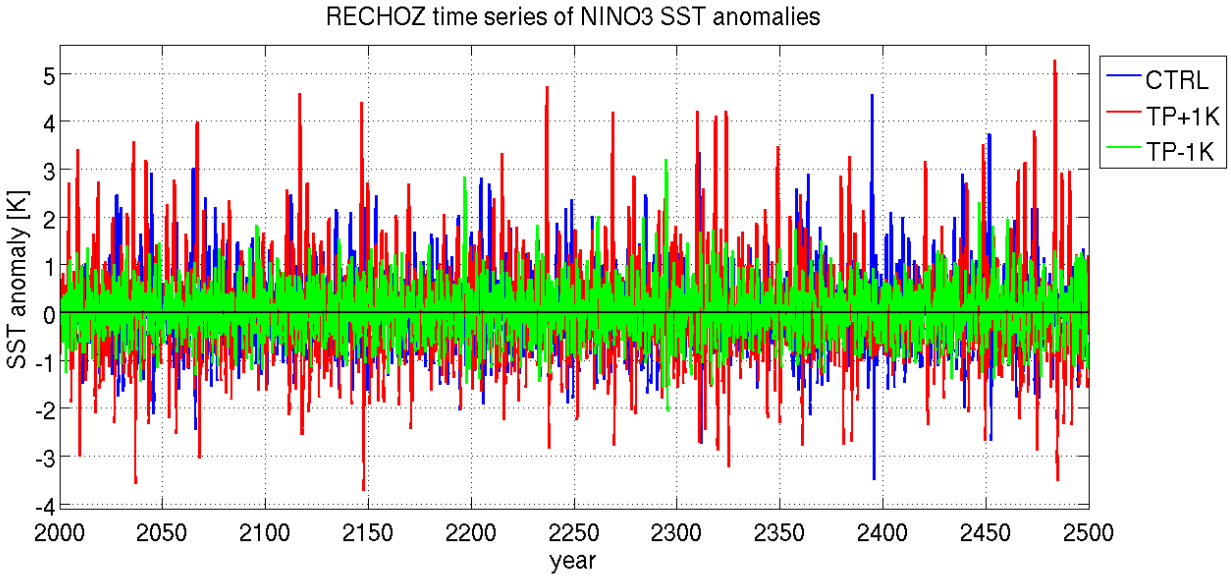

Figure 4.27: Time series of monthly mean NINO3 SST anomalies for the RECHOZ TP-1K (green) and TP+1K (red) experiments compared to observations (blue).

and net heat flux will be analysed. Figure 4.27 shows the time series of NINO3 SST anomalies and equatorial Pacific thermocline depth anomalies for the last 50 years of the TP+1K experiment. The warming of the tropical Pacific mean SST leads to an increase in ENSO variability. Accordingly the variability is reduced when the mean SST is cooled. The standard deviation of NINO3 SST anomalies changes from $\sigma(T_{CTRL}) = 0.8\,K$ in the control run to $\sigma(T_{TP-1K}) = 0.5\,K$ in the run with the colder mean state and $\sigma(T_{TP+1K}) = 1.1\,K$ in the run with a warmer mean state, which corresponds to a decrease of 38% and an increase of 38%. For the TP-1K experiment changes in the thermocline depth variability are of similar magnitude ($\sigma(h_{TP-1K}) = 3.6\,m$ compared to $\sigma(h_{CTRL}) = 5.4\,m$, -33%), but for the TP+1K run there is a much larger increase in thermocline depth variability ($\sigma(h_{TP+1K}) = 9.4\,m$, +74%).

The changes in NINO3 SST variability can also be seen in the spectrum of monthly mean NINO3 SST anomalies (figure 4.28). Additional to the changes in the variability of the NINO3 SST anomalies, the peak of spectrum is shifted towards shorter periods in the TP-1K

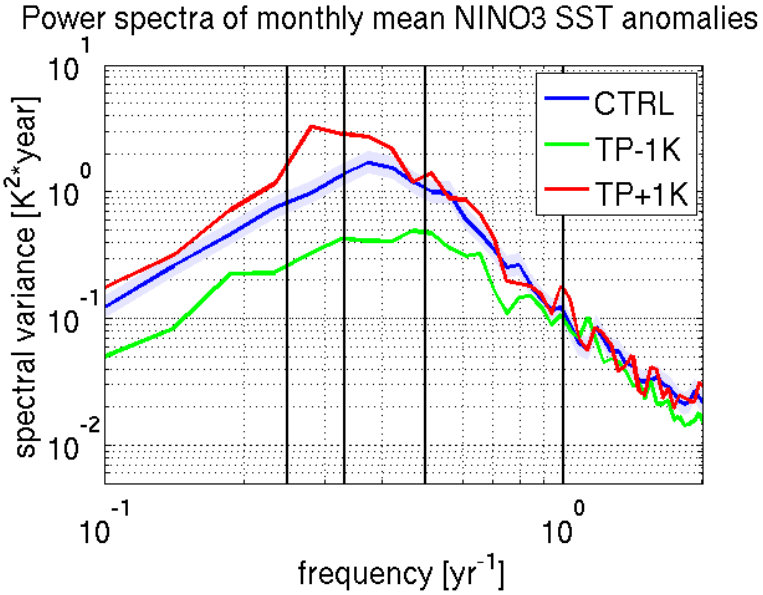

Figure 4.28: Spectra of monthly mean NINO3 SST anomalies for the CTRL run (blue), the TP-1K run (green), and the TP+1K run (red). The violet shading indicates the 80% confidence level of the CTRL run spectrum.

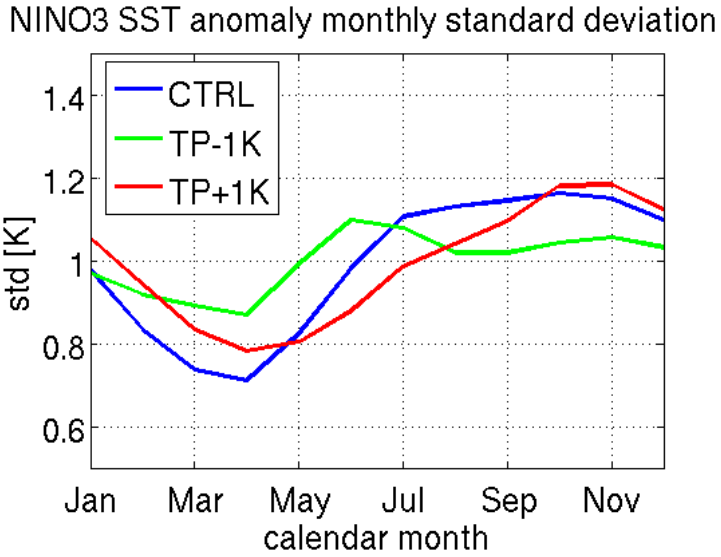

Figure 4.29: Standard deviation of monthly mean NINO3 SST anomalies for each calendar month for the TP-1K experiment (green) and the TP+1K experiment (red) compared to the CTRL experiment (blue). The monthly standard deviations are devided by the total standard deviation of each experiments NINO3 SST anomalies.

Experiment and towards longer periods in the TP+1K experiment.

Also the seasonality of ENSO is influenced by changes in the mean SST (figure 4.29). A colder mean SST leads to a strong reduction of the seasonal cycle, but also in the experiment with warmer mean SST the seasonal cycle is slightly reduced and shifted by approximately one month compared to the control run.

Although there are large changes in the SST variability, the skewness of NINO3 SST anomalies does not change when the mean state changes (figure 4.30). Only the kurtosis of NINO3 SST anomalies is reduced from $\gamma_2(T_{CTRL}) = 1.9$ in the control run to $\gamma_2(T_{TP+1K}) = 1.5$ in the experiment with the warmer mean SST and to $\gamma_2(T_{TP-1K}) = 1.0$ in the experiment with the colder mean SST.

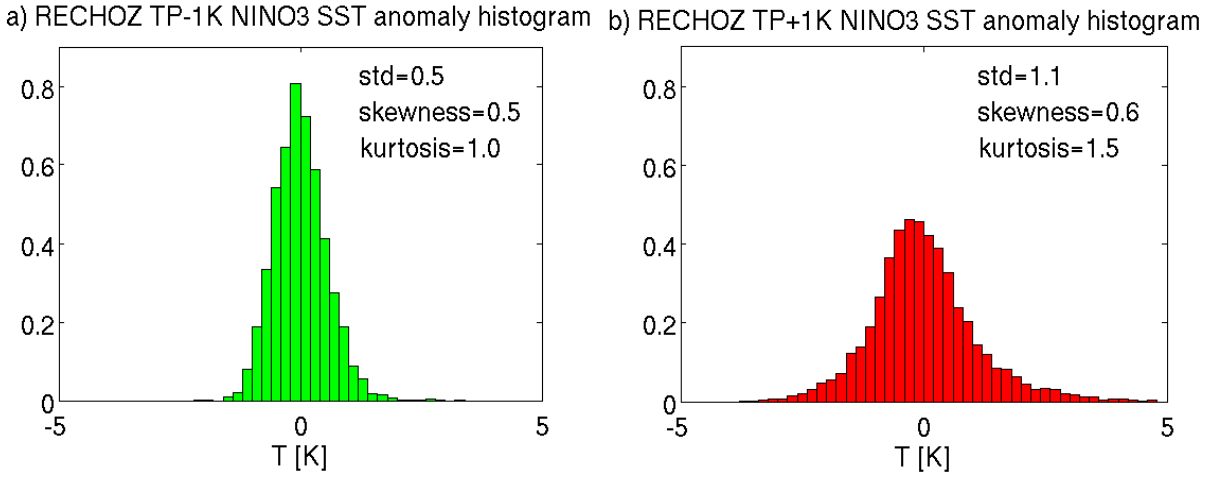

Figure 4.30: Histograms of monthly mean NINO3 SST anomaliess for (a) the TP-1K run and (b) the TP+1K run.

The cross correlation between the equatorial Pacific thermocline depth anomalies and the NINO3 SST anomalies shows only little changes when the mean SST changes (figure 4.31). The values of the maximum correlation are slightly reduced in both mean state experiments. In the TP-1K experiment, the maximum correlations are found one month earlier than in the control experiment, and in the TP+1K experiment, one month later in accordance with the changed periods of ENSO.

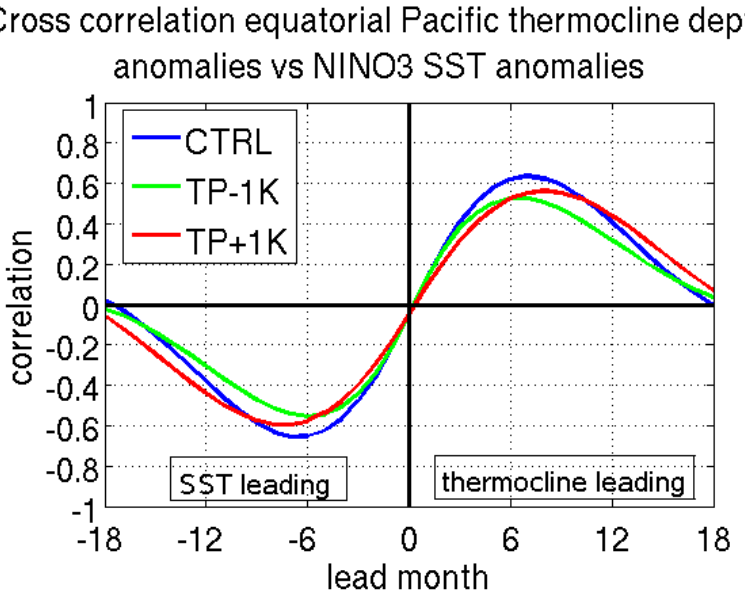

Figure 4.31: Cross correlation between the equatorial Pacific thermocline depth anomalies and the NINO3 SST anomalies for the TP-1K experiment (green) and the TP+1K (red) experiment compared to the control run (blue).

The origin of the changes in SST and thermocline depth variability, ENSO frequency and seasonality, and the relationships between SST and thermocline depth anomalies has to lie in the atmospheric feedbacks. Changes in the mean SST can only influence the NINO3 SST anomalies and the equatorial Pacific thermocline depth anomalies via the NINO3 heat flux anomalies and the central Pacific zonal wind stress anomalies. Computing the regression coefficients between the central Pacific zonal wind stress and the NINO3 SST anomalies and between the NINO3 net heat flux anomalies and the NINO3 SST anomalies shows that the annual mean coupling between the atmosphere and the ocean does not change. The regression between the zonal wind stress and the SST anomalies $r_{T\tau}$ does not change in both experiments compared to the control run and also the regression between the heat flux and the SST anomalies r_{Tf} changes only very little. Thus, changes in the variability or the response of NINO3 heat flux anomalies and central Pacific zonal wind stress anomalies to NINO3 SST anomalies have to be responsible for the changes in the ENSO variability. In figure 4.32 the composites of NINO3 heat flux anomalies are displayed for all ENSO extreme

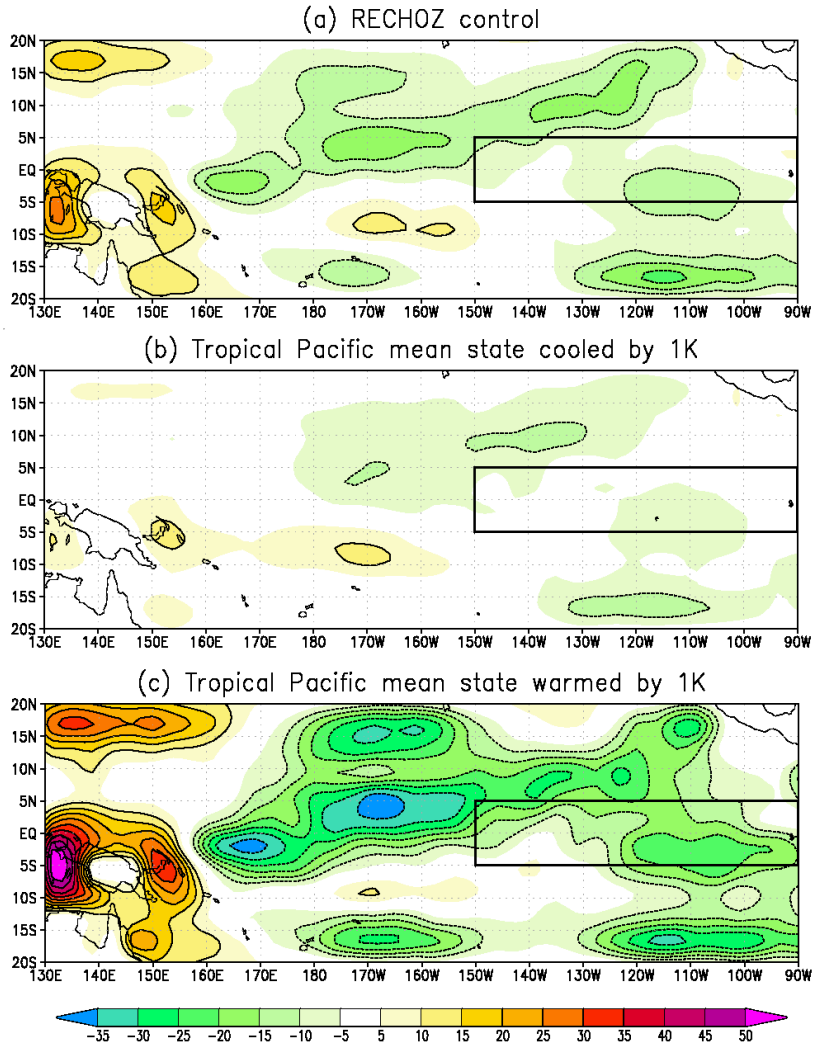

Figure 4.32: Model composite mean values of the net heat flux anomalies for all ENSO extreme years ($|T(December)| > \sigma(T)$) averaged from December to April of the following year for a) the CTRL run, b) the TP-1K run, and c) the TP+1K run. For La Niña events the net heat flux anomalies are considered with reversed sign in the composites mean. Units are in W/m^2. The black box indicates the NINO3 region over which the heat flux anomalies are averaged.

years for both experiments with changed mean SST compared to the control experiment. It can be seen that the already small heat flux anomalies in the control experiment almost vanish when the mean SST of the tropical Pacific is cooled. In contrast they are strongly increased when the mean SST is warmed. Also the variability of the NINO3 heat flux anomalies is reduced (increased) for the TP-1K (TP+1K) experiment. The standard devia-

tion of the NINO3 heat flux anomalies is reduced from $\sigma(f_{CTRL}) = 8.4\,W/m^2$ in the control run to $\sigma(f_{TP-1K}) = 6.7\,W/m^2$ in the TP-1K run. The standard deviation is increased to $\sigma(f_{TP+1K}) = 11.2\,W/m^2$ in the TP+1K run.

The same is true for the zonal wind stress anomalies. The composites of zonal wind stress anomalies for all ENSO extreme years show only very weak wind stress anomalies when

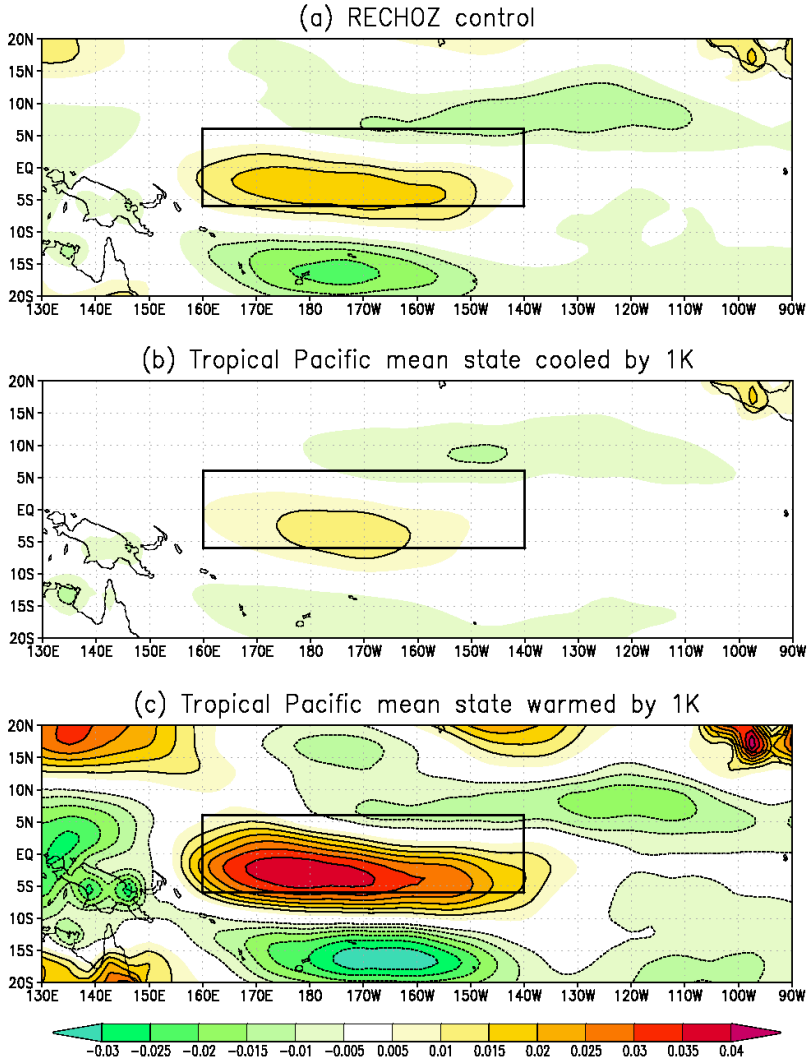

Figure 4.33: Model composite mean values of the zonal wind stress anomalies for all ENSO extreme years ($|T(December)| > \sigma(T)$) averaged from December to April of the following year for a) the CTRL run, b) the TP-1K run, and c) the TP+1K run. For La Niña events the net heat flux anomalies are considered with reversed sign in the composites mean. Units are in Pa. The black box indicates the region over which the wind stress anomalies are averaged.

the mean SST is cooled (figure 4.33 (b)). Again much stronger anomalies are found when the mean state is warmed (figure 4.33 (c)). Also the variability of the central Pacific zonal wind stress anomalies is reduced (increased) for the TP-1K (TP+1K) experiment. The standard deviation of zonal wind stress anomalies is reduced due to a colder mean SST from $\sigma(\tau_{CTRL}) = 0.015\,Pa$ in the control run to $\sigma(\tau_{TP-1K}) = 0.012\,Pa$. Again the standard deviation increases with a warmer mean state ($\sigma(\tau_{TP+1K}) = 0.019\,Pa$). However, the decrease (increase) in the standard deviations of NINO3 heat flux anomalies (-20%/+33%) and central Pacific zonal wind stress anomalies (-20%/+27%) is smaller than for the NINO3 SST anomalies (-38%/+38%) and for the equatorial Pacific thermocline depth anomalies (-33%/+74%).

However, the changes in wind stress and heat flux variability cannot explain the change in the period of ENSO. To understand this change one has to take a look at the persistence of the zonal wind stress anomalies. Figure 4.34 shows the autocorrelations of the central Pacific wind stress anomalies. For the TP-1K experiment the autocorrelation curve of the zonal wind stress anomalies shows a more narrow peak compared to the control run and

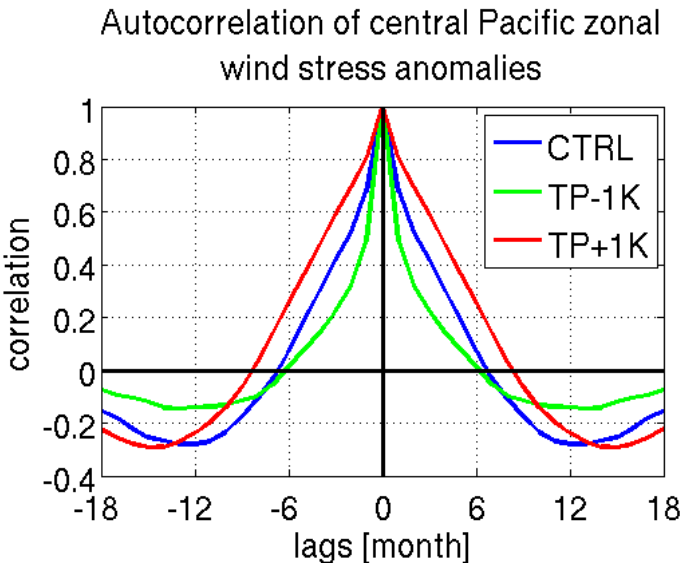

Figure 4.34: Autocorrelation of central Pacific zonal wind stress anomalies for the TP-1K experiment (green) and the TP+1K experiment (red) compared to the CTRl run (blue).

only stays positive for up to 6 months. This means that the wind stress anomalies persist for a shorter time than in the control experiment. For the TP+1K experiment the peak of the autocorrelation curve is wider and the autocorrelation stays positive for up to 8 months, implying a longer persistence.

The changes of the persistence of the wind stress anomalies influence the cross correlation between the central Pacific zonal wind stress anomalies and the NINO3 SST anomalies (figure 4.35). The correlations are slightly increased in the TP+1K experiment and slightly reduced in the TP-1K experiment. In all experiments the maximum correlation is still found when the wind stress is leading by 1 month.

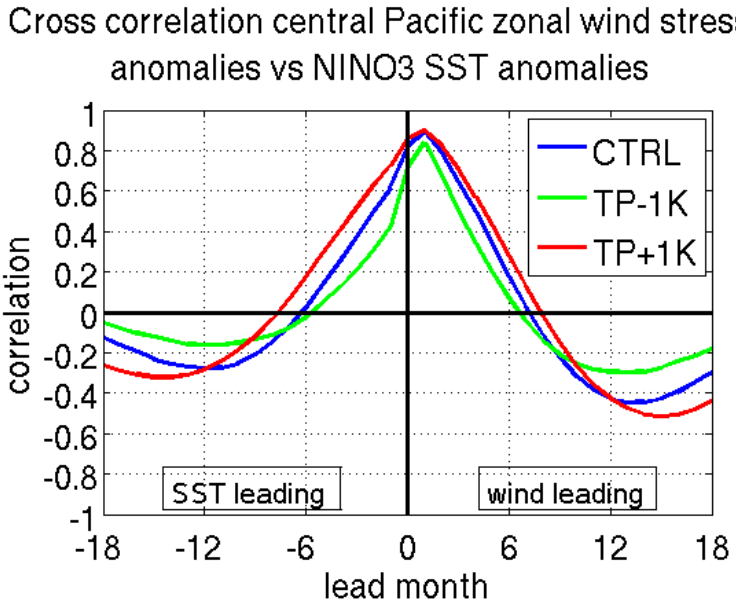

Figure 4.35: Cross correlation between the central Pacific zonal wind stress anomalies and the NINO3 SST anomalies for the TP-1K experiment (green) and the TP+1K experiment (red) compared to the control run (blue).

Also the cross correlation between the central Pacific zonal wind stress anomalies and the equatorial Pacific thermocline depth anomalies is influenced by the longer persistence of the wind stress anomalies (figure 4.36). In the TP-1K experiment the correlations are overall reduced. In the TP+1K experiment the correlations are reduced when the thermocline is leading but increased when the wind stress is leading.

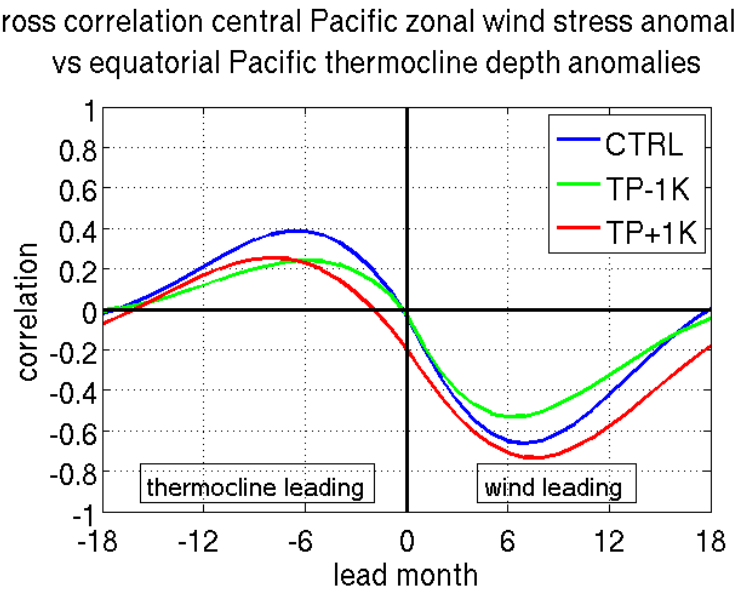

Figure 4.36: Cross correlation between the central Pacific zonal wind stress anomalies and the equatorial Pacific thermocline depth anomalies for the TP-1K experiment (green) and the TP+1K experiment (red) compared to the cotrol run (blue).

Next one can analyse how changes in the mean SST in the tropical Pacific influence the parameters of the recharge oscillator model. Therefore, the parameters of equations 3.9 and 3.10 are fitted to the data resulting from the mean state experiments. The resulting parameter values can be found in table 4.3 at the end of this section. In the experiment with the colder mean SST there are almost no changes found for the damping of the thermocline a_{22} and the two coupling paramters a_{12} and a_{21}. Only the damping of the temperature a_{11} is strongly increased by 69%. Small reductions of 12% and 11% respectively are also found in the standard deviations of the residuals of the parameter fit which correspond to the noise terms s_1 and s_2.

A warmer mean SST in the tropical Pacific influences almost all parameters. Only the coupling of the thermocline to the SST a_{21} shows just a small increase of 1%. The damping of the temperature a_{11} is reduced by 34% compared to the control run. Also the coupling of the temperature to the thermocline a_{12} is reduced by 40% and the damping of the thermocline depth anomalies a_{22} is reduced by 35%. The increase in the standard deviations of the

residuals is of the same size as the reduction in the colder mean SST experiment.

Thus, in the cold mean SST experiment one finds reduced SST variability due to an increased damping of the SST. The increase in damping is caused by weaker wind stress and heat flux variability. The fact that the variability of the thermocline depth is reduced although the damping of the thermocline does not change is due to the strong coupling of the thermocline to the SST. In the warm mean state experiment one finds increased SST variability due to a reduced damping of the SST. The reduction of the damping is caused by increased wind stress and heat flux variability. The stronger increase in thermocline depth variability is due to the strong coupling of the thermocline to the SST and a reduced damping of the thermocline.

To understand the changes in the seasonal cycle one has to take a look at the seasonality of the parameters. Therefore, again a separate parameter fit for each calendar month was performed with a 3-month moving data block. The results are displayed in figure 4.37. The strongest changes are found in the damping of the SST a_{11}. In the cold mean state experiment the damping is strongly increased in summer compared to the CTRL experiment. In the warm mean state experiment the damping even changes into a growing in summer. The changes in the coupling of the thermocline a_{21} seem to be stongly related to the changes in a_{11}. The damping of the thermocline a_{22} is overall reduced in the warm mean state experiment but the seasonal cycle does not change. For the cold mean state experiment a_{22} is increased in summer and autumn. The coupling of the SST to the thermocline a_{12} changes similar to a_{22}.

Also the variability of the heat flux and wind stress anomalies show a seasonal cycle. Changes in the mean state have only little influence on the seasonal cycle of the heat flux anomalies (figure 4.38 (a)). In contrast the seasonal cycle of the wind stress variability is strongly reduced in the cold mean state experiment (figure4.38 (b)). In the warmer mean state experiment the seasonal cycle also seems to be slightly shifted. In both experiments the changes in the seasonality of the wind stress are in accordance with the changes in the SST variabi-

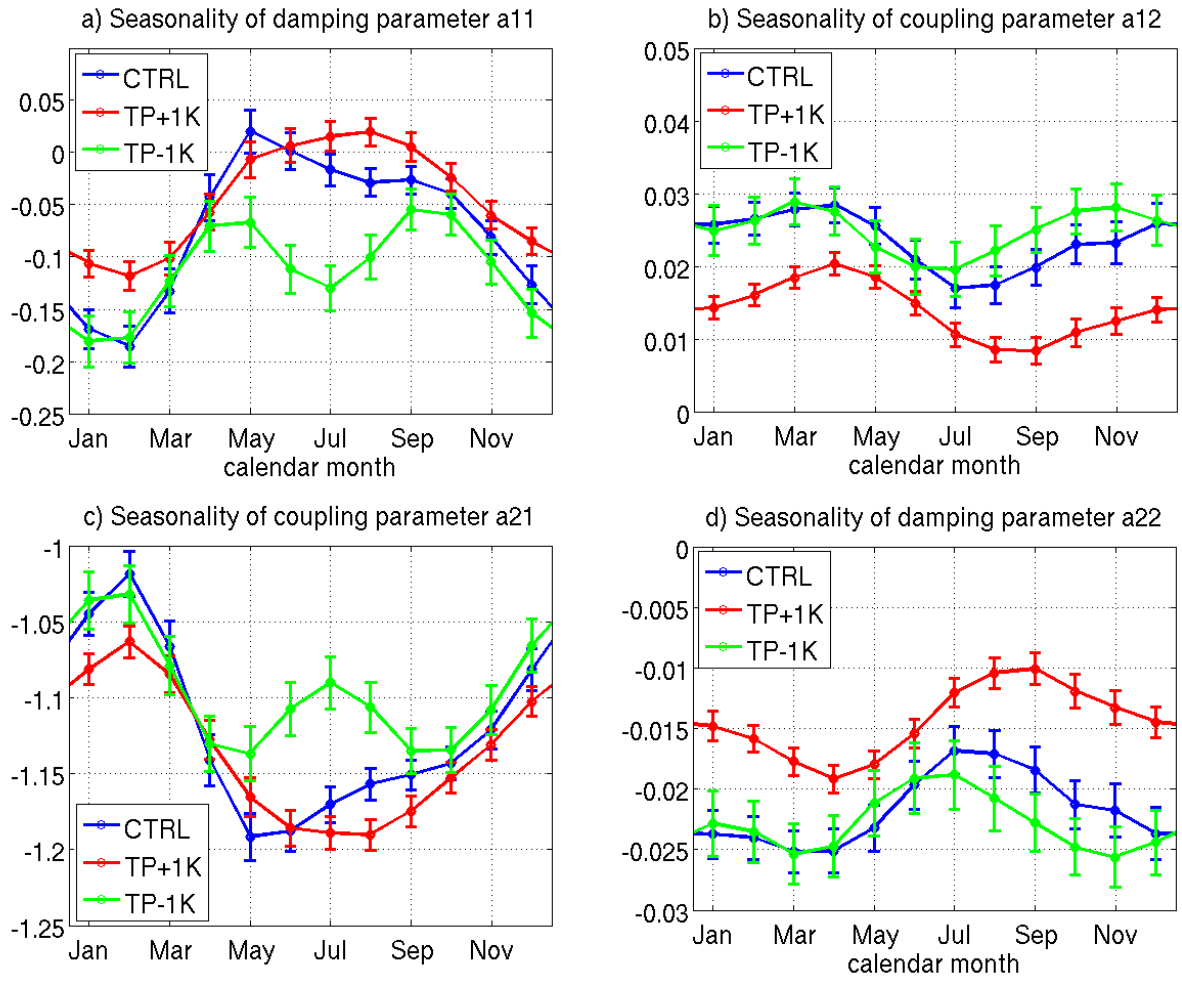

Figure 4.37: Seasonality of the fitted parameters with 95% confident intervals for the TP+1K experiment (red) and the TP-1K experiment (green) compared to the control run (blue).

lity.

The seasonality of the regression between the NINO3 heat flux anomalies and the NINO3 SST anomalies is not influenced by changes in the mean state (figure 4.39 (a)). Also the annual mean regression between the central Pacific zonal wind stress anomalies and the NINO3 SST anomaliesdoes not change the seasonal cycle of the regression is altered when the mean state of the SST changes (figure 4.39 (b)). In both experiments the coupling of the wind stress to the SST is increased in winter. In the warmer mean state this coupling is reduced in spring and early summer and in the cold mean state experiment it is reduced in summer.

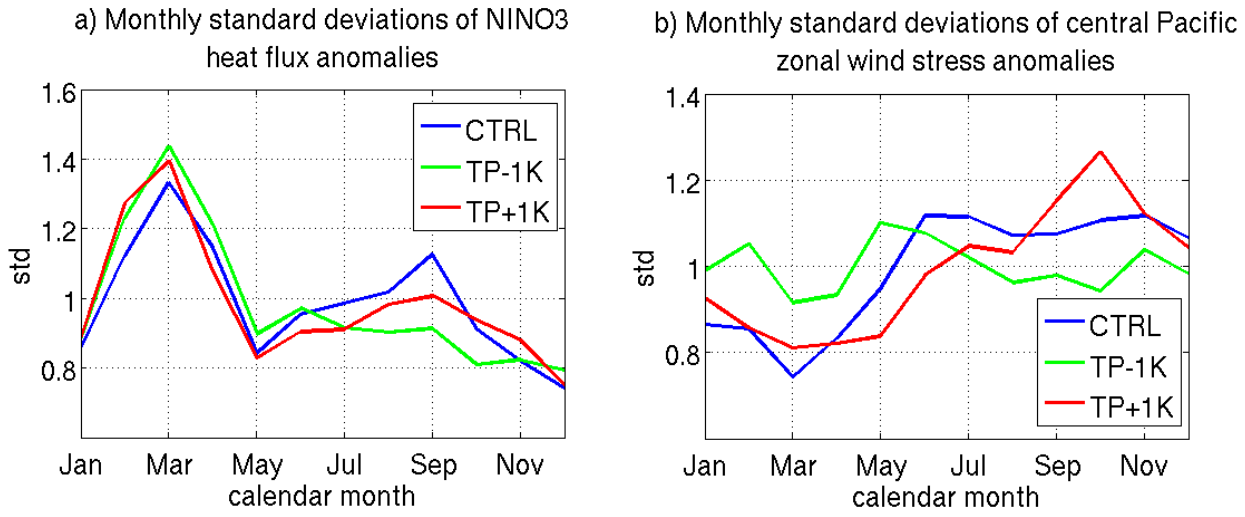

Figure 4.38: Seasonality of a) the the NINO3 heat flux anomalies and b) the central Pacific zonal wind stress anomaliess for the TP-1K experiment (green) and the TP+1K experiment (red) compared to the control run (blue).

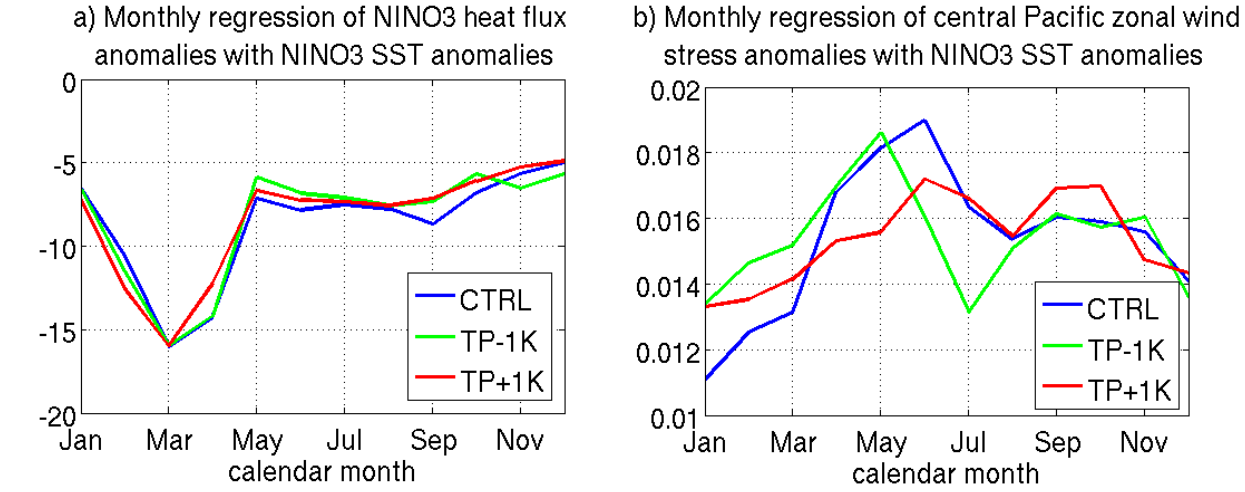

Figure 4.39: Seasonality of the regression between a) the NINO3 heat flux anomalies and the NINO3 SST anomalies and b) the central Pacific zonal wind stress anomalies and the NINO3 SST anomalies for the TP-1K run (green) and the TP+1K run (red) compared to the control run (blue).

The previous analyses showed that changes in the mean state of the tropical Pacific clearly have an influence on the amplitude and frequency of ENSO. However, a uniform cooling or warming of the tropical Pacific is no likely scenario. Therefore, another experiment ENPAT was performed, in which an El Niño-like warming pattern was added to the mean SST of the tropical Pacific. Figure 4.40 shows the changes in the mean SST, zonal wind stress and net heat flux compared to the control run.

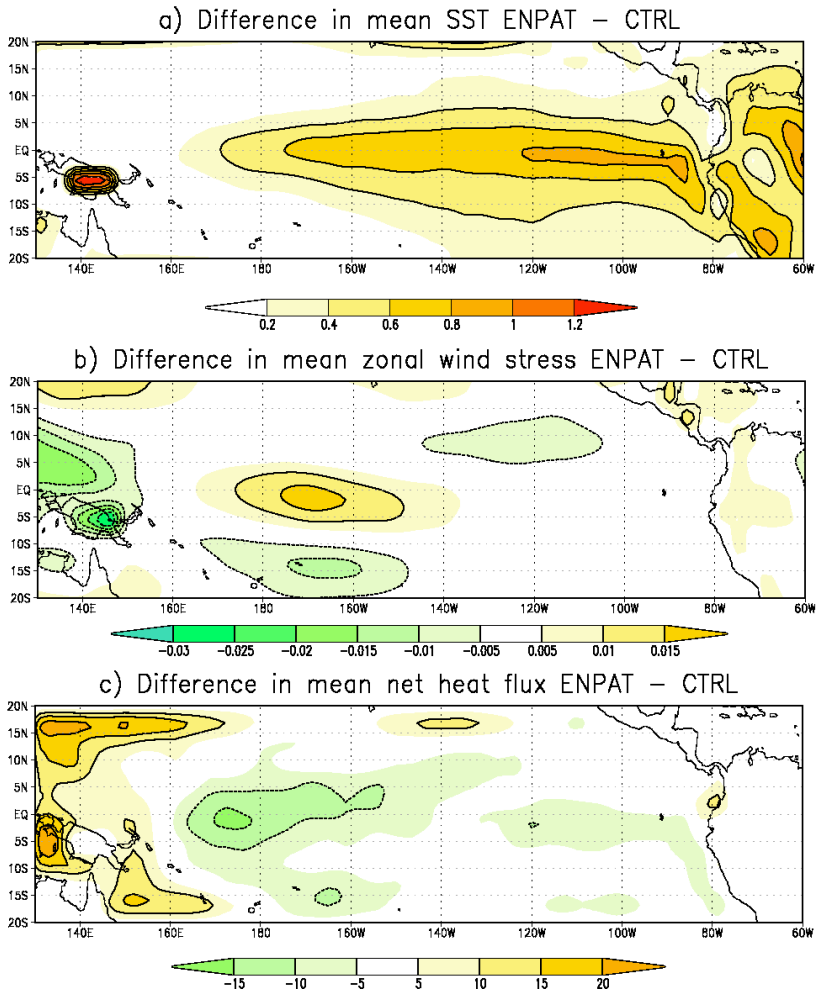

Figure 4.40: Differences in a) mean SST [°C], b) mean zonal wind stress [Pa], and c) mean net heat flux [W/m^2] between the ENPAT experiment and the CTRL run.

The mean SST changes according to the prescribed pattern. The SST is warmed in the central and eastern tropical Pacific and warming is strongest at the equator. Although the amplitude of the warming is smaller than in the TP+1K experiment, the mean wind stress

in the central Pacific shows a stronger reduction than in the TP+1K experiment. In contrast to the TP+1K experiment also the net heat flux in the NINO3 region is slightly reduced. Figure 4.41 shows the power spectra of NINO3 SST anomalies of the ENPAT simulation compared to the CTRL and TP+1K simulations. Although the average warming of the tropical Pacific mean SST is smaller in the ENPAT experiment compared to the TP+1K experiment, a larger increase in NINO3 SST variability is found in the ENPAT experiment. The standard deviation of NINO3 SST anomalies in the ENPAT experiment is $\sigma(T_{ENPAT}) = 1.5\,K$, which is an increase of 88% compared to the control experiment. For the standard deviation of the equatorial Pacific thermocline depth anomalies ($\sigma(h_{ENPAT}) = 11.0\,m$) even an increase of 110% is found. The peak of the ENPAT NINO3 SST anomaly spectrum is shifted to longer periods compared to the spectrum of the CTRL run like in the TP+1K experiment.

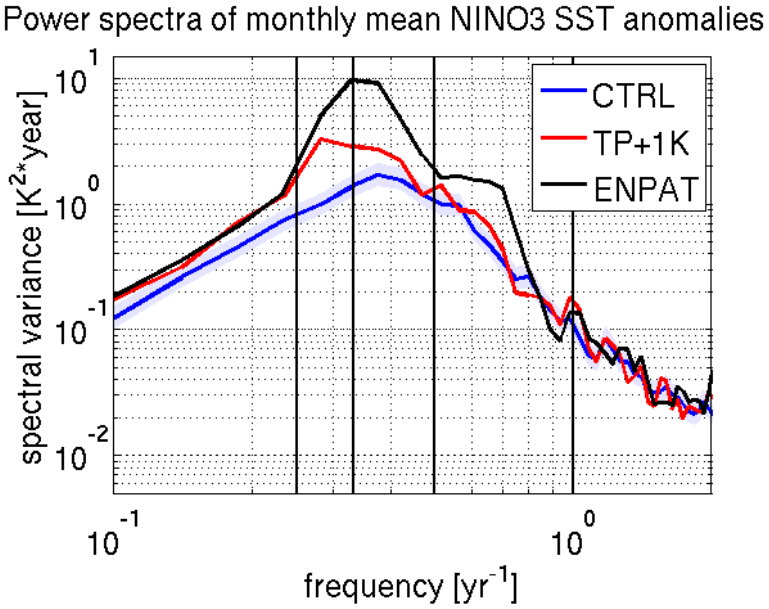

Figure 4.41: Spectra of monthly mean NINO3 SST anomalies for the ENPAT experiment (black) compared to the CTRL run (blue) and the TP+1K experiment (red). The violet shading indicates the 80% confidence level of the CTRL run spectrum.

Also the seasonality of ENSO is influenced by an El Niño-like warming pattern. A stronger seasonal cycle in NINO3 SST anomalies is found compared to both the CTRL and the TP+1K experiments (figure 4.42).

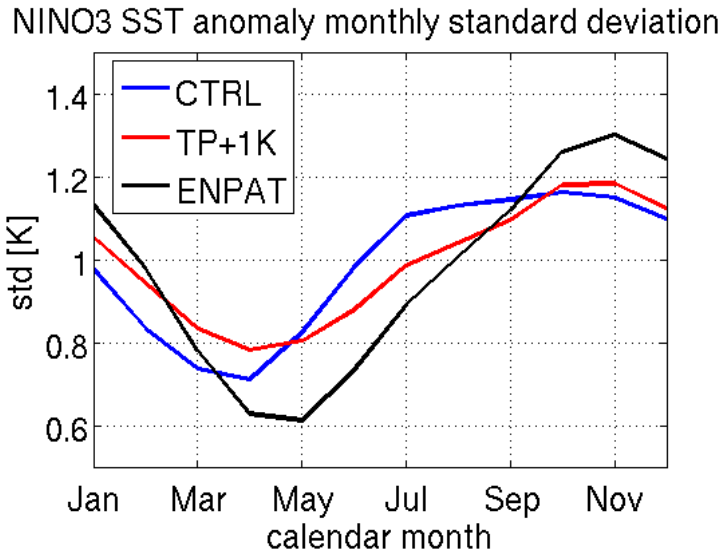

Figure 4.42: Standard deviation of monthly mean NINO3 SST anomalies for each calendar month for the ENPAT experiment (black) compared to the TP+1K experiment (red) and the CTRL experiment (blue). The monthly standard deviations are devided by the total standard deviation of each experiments NINO3 SST anomalies.

An El Niño-like warming also influences the skewness and kurtosis of the NINO3 SST anomalies (figure 4.43). The skewness of the ENPAT NINO3 SST anomalies $\gamma_1(T_{ENPAT}) = 0.4$ is smaller than in the control run ($\gamma_1(T_{CTRL}) = 0.6$) and also the kurtosis $\gamma_2(T_{ENPAT}) = 0.5$ is highly reduced compared to the control run ($\gamma_2(T_{ENPAT}) = 1.9$).

The cross correlation between the equatorial Pacific thermocline depth anomalies and the

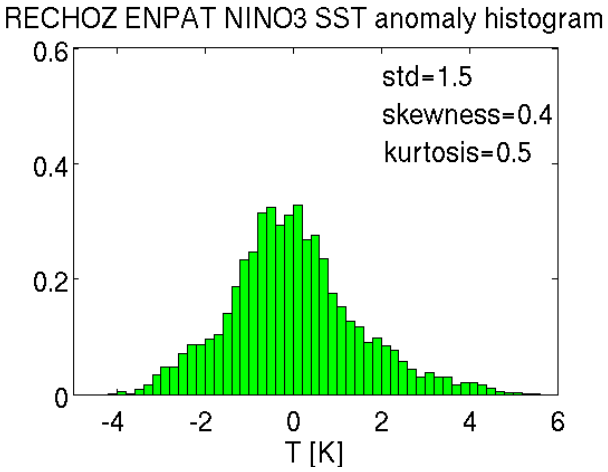

Figure 4.43: Histogram of monthly mean NINO3 SST anomalies for the ENPAT run.

NINO3 SST anomalies shows only small changes compared to the control experiment (figure 4.44). Larger changes are found for the TP+1K experiment.

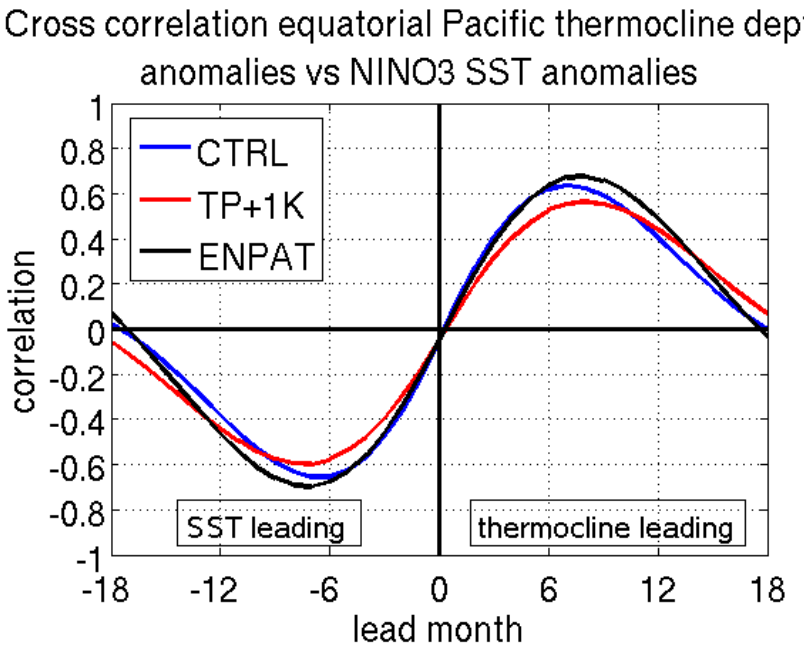

Figure 4.44: Cross correlation of equatorial Pacific thermocline depth anomalies and NINO3 SST anomalies for the ENPAT experiment (black) compared to the CTRL experiment (blue) and the TP+1K experiment (red).

Again atmospheric feedbacks have to be responsible for the changes in the ENSO variability. Like in the TP-1K and TP+1K experiments the regression coefficient between the central Pacific zonal wind stress anomalies and the NINO3 heat flux anomalies $r_{T\tau}$ does not change compared to the CTRL run and the regression coefficient between the NINO3 heat flux anomalies and the NINO3 SST anomalies r_{Tf} changes only very little. Thus, again changes in the variability or the response of central Pacific wind stress anomalies and NINO3 heat flux anomalies to NINO3 SST anomalies have to be the origin of the changes in the ENSO variability. The composite of monthly mean heat flux anomalies for all ENSO extreme years for the ENPAT experiment (figure 4.45) shows no change in the pattern but a large increase in the size of the anomalies compared to the control run (figure 4.32 (a)). Also the variability of the NINO3 heat flux anomalies is strongly increased in the ENPAT experiment. The stan-

dard deviation of the NINO3 heat flux anomalies is $\sigma(f_{ENPAT}) = 13.9\,W/m^2$. The increase in standard deviation of NINO3 heat flux anomalies in the ENPAT experiment compared to the CTRL run (+65%) is twice as large as for the TP+1K experiment (+33%) although the amplitude of the warming is smaller in the ENPAt experiment.

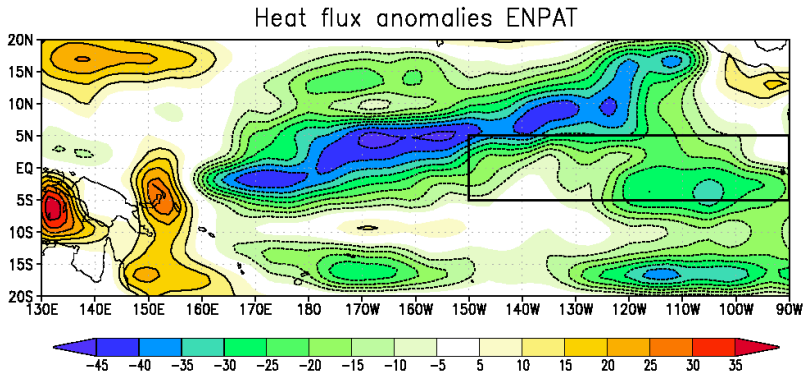

Figure 4.45: Model composite mean values of the net heat flux anomalies for all ENSO extreme years ($|T(December)| > \sigma(T)$) averaged from December to April of the following year for the ENPAT experiment. For La Niña events the net heat flux anomalies are considered with reversed sign in the composites mean. Units are in W/m^2. The black box indicates the NINO3 region over which the heat flux anomalies are averaged.

Also the composites of monthly mean zonal wind stress anomalies for all ENSO extreme years for the ENPAT experiment (figure 4.46) show no change in the pattern of the anomalies but a strong increase in the size of the anomalies compared to the control run (figure 4.33). Also the standard deviation of the central Pacific zonal wind stress anomalies is increased compared to the control run (($\sigma(\tau_{ENPAT}) = 0.025\,Pa$). Again the increase in standard deviation of the central Pacific zonal wind stress anomalies compared to the CTRL run (+66%) is twice as large as for the TP+1K experiment (+26%).

This indicates that the response of the ENSO variability to global warming strongly depends on the pattern of the warming. The changes in the SST gradient along the equator lead to a strong reduction of the trade winds in the central Pacific. Also the net heat flux in the NINO3 region is reduced. This leads to an enhanced variability of central Pacific zonal wind stress anomalies and NINO3 heat flux anomalies and these in turn enhance the ENSO vari-

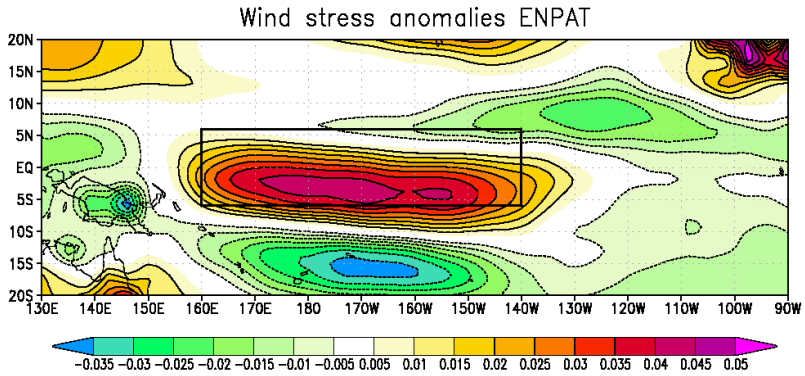

Figure 4.46: Model composite mean values of the zonal wind stress anomalies for all ENSO extreme years ($|T(December)| > \sigma(T)$) averaged from December to April of the following year for the ENPAT experiment. For La Niña events the net heat flux anomalies are considered with reversed sign in the composites mean. Units are in Pa. The black box indicates the region over which the wind stress anomalies are averaged.

ability.

To understand the changes in the period of ENSO again the autocorrelation of central Pacific zonal wind stress anomalies is displayed in figure 4.47. The correlation curve of the ENPAT experiment shows a wider peak compared to the CTRL and TP+1K experiments, but only stays positive for 8 months like in the TP+1K experiment.

The influence of an El Niño-like warming pattern on the parameters of the recharge oscillator was analysed by fitting the parameters to the resulting data from the ENPAT experiment. The resulting parameters can be seen in table 4.3. Again only small changes are found for the coupling of the thermocline to the SST a_{21}. The changes in the damping of the thermocline a_{22} and in the coupling of the SST to the thermocline a_{12} are with -17% and -24% much smaller than in the TP+1K experiment. However, the change in the damping of the SST a_{11} is with -52% much larger than for the TP+1K experiment. Also the increase in the standard deviations of the noise terms (+25% and +26%) is larger than in the TP+1K experiment.

To understand the strong increase of the seasonal cycle of the NINO3 SST anomalies again the seasonal values are the model parameters are displayed in figure 4.48. For all parameters

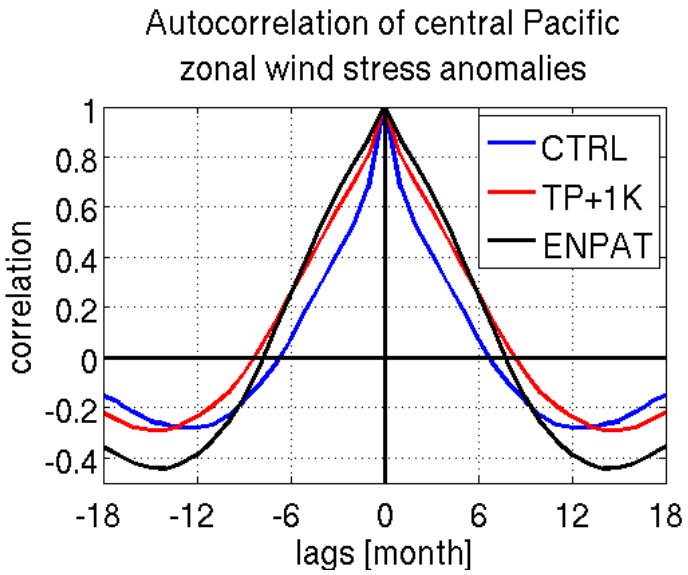

Figure 4.47: Autocorrelation of central Pacific zonal wind stress anomalies for the ENPAT experiment (black) compared to the CTRL experiment (blue) and the TP+1K experiment (red).

a stronger seasonal cycle is found compared to the CTRL and TP+1K experiments.

This goes along with a strong increase in the seasonal cycle of the central Pacific zonal wind stress anomalies (figure 4.49 (b)). Also the seasonal cycle of the regression between the central Pacific zonal wind stress anomalies and the NINO3 SST anomalies is stronger than in the TP+1K experiment (figure 4.50 (b)).

The results of this section indicate that changes in the mean state of the tropical Pacific clearly influence the ENSO variability. A warmer mean state leads to an increase in ENSO variability and a shift of the ENSO period towards longer time scales. A colder mean state leads to a reduction of ENSO variability and also a shorter period of ENSO. The results of the ENPAT experiment show that not only the amplitude of the mean changes is important but also the pattern. Although the amplitude of the change in the mean SST in the ENPAT experiment is smaller than in the TP+1K experiment it shows a larger increase in ENSO variability. However, in this model only changes in the atmospheric feedbacks are considered. Of course also oceanic processes could play a role and maybe also balance the changes. GCM projections indicate for example a shoaling of the equatorial thermocline due

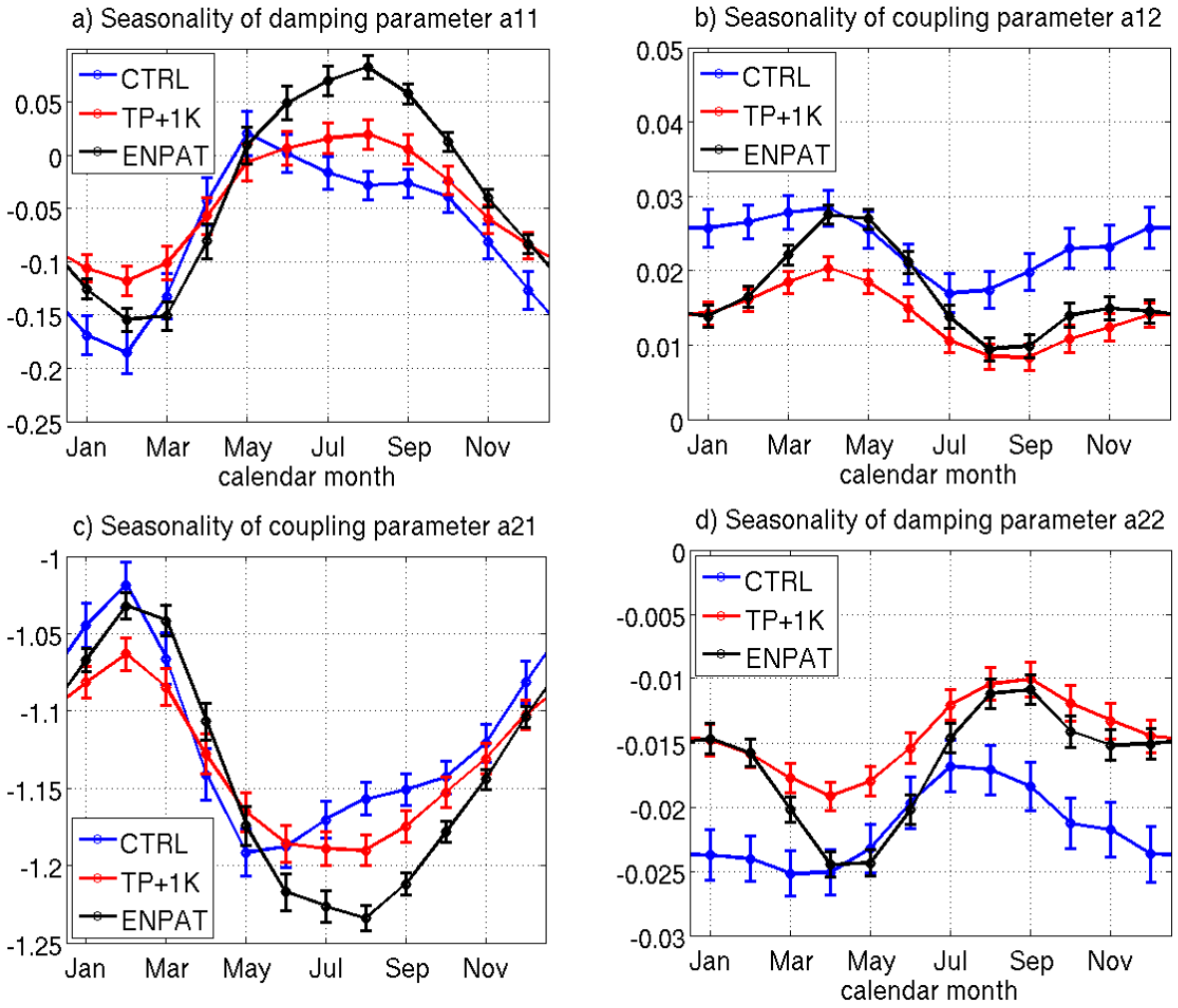

Figure 4.48: Seasonality of the fitted parameters with 95% confident intervals for the ENPAT experiment (black) compared to the control run (blue) and the TP+1K experiment (red).

to reduced equatorial winds and the tendency of surface waters to warm at a faster rate than the deep ocean (Vecchi and Soden, 2007). On the other hand the slope of the thermocline depth is reduced in global warming scenarios of many GCMs which reduces the depth of the thermocline in the east (Collins et al., 2010). Thus, changes in the atmospheric feedbacks due to global warming have an important influence on the properties of ENSO, but to make any satisfying predictions on the future behaviour of ENSO both atmpospheric and oceanic processes have to be considered. Also the simulation of the mean state of the tropical Pacific has to be improved to predict the changes in the ENSO properties.

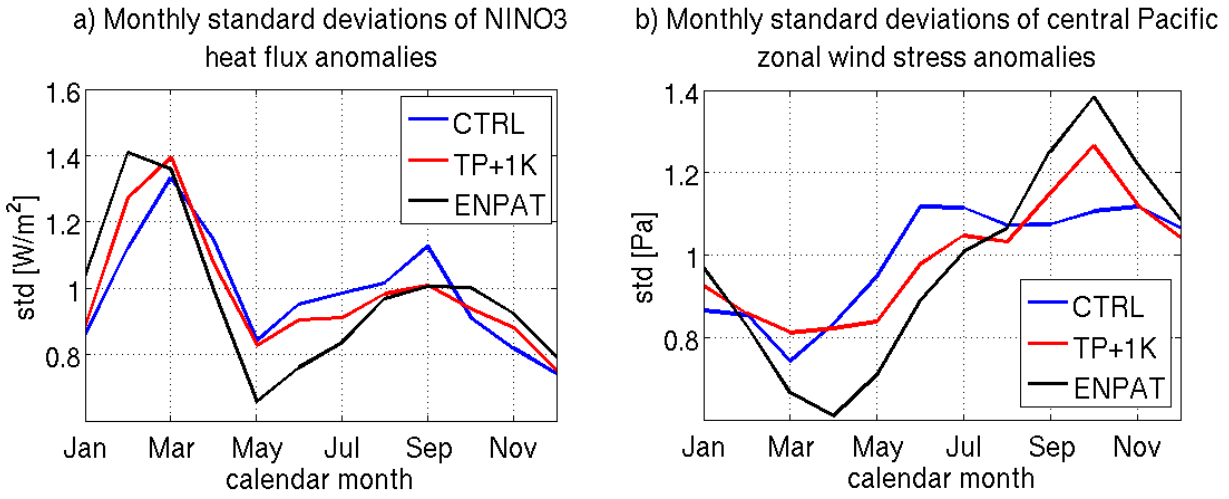

Figure 4.49: Seasonality of a) the the NINO3 heat flux anomalies and b) the central Pacific zonal wind stress anomaliess for the ENPAT experiment (black) compared to the TP+1K experiment (red) and the control run (blue).

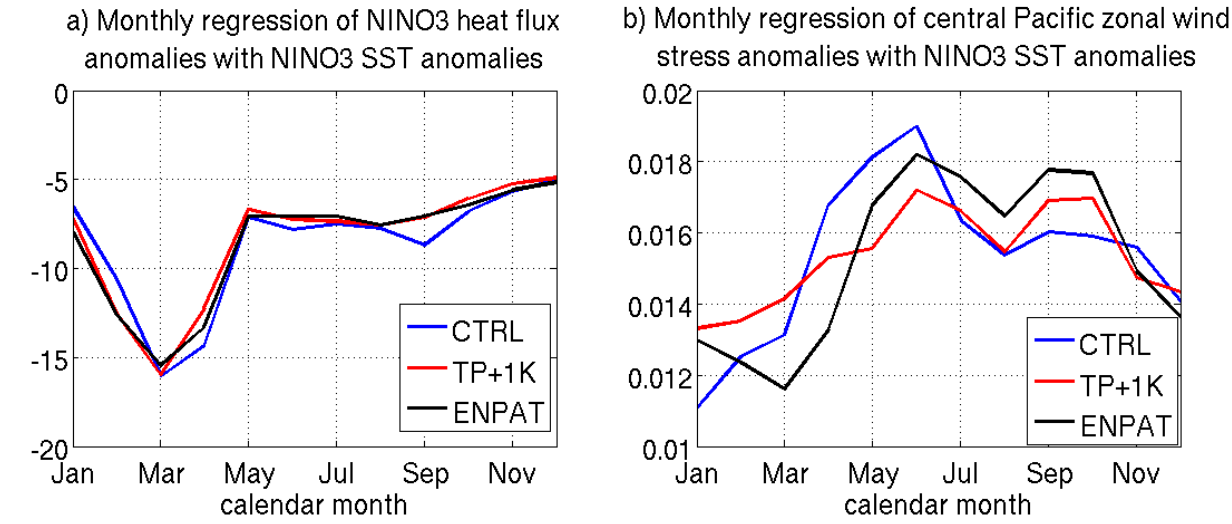

Figure 4.50: Seasonality of the regression between a) the NINO3 heat flux anomalies and the NINO3 SST anomalies and b) the central Pacific zonal wind stress anomalies and the NINO3 SST anomalies for the ENPAT run (black) compared to the TP+1K run (red) and the control run (blue).

	$a_{11}\,[\frac{1}{month}]$	$a_{12}\,[\frac{K}{month\,m}]$	$a_{21}\,[\frac{m}{K\,month}]$	$a_{22}\,[\frac{1}{month}]$	$\sigma(s_1)\,[\frac{K}{month}]$	$\sigma(s_2)\,[\frac{m}{month}]$
CTRL	-0.065 ± 0.009	0.025 ± 0.001	-1.126 ± 0.006	-0.023 ± 0.001	0.272	0.207
TP-1K	-0.110 ± 0.011	0.025 ± 0.002	-1.098 ± 0.009	-0.023 ± 0.001	0.240	0.185
TP+1K	-0.043 ± 0.001	0.015 ± 0.001	-1.137 ± 0.005	-0.015 ± 0.001	0.304	0.231
ENPAT	-0.031 ± 0.001	0.020 ± 0.001	-1.144 ± 0.004	-0.019 ± 0.001	0.334	0.256

Table 4.3: Resulting model parameters from the TP-1K, TP+1K, and ENPAT experiments compared to the CTRL run with 95% confident intervals.

4.5 Interactions of the tropical oceans with ENSO

Recent studies suggest that tropical Indian Ocean and the tropical Atlantic Ocean may not only react to the ENSO mode but are influencing ENSO themselves. Most studies focus on a possible feedback of the tropical Indian Ocean on the ENSO dynamics (Liu, 2002; Yu et al., 2002; Wu and Kirtman, 2004; Annamalai et al., 2005; Kug and Kang, 2006; Dommenget et al., 2006; Jansen et al., 2009). Liu (2002) showed in model studies that ENSO variability can be supressed if it is influenced by an external (outside the tropical Pacific) periodical forcing. Following this study a possible source of this forcing could be the tropical Indian Ocean. Yu et al. (2002), Wu and Kirtman (2004), and Dommenget et al. (2006) analysed coupled ocean atmosphere GCMs in which the influence of the Indian Ocean was supressed. In the studies of Yu et al. (2002) and Wu and Kirtman (2004) the ENSO variability was enhanced if the SST variability of the Indian Ocean was active. However, they find contradictory results regarding the periodicity of ENSO. Both studies are based on relatively short time series which do not allow statistically reliable statements on the changes of the period of ENSO. Dommenget et al. (2006) analysed 500-year-long coupled GCM simulations and found an increase in ENSO variability, and a shift of ENSO period towards longer periods, if the SST variability in the tropical Indian Ocean was supressed. This is also in agreement with a conceptual model study of Jansen et al. (2009) where they found an ENSO period shift from 4 to about 5 years, and an increase in NINO3 SST variability of about 40%, if the feedback of the Indian Ocean is switched off.

In the opinion of Wu and Kirtman (2004) and Kug and Kang (2006), the observations suggest an influence of the SST anomalies in the tropical Indian Ocean on the ENSO dynamics, too. Kug and Kang (2006) found a shortening of the ENSO period because the Indian Ocean SST anomalies induce easterlies in the western Pacific which lead to faster reversal of the ENSO cycle. However, these studies are only of limited significance primarily due to the short time series of observed SSTs. Another problem is the difficulty in quantifying the influence of the

Indian Ocean on ENSO because the Indian Ocean is primarily influenced by ENSO, and the feedback of the Indian Ocean on ENSO is only a secondary effect. In principle, it could be possible to explain the observations without a feedback of the Indian Ocean on ENSO.

The Indian Ocean also seems to develop global teleconnections independent of ENSO (Deser et al. (2004) and Bader and Latif (2005)). Deser et al. (2004) found that atmospheric fluctuations over the North Pacific are driven by the SST anomalies in the Indian Ocean. Bader and Latif (2005) showed that the North Atlantic Oscillation (NAO) is driven by the SST trend in the tropical Indian Ocean.

Some studies also propose an influence of the Atlantic Ocean on ENSO. An early study by Wright (1986) gives some indirect hints on the possible influence of SST anomalies in the tropical Atlantic on ENSO. A study by Dong et al. (2006) shows that multidecadal fluctuations of the tropical Atlantic SST anomalies influence the strength of ENSO. Dommenget et al. (2006) found, in a coupled GCM study, a shift in ENSO period towards longer periods and an increase in ENSO variability if the SST variability in the tropical Atlantic Ocean is supressed. Very recently, Jansen et al. (2009) found that an inclusion of the Atlantic Ocean can improve the ENSO forecast skill of their conceptual model, and the study of Rodriguez-Fonseca et al. (2009) gives some indications from observations that the summer Atlantic Niños (Niñas) alter the tropical circulation which favors the development of a Pacific La Niña (El Niño) in the following winter.

Thus, many studies indicate possible influences of the tropical Indian and Atlantic Oceans on ENSO, but the exact mechanisms of these teleconnections are not yet fully understood and need further investigation.

To study the interactions of the tropical Indian Ocean and the tropical Atlantic Ocean with ENSO three sensitivity experiments were performed in which the SST in a specific region is prescribed by monthly varying climatologies obtained from the control run. First the SST in the tropical Atlantic ($30°S - 30°N$) is prescribed (NOAT), then the SST in the tropical Indian Ocean ($30°S$-northern boundary)(NOIND) and finally the SST in both the tropical

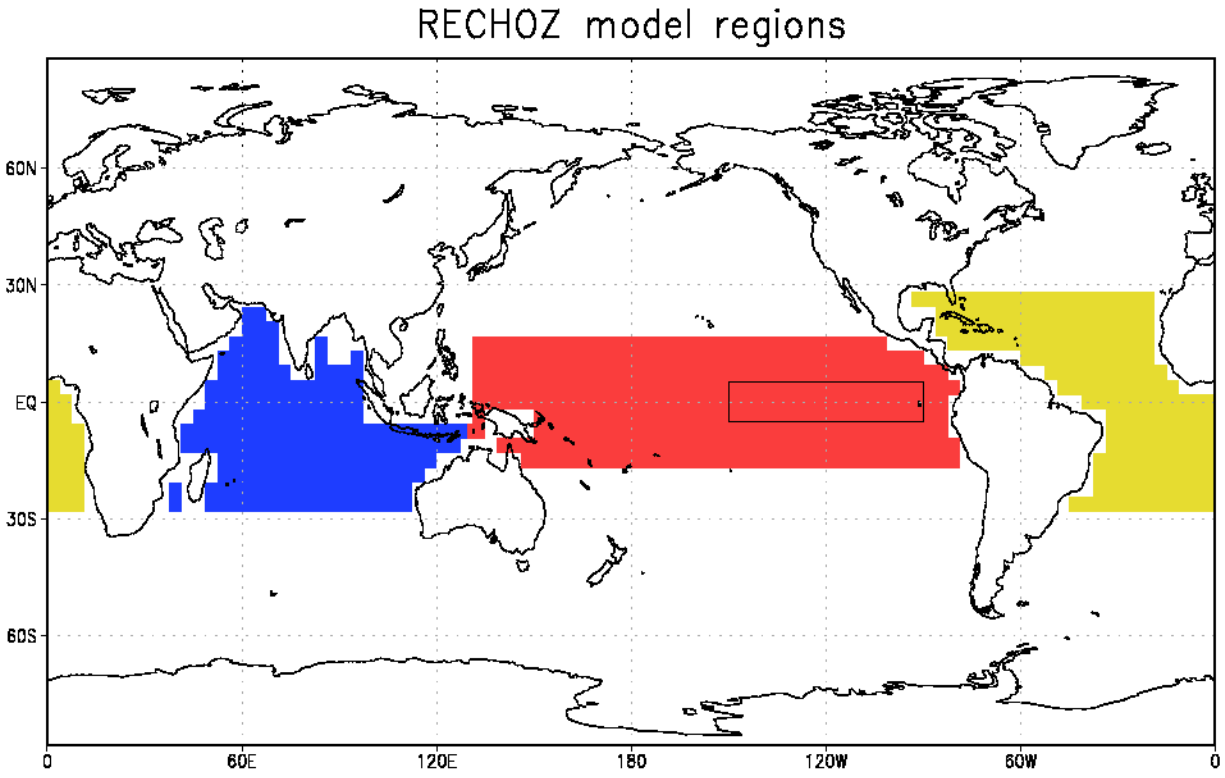

Figure 4.51: Different RECHOZ model regions. Red indicates the region in which the recharge oscillator ocean model is used. The black box inside shows the NINO3 region. Blue represents the region in which the SST is prescribed in the NOIND experiment. Yellow highlights the region where the SST is presribed in the NOAT experiment. In the NOAI experiment the SST is prescribed in both the blue and the yellow regions.

Atlantic and the tropical Indian Ocean is prescribed (NOAI). The different regions in which the SST is prescribed can be seen in figure 4.51. An overview of the different sensitivity experiments performed is given in table 4.4.

First it is analysed how the mean SST, zonal wind stress and net heat flux in the tropical Pacific are influenced by decoupling one or both of the other tropical oceans. In all 3 sensitivity experiments the mean SST in the tropical Pacific does not change compared to the CTRL run (not shown). The changes in the mean zonal wind stress and mean net heat flux for the NOIND experiment are shown in figure 4.52. The strongest changes in zonal wind stress are found in the far western Pacific where the zonal wind stress is reduced. Also in the central equatorial Pacific and from 10 to 20° N the zonal wind stress is slightly reduced.

Exp. ID	Years	Modifications with respect to the CTRL experiment
CTRL	500	Control run of the RECHOZ model
NOAT	500	Experiment with the SST in the tropical Atlantic Ocean prescribed
NOIND	500	Experiment with the SST in the tropical Indian Ocean prescribed
NOAI	500	Experiment with the SST in the tropical Atlantic and the tropical Indian Ocean prescribed

Table 4.4: RECHOZ model sensitivity experiments used to study the interactions of the tropical oceans with ENSO.

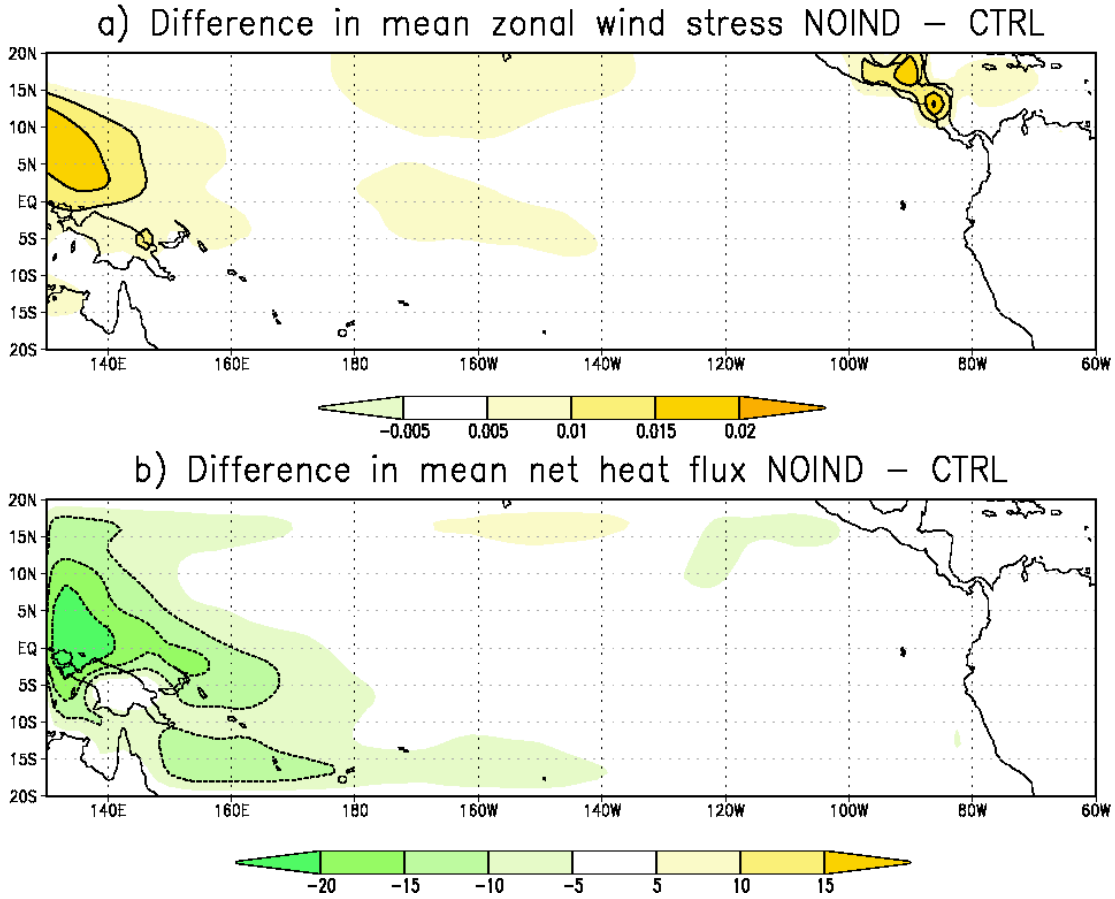

Figure 4.52: Differences in a) mean zonal wind stress [Pa] and b) mean net heat flux [W/m^2] between the NOIND experiment and the CTRL run.

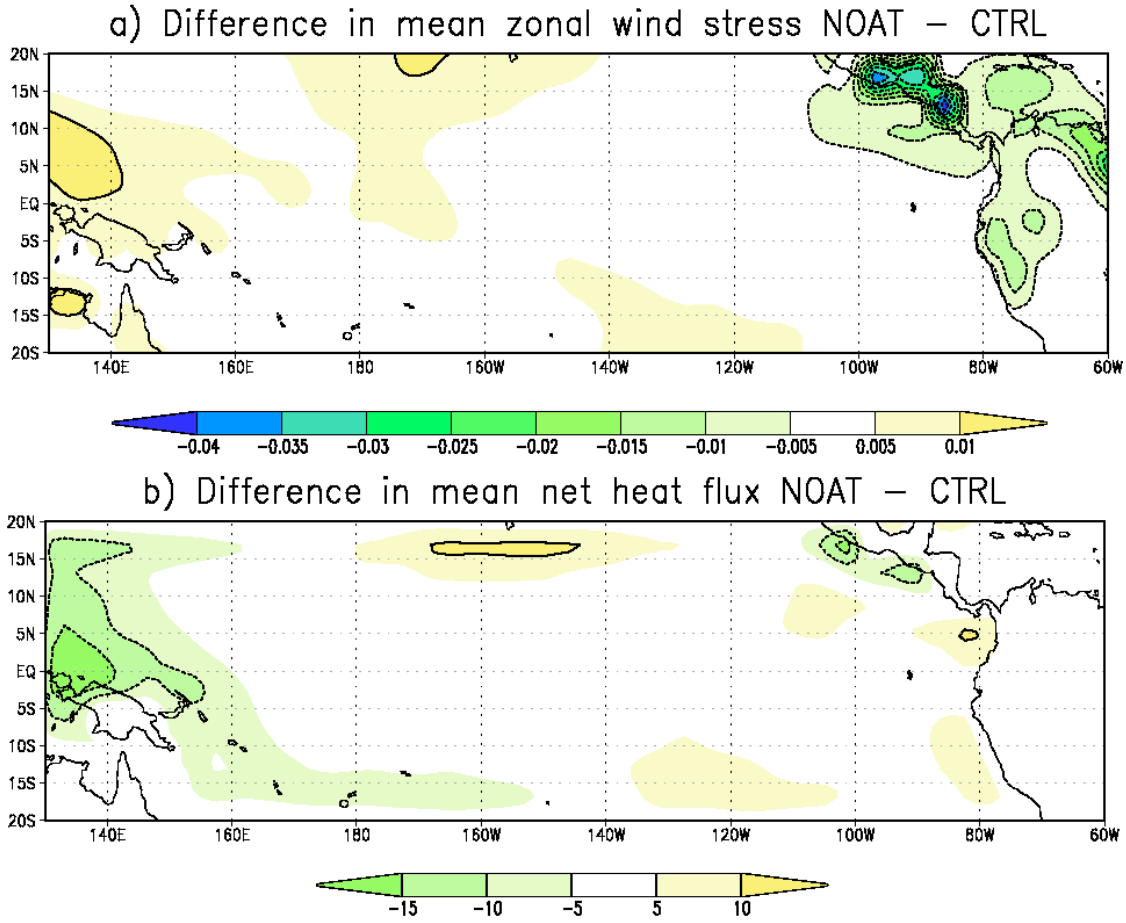

Figure 4.53: Differences in a) mean zonal wind stress [Pa] and b) mean net heat flux [W/m^2] between the NOAT experiment and the CTRL run.

For the net heat flux also a reduction is found in the western Pacific.

The changes in mean zonal wind stress and net heat flux for the NOAT experiment are shown in figure 4.53. The zonal wind stress is increased compared to the CTRL run in eastern Pacific along the coast of Central America. In the western and the central Pacific small areas of reduced zonal wind stress are found. For the net heat flux again the largest change is found in the western Pacific. In the following again only the anomalies of the SST, thermocline depth, zonal wind stress and net heat flux will be analysed.

In figure 4.54, as an example, the SST anomaly time series of the NOIND run is shown compared to the CTRL run. It can be seen that decoupling the tropical Indian Ocean leads to a strong increase in variability of NINO3 SST anomalies. Also decoupling the tropical Atlantic

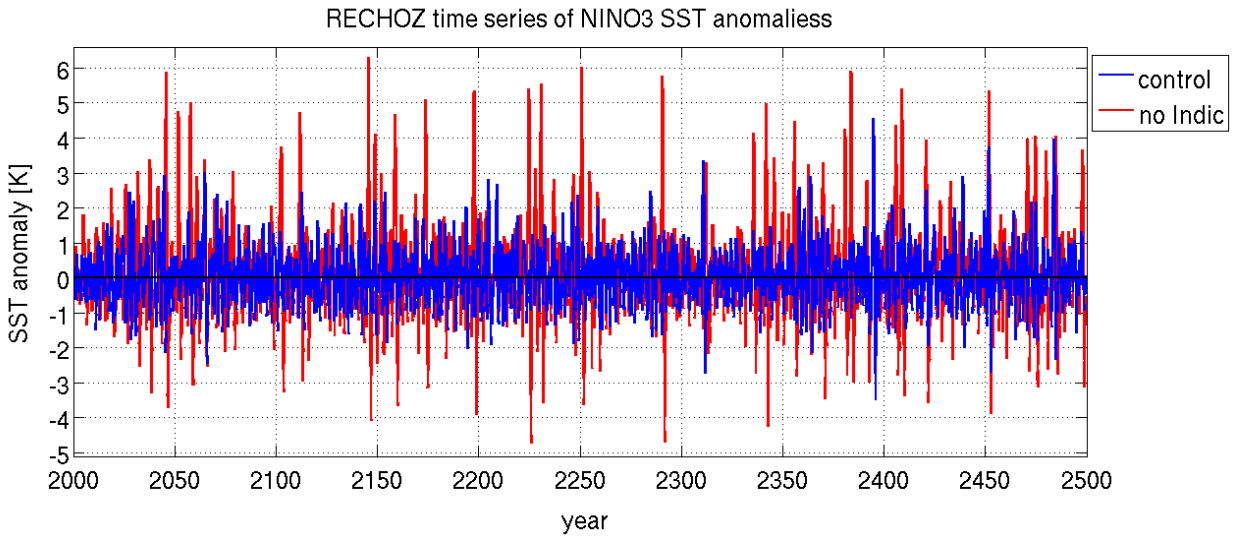

Figure 4.54: Time series of monthly mean NINO3 SST anomalies for the NOIND run for the period from 2000 to 2500 (red) compared to the CTRL run (blue).

Ocean leads to a small increase in SST variability. The standard deviation of NINO3 SST anomalies increases from $\sigma(T_{CTRL}) = 0.8\,K$ in the control run to $\sigma(T_{NOAT}) = 1.0\,K$ in the run with the tropical Atlantic Ocean decoupled to $\sigma(T_{NOIND}) = \sigma(T_{NOAI}) = 1.3\,K$ in the runs with the tropical Indian Ocean and both tropical oceans decoupled. This is an increase of 25% for the NOAT experiment and of 63% for the NOIND and NOAI experiments. The increase in thermocline depth variability is even stronger. The standard deviation of equatorial Pacific thermocline depth anomalies increases from $\sigma(h_{CTRL}) = 5.4\,m$ in the control run to $\sigma(h_{NOAT}) = 6.9\,m$ in the experiment with the tropical Atlantic Ocean decoupled to $\sigma(h_{NOIND}) = 10.4\,m$ for the experiment with the tropical Indian Ocean decoupled and $\sigma(h_{NOAI}) = 10.5\,m$ in the experiment with both tropical oceans decoupled, which corresponds to an increase of 28%, 93%, and 94% respectively.

The increase in NINO3 SST variability can also be seen in the power spectra of NINO3 SST anomalies for the three sensitivity experiments compared to the control run (figure 4.55). When the tropical Indian Ocean or both tropical oceans are decoupled also the peak of the NINO3 SST anomaly spectrum is shifted towards longer periods. This effect is stronger when

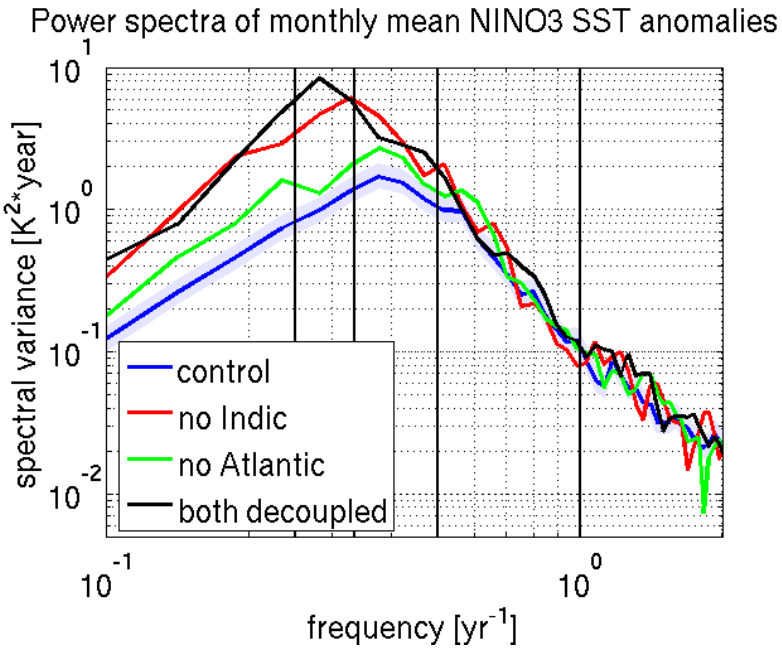

Figure 4.55: Spectra of monthly mean NINO3 SST anomalies for the CTRL run (blue), the NOIND experiment (red), the NOAT experiment (green), and the NOAI experiment (black). The violet shading indicates the 80% confidence level of the CTRL run spectrum.

both tropical oceans are decoupled than for the tropical Indian Ocean decoupled. These results are in good agreement with the studies of Dommenget et al. (2006) and Jansen et al. (2009). Only the increase in the NINO3 SST variability is much stronger than in the previous studies.

Despite the large increase in SST variability in the sensitivity experiments the skewness and kurtosis of the NINO3 SST anomalies in the sensitivity experiments (figure 4.56) do not change significantly compared to the control run (figure 4.8 (a)).

If one takes a look at the cross correlation between the NINO3 SST anomalies and the equatorial Pacific thermocline depth anomalies (figure 4.57) one finds almost no change in the NOAT experiment, where the tropical Atlantic ocean is decoupled, but for the NOIND and the NOAI experiments, where the tropical Indian and both tropical oceans are decoupled, one finds sligthly larger correlations and a shift of the maximum correlations from lead times around 6 - 7 months to lead times of about 9 months.

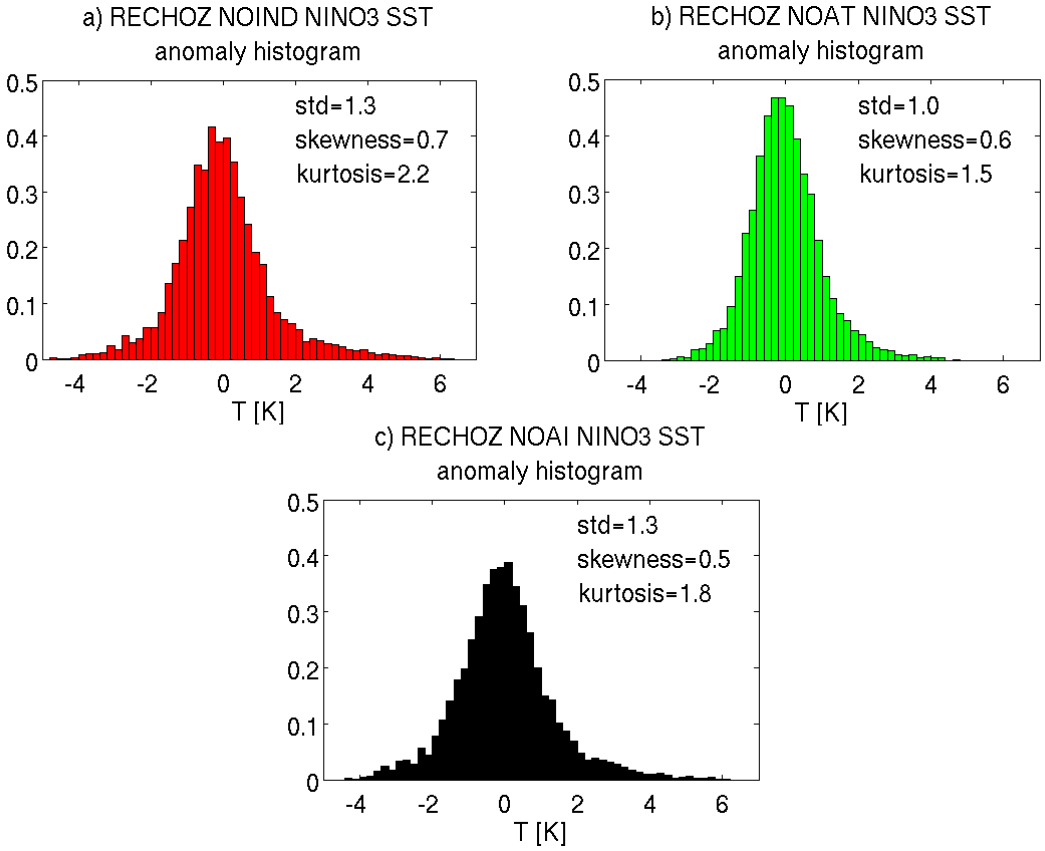

Figure 4.56: Histograms of monthly mean NINO3 SST anomaliess for (a) the NOIND run, (b) the NOAT run, and (c) the NOAI run.

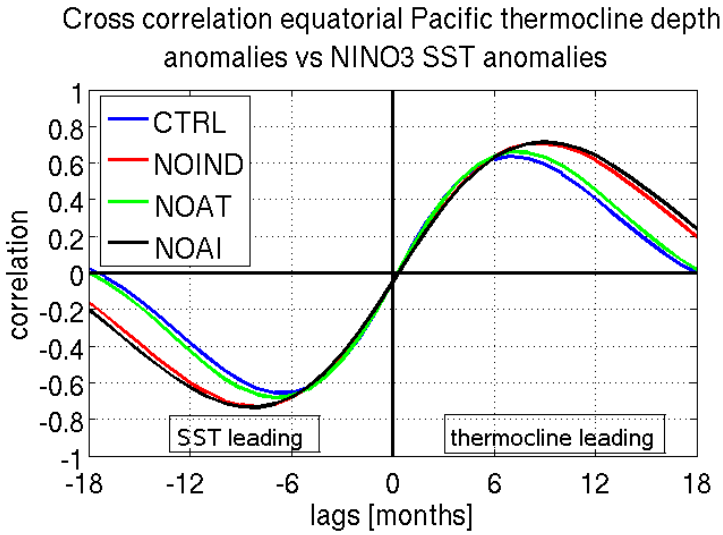

Figure 4.57: Cross correlation between the equatorial Pacific thermocline depth anomalies and the NINO3 SST anomalies for the NOIND experiment (red), the NOAT experiment (green), and the NOAI experiment (black) compared to the control run (blue).

The changes in the variability and seasonality of ENSO and in the relationships between the SST and thermocline depth anomalies can again only be caused by the atmospheric properties. Therefore, first the changes in the patterns of the heat flux anomalies are analysed. Figure 4.58 shows the composites of the heat flux anomalies for all ENSO extreme years. It can be seen that the pattern of the heat flux anomalies does not change in all three sensitivity experiments. Only the strength of the heat fluxes increases. This is also supported by the increase of the standard deviations of NINO3 heat flux anomalies. The standard deviation increases from $\sigma(f_{CTRL}) = 8.4\,W/m^2$ in the control run to $\sigma(f_{NOAT}) = 9.0\,W/m^2$ in the NOAT experiment, $\sigma(f_{NOIND}) = 11.3\,W/m^2$ in the NOIND experiment, and $\sigma(f_{NOAI}) = 11.1\,W/m^2$, what corresponds to an increase of 7%, 35%, and 32% respectively. However, the increase in NINO3 heat flux anomalies is smaller than the increase in NINO3 SST anomalies.

Figure 4.59 shows the composites of the zonal wind stress anomalies for all ENSO extreme years. Again the pattern does not change for all three sensitivity experiments and only the strength is increased. The standard deviation of central Pacific zonal wind stress anomalies increases from $\sigma(\tau_{CTRL}) = 0.015\,Pa$ in the control run to $\sigma(\tau_{NOAT}) = 0.018\,Pa$ in the NOAT run and $\sigma(\tau_{NOAT}) = \sigma(\tau_{NOAI}) = 0.023\,Pa$ in the NOIND and NOAI runs. This is an increase of 20% in the NOAT run and 53% in the NOIND and NOAI runs.

Again the increase in standard deviation of the zonal wind stress anomalies is smaller than for the NINO3 SST anomalies or the equatorial Pacific thermocline depth anomalies. So, this does still not explain the large increases in standard deviation of NINO3 SST anomalies and especially in standard deviation of equatorial Pacific thermocline depth anomalies. Also it is still unclear, what is causing the shift in the peak of the NINO3 SST anomaly spectrum towards longer periods.

To understand the shift of the period one has again to take a look at the persistence of the central Pacific zonal wind stress anomalies. Therefore, again the autocorrelations of the central Pacific zonal wind stress anomalies are plotted in figure 4.60.

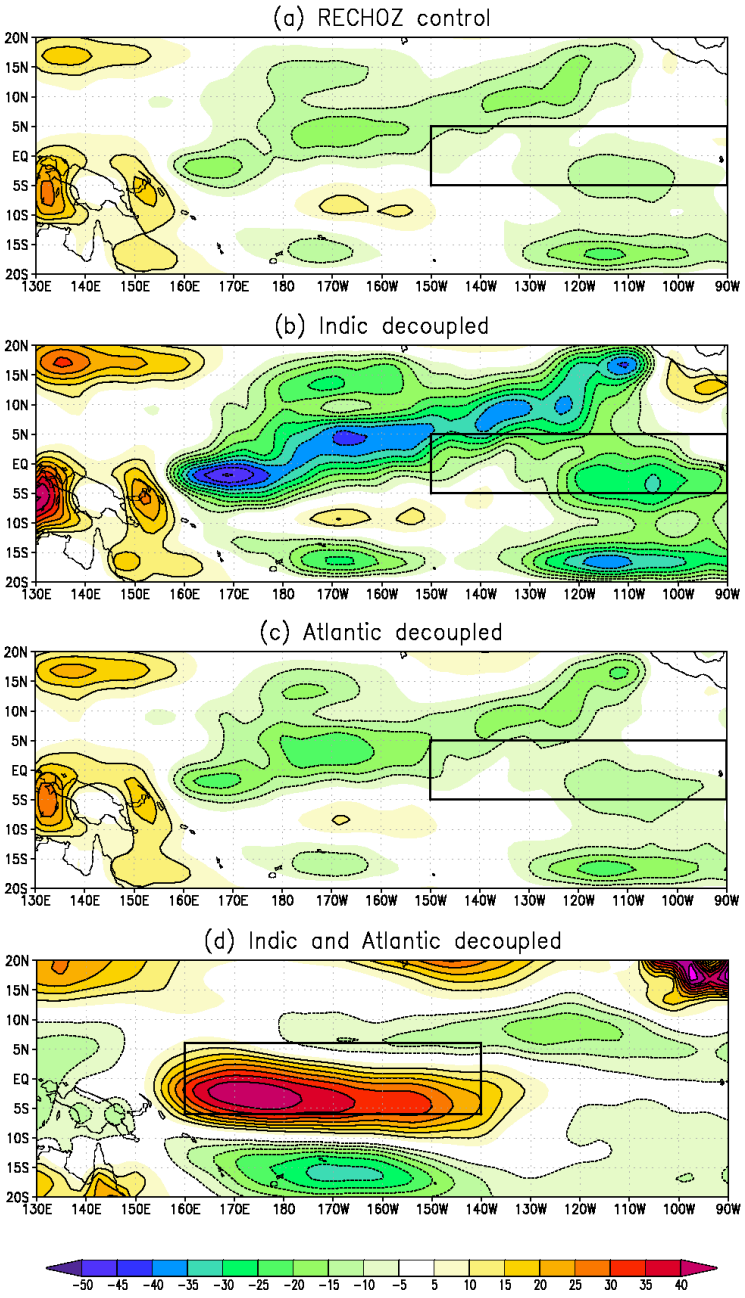

Figure 4.58: Model composite mean values of the net heat flux anomalies for all ENSO extreme years ($|T(December)| > \sigma(T)$) averaged from December to April of the following year for a) the CTRL run, b) the NOIND run, c) the NOAT run, and d) the NOAI run. For La Niña events the net heat flux anomalies are considered with reversed sign in the composites mean. Units are in W/m^2. The black box indicates the NINO3 region over which the heat flux anomalies are averaged.

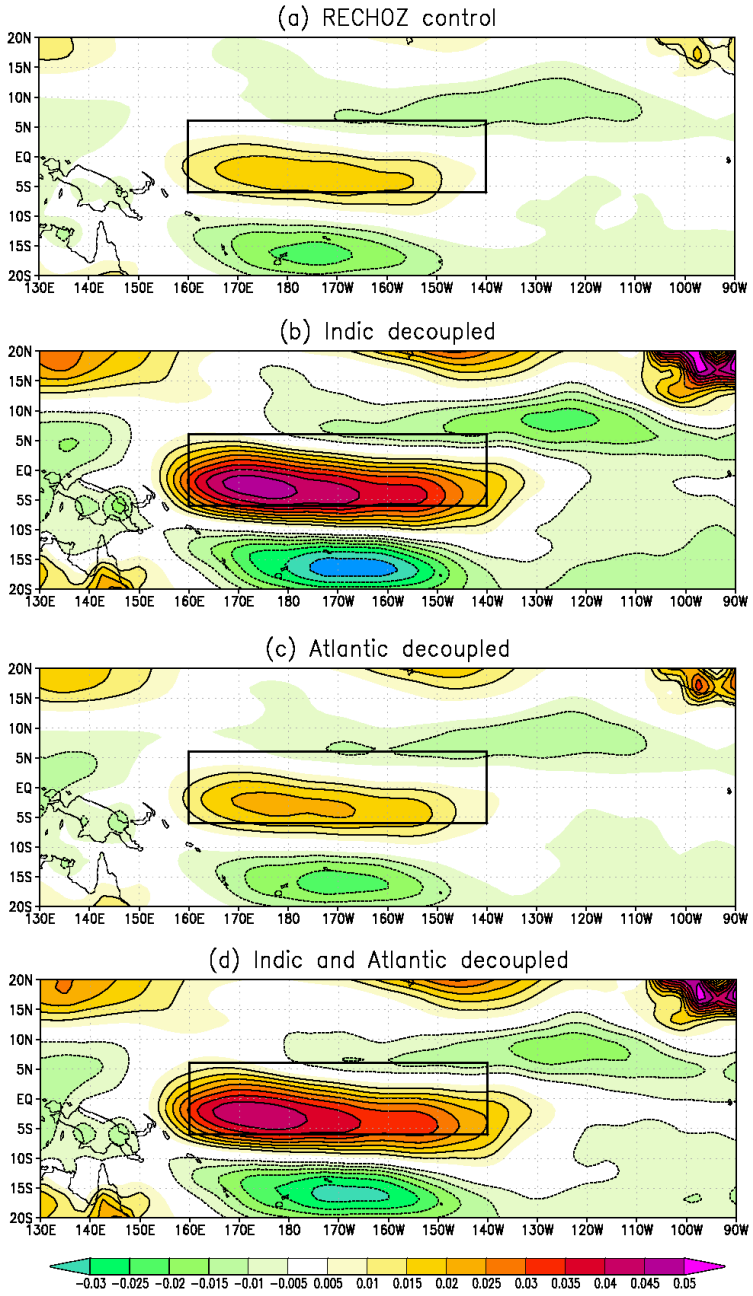

Figure 4.59: Model composite mean values of the zonal wind stress anomalies for all ENSO extreme years ($|T(December)| > \sigma(T)$) averaged from December to April of the following year for a) the CTRL run, b) the NOIND run, c) the NOAT run, and d) the NOAI run. For La Niña events the net heat flux anomalies are considered with reversed sign in the composites mean. Units are in Pa. The black box indicates the region over which the wind stress anomalies are averaged.

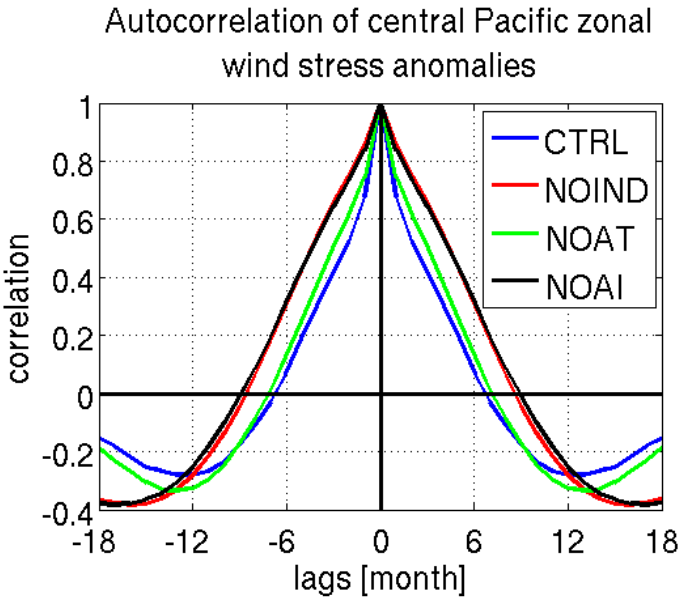

Figure 4.60: Autocorrelation of central Pacific zonal wind stress anomalies for the NOIND experiment (red), the NOAT experiment (green), and the NOAI experiment (black) compared to the CTRl run (blue).

While for the NOAT experiment again almost no changes are found, the NOIND and the NOAI experiments show a wider peak of the autocorrelation curve and stay positive for longer times compared to the control run. This means that the zonal wind stress anomalies persist longer. So, this can explain the shift in the NINO3 SST anomaly spectrum towards longer periods especially when the tropical Indian Ocean is decoupled. This is in good agreement with the results of Dommenget et al. (2006).

The cross correlation between the central Pacific zonal wind stress anomalies and the NINO3 SST anomalies does not change in the NOAT experiment (figure 4.61). In the NOIND and the NOAI experiments the maximum correlation is still found when the wind stress is leading the SST for about 1 month, but the time the correlation stays positive increases and the correlations for lead times longer than one year increase, too.

The cross correlation between the central Pacific zonal wind stress anomalies and the equatorial Pacific thermocline depth anomalies again do not change significantly in the NOAT experiment (figure 4.62). For the NOIND and the NOAI experiments the correlations increase

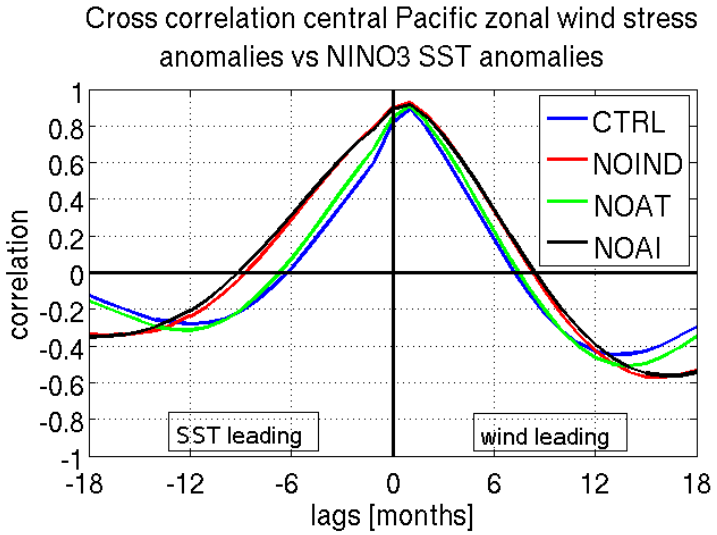

Figure 4.61: Cross correlation between the central Pacific zonal wind stress anomalies and the NINO3 SST anomalies for the NOIND experiment (red), the NOAT experiment (green), and the NOAI experiment (black) compared to the control run (blue).

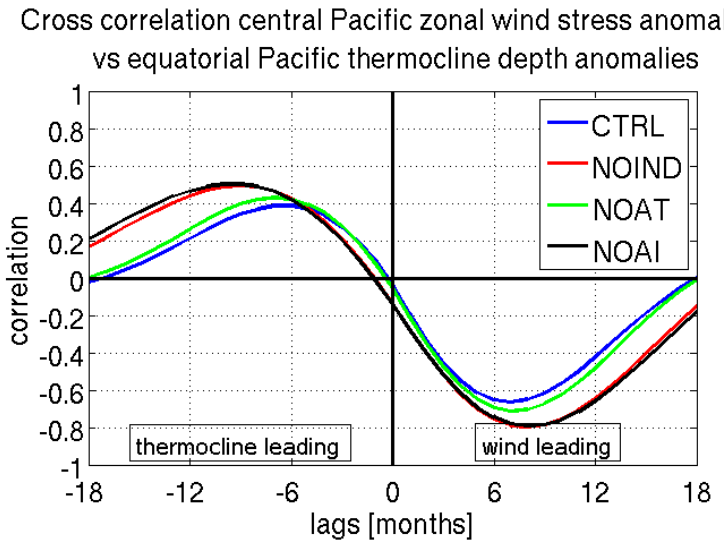

Figure 4.62: Cross correlation between the central Pacific zonal wind stress anomalies and the equatorial Pacific thermocline depth anomalies for the NOIND experiment (red), the NOAT experiment (green), and the NOAI experiment (black) compared to the cotrol run (blue).

for lead times larger than 6 months.

The next thing one can do is to analyse how the parameters of the recharge oscillator model (equations 3.9 and 3.10) change if there is no SST variability in the other tropical oceans. Therefore, again a linear regression was performed to fit the parameters to the resulting data of the sensitivity experiments. Table 4.5 at the end of this section shows the values resulting from these parameter fits. No significant changes are found for the NOAT experiment. The changes for the NOIND and NOAI experiments are of similar magnitude. Thus, in the following, only the changes in the NOIND experiment will be analysed. The strongest change is found in the damping of the SST a_{11} which is reduced by 52%. Also the coupling of the SST to the thermocline a_{12} is reduced by 24%. The damping of the thermocline is reduced by 22%, but the coupling of the thermocline to the SST is only slightly increased by 2%. The standard deviations of the residuals which correspond to the noise terms s_1 and s_2 are increased by 13% each. What these changes in the parameters imply can be analysed if one includes these parameters in the REOSC-MC model. Different experiments with the REOSC-MC model were performed in which the resulting parameters of the CTRL and the NOIND experiment and combinations of these parameters were used. Figure 4.63 shows the spectra of monthly mean NINO3 SST anomalies resulting from this experiments. It can be seen that the changes in the coupling of the thermocline depth anomalies to the SST anomalies a_{21} and in the damping of the thermocline depth anomalies a_{22} have no influence on the frequency and amplitude of ENSO. The changes in the standard deviation of the noise terms lead to enhanced variability on all time scales. The change of the damping of the SST anomalies a_{11} leads to enhanced variability on ENSO time scales. Only the change in the coupling of the SST anomalies to the thermocline depth anomalies a_{12} leads to a decrease of variability on time scales up to 4 years and shifts the peak of the spectrum towards longer periods.

In summary, one can say that a clear influence of the tropical Indian Ocean on the SST variability in tropical Pacific is found while it is difficult to detect an influence of the tropical

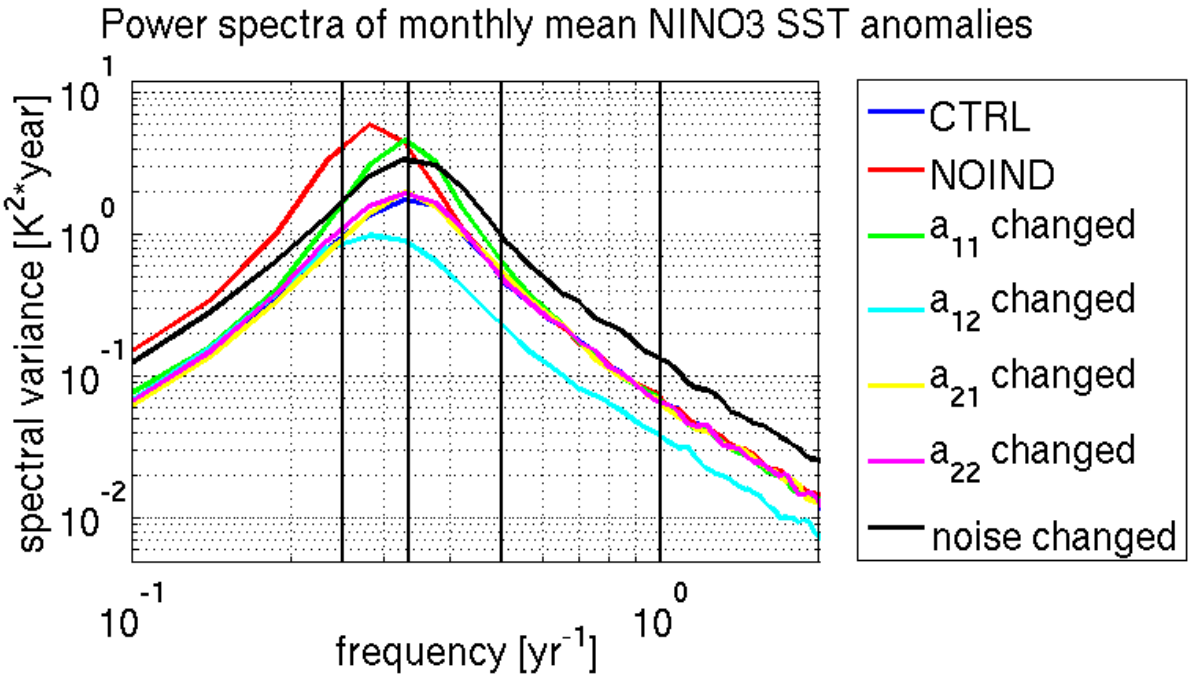

Figure 4.63: Spectra of monthly mean NINO3 SST anomalies for the REOSC-MC experiments with the parameters obtained from the CTRL run (blue), the NOIND run (red) and all parameters from the CTRL run despite a_{11} from the NOIND run (green), a_{12} from the NOIND run (cyan), a_{21} from the NOIND run (yellow), a_{22} from the NOIND run (magenta), and the standard deviations of the noise terms from the NOIND run (black).

Atlantic ocean. Decoupling the tropical Atlantic ocean leads to a small increase in NINO3 SST and equatorial Pacific thermocline depth variability due to stronger zonal wind stress and heat flux variability. However, the parameters of the recharge oscillator are not significantly changed compared to the control experiment. Only a small increase in the standard deviation of the noise terms is found. Decoupling the tropical Indian Ocean leads to a large increase in NINO3 SST and equatorial Pacific thermocline depth variability. Also the peak of the NINO3 SST anomaly spectrum is shifted towards longer periods. The increase in SST variability is due to a reduced damping of the SST and a stronger noise forcing. The larger changes in thermocline depth variability are also due to a reduced damping of the thermocline and an increased noise forcing and also the strong coupling to the SST. The decrease of the damping terms and the increase of the noise terms are due to an increased

variability of zonal wind stress and net heat flux anomalies. The longer persistence of the zonal wind stress anomalies reduces the coupling of the SST to the thermocline and with it shifts the peak of the SST spectrum towards longer periods. Decoupling both tropical oceans has no additional influence on ENSO.

	$a_{11}\,[\frac{1}{month}]$	$a_{12}\,[\frac{K}{month\,m}]$	$a_{21}\,[\frac{m}{K\,month}]$	$a_{22}\,[\frac{1}{month}]$	$\sigma(s_1)\,[\frac{K}{month}]$	$\sigma(s_2)\,[\frac{m}{month}]$
CTRL	-0.065 ± 0.009	0.025 ± 0.001	-1.126 ± 0.006	-0.023 ± 0.001	0.272	0.207
NOIND	-0.031 ± 0.006	0.019 ± 0.001	-1.145 ± 0.005	-0.018 ± 0.001	0.308	0.234
NOAT	-0.059 ± 0.008	0.024 ± 0.001	-1.132 ± 0.006	-0.022 ± 0.001	0.297	0.227
NOAI	-0.035 ± 0.006	0.018 ± 0.001	-1.139 ± 0.005	-0.018 ± 0.001	0.330	0.256

Table 4.5: Resulting model parameters from the NOIND, NOAT, and NOAI experiments compared to the CTRL run with 95% confident intervals.

5 Conclusions

5.1 Results and Discussion

For seasonal and long-term global climate predictions a detailed understanding of the ENSO phenomenon is necessary. Although there have been large improvements in the understanding of the ENSO mode and the ability to predict ENSO in the recent decades, there are still aspects of ENSO which are not yet fully understood and which are not simulated correctly by most models. Thus, the aim of this thesis was to enhance the understanding of different aspects of ENSO. For this purpose the new HCM RECHOZ was developed which couples a complex atmospheric GCM to the simple two-dimensional linear recharge oscillator ocean model in the tropical Pacific. Then it was analysed how ENSO is simulated in this model and different key questions were adressed with the help of this model. The results will be summarised in the following.

- ENSO in the RECHOZ model

In section 4.1 it was examined how the ENSO phenomenon is simulated in the RECHOZ model. Many state-of-the-art GCMs have problems simulating the seasonality and nonlinearity of ENSO correctly (Guilyardi et al., 2009b; van Oldenborgh et al., 2005). It was shown that although the RECHOZ model has only a minimum complex representation of ENSO it produces a very good simulation of it. The model is able to simulate the main statistical properties of ENSO like its variance, period, seasonality, skewness, and kurtosis. Thus, the

model is very suitable to analyse the origins of the seasonality and nonlinearity of ENSO and to study the influences of remote forcings onto ENSO.

- Which atmospheric processes lead to the phase locking of ENSO, with El Niño and La Niña events typically peaking in early boreal winter?

The seasonal cycle in the strength of the ENSO amplitudes can be attributed to the seasonal varying sensitivity of the atmosphere to SST anomalies. In section 4.2 it was pointed out that a stronger coupling of zonal wind stress to SST in spring and summer reduces the damping of SST. The weaker coupling of zonal wind stress increases the damping of the ENSO events in winter and early spring.

- What are possible atmospheric causes for the amplitude asymmetry between El Niño and La Niña events?

Many studies see the origin of the ENSO nonlinearity in the ocean dynamics (Jin et al., 2003; An and Jin, 2004; Su et al., 2010). The origin of the nonlinearities in the ENSO cycle in the RECHOZ model has to lie in the atmospheric forcings because the model by construction only allows linear feedbacks in the ocean processes. In section 4.3 it was shown that a nonlinear zonal wind response to equal-strength but opposite SSTAs can explain the asymmetry between eastern Pacific SSTAs during El Niño and La Niña events, which is in agreement with the results of Kang and Kug (2002). So the fact that this simple model with only parameterized ocean dynamics can reproduce the ENSO amplitude asymmetry shows that atmospheric nonlinearities have an important influence on the SST skewness in the eastern tropical Pacific.

- In which way are changes in the mean state of the tropical Pacific affecting ENSO through atmospheric feedbacks?

The possible changes of ENSO due to global warming are currently very strongly discussed. For the changes in the mean state of the tropical Pacific studies range from no change at all

(Collins and CMIP Modeling Groups, 2005) over an El Niño-like warming pattern (Meehl et al., 2007) to an enhanced equatorial warming (Liu et al., 2005). Also the future strength of ENSO simulated by state-of-the-art GCMs shows a large spread of results (Meehl et al., 2007). In section 4.4 different sensitivity experiments were analysed to improve the understanding of possible influences of changes in the mean state on ENSO through atmospheric feedbacks. It was found that changes in the mean state of the tropical Pacific have a large influence on ENSO. An overall cooling of the mean SST leads to reduced ENSO variability and a shorter ENSO period due to reduced variability of the NINO3 heat flux anomalies and the central Pacific zonal wind stress anomalies and a shorter persistence of the zonal wind stress anomalies. In contrast an overall warming leads increased variability of NINO3 heat flux anomalies and central Pacific zonal wind stress anomalies and thus increases the ENSO variability. A longer persistence of the zonal wind stress anomalies leads to a longer ENSO period. However, the results strongly depend on the pattern of the mean state change. An El Niño-like warming pattern with a smaller amplitude of tropical Pacific warming leads to a stronger increase in NINO3 heat flux anomaly and central Pacific zonal wind stress anomaly variability and thus also a larger increase in ENSO variability than a uniform warming pattern. However, also ocean dynamics have to be considered to be able to predict the future behaviour of ENSO.

- How are the tropical Indian Ocean and the tropical Atlantic Ocean influencing ENSO?

Many recent studies suggest that the tropical Indian and the tropical Atlantic Ocean are not only influenced by ENSO but also have a feedback on ENSO themselves (see for example Dommenget et al. (2006); Jansen et al. (2009); Rodriguez-Fonseca et al. (2009). The results of section 4.5 show that decoupling the tropical Atlantic Ocean has little influence on the SST variability in the tropical Pacific, while decoupling the tropical Indian Ocean has a large effect. Increased variability of zonal wind stress anomalies and heat flux anomalies reduces the damping of the SST and the thermocline depth and so increases the variability of SST

and thermocline depth anomalies. A longer persistence of the zonal wind stress anomalies reduces the coupling of the SST anomalies to the thermocline depth anomalies and with it leads to a shift of the peak of the NINO3 SST anomaly spectrum towards longer periods. The results are in good agreement with Dommenget et al. (2006).

The results of this thesis show that in order to improve the simulation of ENSO in climate models one has to improve the representation of the atmospheric feedbacks. However, ocean processes are also an important factor for ENSO. To improve the predictions of ENSO it could be helpful to include the tropical Indian Ocean, though one still has to consider that the tropical Indian Ocean primary is influenced by ENSO itself. On the other hand, although only little influence of the Atlantic ocean on ENSO was found, this could be more important for ENSO predictions because the tropical Atlantic Ocean is less influenced by ENSO. At the current point in time it is not possible to say how ENSO will be altered by global warming. As long as the models do not agree in which way the mean state of the tropical Pacific will change, one cannot make faithful predictions on how ENSO will change. However, the model results indicate that a warmer mean state of the tropical Pacific will lead to increased ENSO variability.

5.2 Outlook

The RECHOZ model proved to be a very useful tool to analyse the mechanisms and interactions of ENSO. It helped to gain a better understanding of some aspects of ENSO. However, there are still other aspects of ENSO which are matter of ongoing research where the RECHOZ model could help to improve the understanding. Two recent areas of ENSO research are the predictability of ENSO and possible changes of ENSO under global warming.

5.2.1 ENSO predictions

The prediction of El Niño and La Niña events is of great importance because of their large socio-economic impacts. One way to improve ENSO forecasts could be to include effects of the Indian and the Atlantic Ocean in the forecasts. The good representation of the ENSO statistics in the RECHOZ model and the possibility to easily control SST variations in different regions of the oceans without essentially disturbing the system form a good background for ENSO predictability studies. In chapter 4.5 it was illustrated that especially the tropical Indian Ocean has an influence on the ENSO variability and period. Therefore, the RECHOZ model is also very appropiate to analyse the influences of these regions on ENSO predictability.

5.2.2 Changes in ENSO variability due to global warming

Another area of ongoing research is how global warming will influence ENSO. In section 4.4 it was shown that the RECHOZ model can be used to study the influence of changes in the mean state of the tropical Pacific on ENSO. Thus, the model could be used to perform sensitivity studies with different mean SST climatologies obtained from different future climate projections from the database of the IPCC. Then the influence of these different mean states on the recharge oscillator model parameters can be analysed. Also the influences of changes in the mean state in other regions on ENSO can be studied.

List of Figures

List of Tables

Bibliography

Alexander, M. A. and C. Penland, 1996: Variability in a Mixed Layer Ocean Model Driven by Stochastic Atmospheric Forcing. *J. Climate*, **9**, 2424–2442.

An, S.-I. and F.-F. Jin, 2004: Nonlinearity and Asymmetry of ENSO. *J. Climate*, **17**, 2399–2412.

Annamalai, H., S. P. Xie, J. P. McCreary, and R. Murtugudde, 2005: Impact of Indian Ocean Sea Surface Temperature on Developing El Niño. *J. Climate*, **18**, 302–319.

Bader, J. and M. Latif, 2005: North Atlantic Oscillation Response to Anomalous Indian Ocean SST in a Coupled GCM. *J. Climate*, **18**, 5382–5389, doi:10.1175/JCLI3577.1.

Baquero-Bernal, A., M. Latif, and S. Legutke, 2002: On Dipolelike Variability of Sea Surface Temperature in the Tropical Indian Ocean. *J. Climate*, **15**, 1358–1368.

Battisti, D. S., 1988: The Dynamics and Thermodynamics of a Warming Event in a Coupled Tropical Atmosphere-Ocean Model. *J. Atmos. Sci.*, **45**(20), 2889–2919.

Battisti, D. S. and A. C. Hirst, 1989: Interannual Variability in a Tropical Atmosphere-Ocean Model: Influence of the Basic State, Ocean Geometry and Nonlinearity. *J. Atmos. Sci.*, **46**(12), 1687–1712.

Behera, S. K., J. J. Luo, S. Masson, S. A. Rao, H. Sakum, and T. Yamagata, 2006: A CGCM Study on the Interaction between IOD and ENSO. *J. Climate*, **19**, 1688–1705.

Bjerknes, J., 1969: Atmospheric teleconnections from the equatorial Pacific. *Mon. Weather Rev.*, **97**(3), 163–172.

Boer, G. J. and B. Yu, 2003: Dynamical aspects of climate sensitivity. *Geophys. Res. Lett.*, **30**(3), 1135, doi:10.1029/2002GL016549.

Burgers, G., F.-F. Jin, and G. J. van Oldenborgh, 2005: The simplest ENSO recharge oscillator. *Geophys. Res. Lett.*, **32**(L13706), doi: 10.1029/2005GL022951.

Burgers, G. and D. B. Stephenson, 1999: The "normality" of El Niño. *Geophys. Res. Lett.*, **26**(8), 1027–1030, doi:10.1029/1999GL900161.

Cane, M. A., A. C. Clement, A. Kaplan, Y. Kushnir, D. Pozdnyakov, R. Seager, S. E. Zebiak, and R. Murtugudde, 1997: Twentieth-Century Sea Surface Temperature Trends. *Science*, **275**(5302), 957–960.

Capotondi, A., A. Wittenberg, and S. Masina, 2006: Spatial and temporal structure of Tropical Pacific interannual variability in 20th century coupled simulations. *Ocean Model.*, **15**(3-4), 274–298.

Clement, A. C., R. Seager, M. A. Cane, and S. E. Zebiak, 1996: An Ocean Dynamical Thermostat. *J. Climate*, **9**, 2190–2196.

Collins, M., S.-I. An, W. Cai, A. Ganachaud, E. Guilyardi, F.-F. Jin, M. Jochum, M. Lengaigne, S. Power, A. Timmermann, G. Vecchi, and A. Wittenberg, 2010: The impact of global warming on the tropical Pacific Ocean an El Niño. *Nat. Geosci.*, **3**, 391–397, doi:10.1038/ngeo868.

Collins, M. and CMIP Modeling Groups, 2005: El Niño- or La Niña-like climate change? *Clim. Dyn.*, **24**(1), 89–104.

Deser, C., A. S. Phillips, and J. W. Hurrell, 2004: Pacific Interdecadal Climate Variability: Linkages between the Tropics and the North Pacific during Boreal Winter since 1900. *J. Climate*, **17**, 3109–3124.

DiNezio, P. N., A. C. Clement, G. A. Vecchi, B. J. Soden, B. P. Kirtman, and S.-K. Lee, 2009: Climate Response of the Equatorial Pacific to Global Warming. *J. Climate*, **22**, 4873–4892.

Dommenget, D., 2007: Evaluating EOF modes against a stochastic null hypothesis. *Clim. Dyn.*, **28**(5), 517–531, doi:10.1007/s00382-006-0195-8.

Dommenget, D. and M. Latif, 2008: Generation of hyper climate modes. *Geophys. Res. Lett.*, **35**(L02706), doi:10.1029/2007GL031087.

Dommenget, D., V. Semenov, and M. Latif, 2006: Impacts of the tropical Indian and Atlantic Oceans on ENSO. *Geophys. Res. Lett.*, **33**(L11701), doi:10.1029/2006GL025871.

Dong, B., R. T. Sutton, and A. A. Scaife, 2006: Multidecadal modulation of El Niño-Southern Oscillation (ENSO) variance by Atlantic Ocean sea surface temperatures. *Geophys. Res. Lett.*, **33**(L08705), doi:10.1029/2006GL025766.

Enfield, D. B. and D. A. Mayer, 1997: Tropical Atlantic sea surface temperature variability an its relation to El Niño-Southern Oscillation. *J. Geophys. Res.*, **102**(C1), 929–945, doi:10.1029/96JC03296.

Fedorov, A. V. and S. G. Philander, 2001: A Stability Analysis of Tropical Ocean-Atmosphere Interactions: Bridging Measurements and Theory for El Niño. *J. Climate*, **14**, 3086–3101.

Fischer, A. S., P. Terray, E. Guilyardi, S. Gualdi, and P. Delecluse, 2005: Two Independent Triggers for the Indian Ocean Dipole/Zonal Mode in a Coupled GCM. *J. Climate*, **18**, 3428–3449, doi:10.1175/JCLI3478.1.

Galanti, E. and E. Tziperman, 2000: ENSO's Phase Locking to the Seasonal Cycle in the Fast-SST, Fast-Wave, and Mixed-Mode Regimes. *J. Atmos. Sci.*, **57**, 2936–2950.

Guilyardi, E., 2006: El Niño-mean state-seasonal cycle interactions in a multi-model ensemble. *Clim. Dyn.*, **26**(4), 329–348, doi:10.1007/s00382-005-0084-6.

Guilyardi, E., P. Braconnot, F.-F. Jin, S. T. Kim, M. Kolasinski, T. Li, and I. Musat, 2009a: Atmosphere Feedbacks during ENSO in a Coupled GCM with a Modified Atmospheric Convection Scheme. *J. Climate*, **22**, 5698–5718, doi:10.1175/2009JCLI2185.1.

Guilyardi, E., S. Gualdi, J. Slingo, A. Navarra, P. Delecluse, J. Cole, G. Madec, M. Roberts, M. Latif, and L. Terray, 2004: Representing El Niño in Coupled Ocean-Atmosphere GCMs: The Dominant Role of the Atmospheric Component. *J. Climate*, **17**, 4623–4629, doi:10.1175/JCLI-3260.1.

Guilyardi, E., A. Wittenberg, A. Fedorov, M. Collins, C. Wang, A. Capotondi, G. J. van Oldenborgh, and T. Stockdale, 2009b: Understanding El Niño in Ocean-Atmosphere General Circulation Models: Progress and Challenges. *Bull. Amer. Meteor. Soc.*, **90**, 325–340.

Hastenrath, S., L. C. de Castro, and P. Aceituno, 1987: The Southern Oscillation in the Tropical Atlantic Sector. *Contrib. Atmos. Phys.*, **60**, 447–463.

Held, I. M. and B. J. Soden, 2006: Robust Response of the Hydrological Cycle to Global Warming. *J. Climate*, **19**, 5686–5699.

Hirst, A. C., 1986: Unstable and Damped Equatorial Modes in Simple Coupled Ocean-Atmosphere Models. *J. Atmos. Sci.*, **43**(6), 606–632.

Hoerling, M. P., A. Kumar, and M. Zhong, 1997: El Niño, La Niña, and the Nonlinearity of Their Teleconnections. *J. Climate*, **10**, 1769–1786.

Huang, B., 2004: Remotely forced variability in the tropical Atlantic Ocean. *Clim. Dyn.*, **23**(2), 133–152, doi:10.1007/s00382-004-0443-8.

Jansen, M. F., D. Dommenget, and N. Keenlyside, 2009: Tropical Atmosphere-Ocean Interactions in a Conceptual Framework. *J. Climate*, **22**, 550–567, doi:10.1175/2008JCLI2243.1.

Jin, F.-F., 1997: An Equatorial Ocean Recharge Paradigm for ENSO. Part 1: Conceptual Model. *J. Atmos. Sci.*, **54**, 811–829.

Jin, F.-F., S.-I. An, A. Timmermann, and J. Zhao, 2003: Strong El Niño events and nonlinear dynamical heating. *Geophys. Res. Lett.*, **30**(3), 1120, doi:10.1029/2002GL016356.

Kalnay, E. and Coauthors, 1996: The NCEP/NCAR 40-Year Reanalysis Project. *Bull. Amer. Meteor. Soc.*, **77**, 437–471.

Kang, I.-S. and J.-S. Kug, 2002: El Niño and La Niña sea surface temperature anomalies: Asymmetry characteristics associated with their wind stress anomalies. *J. Geophys. Res.*, **107**(D19), 4372, doi:10.1029/2001JD000393.

Keenlyside, N. S. and M. Latif, 2007: Understanding Atlantic Interannual Variability. *J. Climate*, **20**, 131–142.

Knutson, T. R. and S. Manabe, 1995: Time-Mean Response over the Tropical Pacific to Increased CO_2 in a Coupled Ocean-Atmosphere Model. *J. Climate*, **8**, 2181–2199.

Knutson, T. R. and S. Manabe, 1998: Model Assessment of Decadal Variability and Trends in the Tropical Pacific Ocean. *J. Climate*, **11**, 2273–2296.

Kug, J.-S. and I.-S. Kang, 2006: Interactive Feedback between ENSO and the Indian Ocean. *J. Climate*, **19**, 1784–1801.

Large, W. G. and S. G. Yeager, 2008: The global climatology of an interannually varying air-sea flux data set. *Clim. Dyn.*, **33**, 341–364, doi:10.1007/s00382-008-0441-3.

Latif, M., D. Anderson, T. Barnett, M. Cane, R. Kleeman, A. Leetmaa, J. O'Brien, A. Rosati, and E. Schneider, 1998: A review of the predictability and prediction of ENSO. *J. Geophys. Res.*, **103**(C7), 14375–14393, doi:10.1029/97JC3413.

Latif, M. and T. P. Barnett, 1995: Interactions of the Tropical Oceans. *J. Climate*, **8**, 952–964.

Latif, M. and Coauthors, 2001: ENSIP: the El Niño simulation intercomparison project. *Clim. Dyn.*, **18**(3-4), 255–276, doi:10.1007/s003820100174.

Levitus, S., R. Burgett, and T. P. Boyer, 1994: Salinity. Vol. 3, World Ocean Atlas 1994. *NOAA Atlas NESDIS 3*, p. 111pp.

Li, T. and S. G. H. Philander, 1996: On the Annual Cycle of the Eastern Equatorial Pacific. *J. Climate*, **9**, 2986–2998.

Lin, J.-L., 2007: The Double-ITCZ Problem in IPCC AR4 Coupled GCMs: Ocean-Atmosphere Feedback Analysis. *J. Climate*, **20**, 4497–4525.

Liu, Z., 2002: A Simple Model Study of ENSO Suppression by External Periodic Forcing. *J. Climate*, **15**, 1088–1098.

Liu, Z., S. Vavrus, F. He, N. Wen, and Y. Zhong, 2005: Rethinking Tropical Ocean Response to Global Warming: The Enhanced Equatorial Warming. *J. Climate*, **18**, 4684–4700.

Marsland, S., H. Haak, J. Jungclaus, M. Latif, and F. Röske, 2003: The Max-Planck-Institute global ocean/sea ice model with orthogonal curvilinear coordinates. *Ocean Model.*, **5**(2), 91–127.

Massey, F. J., 1951: The Kolmogorov-Smirnov Test for Goodness of Fit. *Journal of the American Statistical Association*, **46**, 68–78.

Meehl, G. A., T. F. Stocker, W. D. Collins, P. Friedlingstein, A. T. Gaye, J. M. Gregory, A. Kitoh, R. Knutti, J. M. Murphy, A. Noda, S. C. B. Raper, I. G. Watterson, A. J. Weaver, and Z.-C. Zhao, 2007: Global Climate Projections. In: S. Solomon, D. Qin, M. Manning, Z. Chen, M. Marquis, K. B. Averyt, M. Tignor, and H. L. Miller, eds., *Climate Change 2007: The Physical Science Basis. Contribution of Working Group I to the Fourth Assessment Report of the Intergovernmental Panel on Climate Change*, p. 996 pp. Cambridge University Press.

Meehl, G. A. and W. M. Washington, 1996: El Niño-like climate change in a model with increased atmospheric CO_2 concentrations. *Nature*, **382**, 56–60, doi:10.1038/382056a0.

Mo, K. C. and S. Häkkinen, 2001: Interannual Variability in the Tropical Atlantic and Linkages to the Pacific. *J. Climate*, **14**, 2740–2762.

Niiler, P. P. and E. B. Kraus, 1977: One dimension models of the upper ocean. In: E. B. Kraus, ed., *Modeling and Prediction of Upper Layers of the Ocean*, pp. 143–172. Pergamon, New York.

Philander, S. G. H., 1983: El Niño Southern Oscillation phenomena. *Nature*, **302**, 295–301.

Philander, S. G. H., 1985: El Niño and La Niña. *J. Atmos. Sci.*, **42**(23), 2652–2662.

Philip, S. and G. J. van Oldenborgh, 2009: Significant Atmospheric Nonlinearities in the ENSO Cycle. *J. Climate*, **22**, 4014–4028, doi:10.1175/2009JCLI2716.1.

Rasmusson, E. and T. Carpenter, 1982: Variations in Tropical Sea Surface Temperature and Surface Wind Fields Associated with the Southern Oscillation/El Niño. *Mon. Wea. Rev.*, **110**(5), 354–384.

Rayner, N. A., D. E. Parker, E. B. Horton, C. K. Folland, L. V. Alexander, D. P. Rowell, E. C. Kent, and A. Kaplan, 2003: Global analyses of sea surface temperature, sea ice, and night marine air temperature since the late nineteenth century. *J. Geophys. Res.*, **108**(D14), 4407, doi:10.1029/2002JD002670.

Rodriguez-Fonseca, B., I. Polo, J. Garcia-Serrano, T. Losada, E. Mohino, C. R. Mechoso, and F. Kucharski, 2009: Are Atlantic Niños enhancing Pacific ENSO events in recent decades? *Geophys. Res. Lett.*, **36**(L20705), doi:10.1029/2009GL040048.

Roeckner, E., R. Brokopf, M. Esch, M. Giorgetta, S. Hagemann, L. Kornblueh, E. Manzini, U. Schlese, and U. Schulzweida, 2004: Sensitivity of Simulated Climate to Horizontal and Vertical Resolution. *Rep. 354, Max-Planck-Inst. for meteorol., Hamburg, Germany*.

Roeckner, E. et al., 2003: The atmospheric general circulation model ECHAM5. Part I: Model description. *Rep. 349, Max-Planck-Inst. for meteorol., Hamburg, Germany*.

Ropelewski, C. F. and M. S. Halpert, 1987: Global and Regional Scale Precipitation Patterns Associated with the El Niño/Southern Oscillation. *Mon. Wea. Rev.*, **115**(8), 1606–1626.

Schneider, E. K., 2002: Understanding Differences between the Equatorial Pacific as Simulated by Two Coupled GCMs. *J. Climate*, **15**, 449–469.

Schott, F. A., S.-P. Xie, and J. P. McCreary Jr., 2009: Indian Ocean circulation and climate variability. *Rev. Geophys.*, **47**(RG1002), doi:10.1029/2007RG000245.

Smith, N. R., 1995: An Improved System for Tropical Ocean Subsurface Temperature Analyses. *J. Atmos. Ocean. Technol.*, **12**, 850–870.

Su, J., R. Zhang, T. Li, X. Rong, J.-S. Kug, and C.-C. Hong, 2010: Causes of the El Niño and La Niña Amplitude Asymmetry in the Equatorial Eastern Pacific. *J. Climate*, **23**, 605–617, doi:10.1175/2009JCLI2894.1.

Suarez, M. J. and P. S. Schopf, 1988: A Delayed Action Oscillator for ENSO. *J. Atmos. Sci.*, **45**(21), 3283–3287.

Tziperman, E., M. A. Cane, S. E. Zebiak, Y. Xue, and B. Blumenthal, 1998: Locking of El Niño's Peak Time to the End of the Calendar Year in the Delayed Oscillator Picture of ENSO. *J. Climate*, **11**, 2191–2199.

van Oldenborgh, G. J., S. Y. Philip, and M. Collins, 2005: El Niño in a changing climate: a multi-model study. *Ocean Science*, **1**(2), 81–95.

Vavrus, S. and Z. Liu, 2002: Toward understanding the response of the tropical atmosphere-ocean system to increased CO2 using equilibrium asynchronous coupling. *Clim. Dyn.*, **19**(3-4), 355–369, doi:10.1007/s00382-002-0232-1.

Vecchi, G. A., A. Clement, and B. J. Soden, 2008: Examining the tropical Pacifics response to global warming. *EOS,Trans. Amer. Geophys. Union*, **89**, 81,83.

Vecchi, G. A. and B. J. Soden, 2007: Global Warming and the Weakening of the Tropical Circulation. *J. Climate*, **20**, 4316–4340.

Venzke, S., M. Latif, and A. Villwock, 2000: The Coupled GCM ECHO-2. Part II: Indian Ocean Response to ENSO. *J. Climate*, **13**, 1371–1383.

Walker, G. T., 1924: Correlation of seasonal variations in weather IX: A further study of world weather. *Mem. Indian Meteorol. Dep.*, **24**, 275–332.

Wang, B. and S.-I. An, 2001: Why the properties of El Niño changed during the late 1970s. *Geophys. Res. Lett.*, **28**(19), 3709–3712, doi:10.1029/2001GL012862.

Wittenberg, A. T., 2004: Extended Wind Stress Analyses for ENSO. *J. Climate*, **17**, 2526–2540.

Wright, P. B., 1986: Precursors of the Southern Oscillation. *J. Climatol.*, **6**, 17–30.

Wu, R. and B. P. Kirtman, 2004: Understanding the Impacts of the Indian Ocean on ENSO Variability in a Coupled GCM. *J. Climate*, **17**, 4019–4031.

Yamaguchi, K. and A. Noda, 2006: Global warming patterns over the North Pacific: ENSO versus AO. *J. Meteorol. Soc. Japan*, **84**, 221–241.

Yu, B. and G. Boer, 2002: The roles of radiation and dynamical processes in the El Niño-like response to global warming. *Clim. Dyn.*, **19**(5-6), 539–554, doi:10.1007/s00382-002-0244-x.

Yu, J.-Y., C. R. Mechoso, J. C. McWilliams, and A. Arakawa, 2002: Impacts of the Indian Ocean on the ENSO cycle. *Geophys. Res. Lett.*, **29**(1204), doi:10.1029/2001GL014098.

Abbreviations

AR(1)	First order autoregressive process
AR4	Fourth assesment report of the IPCC
ATL3	Region in the eastern equatorial Atlantic ocean ($20°W - 0°E, 3°S - 3°N$)
CMIP	Coupled Model Intercomparison Project
ECHAM5	Hamburg version of the ECMWF atmospheric model
ECMWF	European Center for Medium Range Weather Forecast
ENSO	El Niño Southern Oscillation
EOF	Empirical orthogonal function
GCM	General circulation model
HCM	Hybrid coupled model
IOD	Indian Ocean dipole mode
IPCC	Intergovernmental Panel on Climate Change
ITCZ	Intertropical convergence zone
MPI-OM	Max Planck Institute Ocean Model
NAO	North Atlantic Oscillation

NCEP-NCAR	Reanalysis data set of the National Centers for Environmental Prediction and the National Center for Atmospheric Research
NINO3	Region in the eastern equatorial Pacific ($90°W - 150°W, 5°S - 5°N$)
NINO3.4	Region in the central equatorial Pacific ($120°W - 170°W, 5°S - 5°N$)
NINO4	Region in the central equatorial Pacific ($160°E - 150°W, 5°S - 5°N$)
OZ	Simple mixed layer ocean model
RECHOZ	Hybrid coupled model consisting of the ECHAM5 atmosphere model, the OZ mixed layer ocean model and the recharge oscillator ocean model
REOSC-MC	Simple Monte Carlo version of the recharge oscillator ocean model
SLP	Sea level pressure
SO	Southern Oscillation
SST	Sea surface temperature
SSTA	Sea surface temperature anomalies
TAO	Tropical Atmosphere Ocean - Array of buoys in the tropical Pacific recording air and sea temperature
WIO	Region in the western tropical Indian Ocean ($50°E - 70°E, 10°S - 10°N$)

Danksagung

An dieser Stelle möchte ich mich bei all jenen bedanken, die durch praktische oder moralische Unterstützung zum Entstehen dieser Arbeit beigetragen haben.
Ganz besonders gilt mein Dank Dr. Dietmar Dommenget, der es mir überhaupt erst ermöglicht hat, an diesem interessanten Thema zu arbeiten und darüber zu promovieren. Außerdem möchte ich mich für die tolle Betreuung während der gesamten Zeit sowohl in Kiel als auch von Melbourne aus bedanken.
Auch bei Prof. Dr. Mojib Latif möchte ich mich für die Unterstützung bedanken und sowie auch bei Dr. Noel Keenlyside und der gesamten Arbeitsgruppe für die vielen hilfreichen Diskussionen und Kommentare, die maßgeblich zur Entstehung dieser Arbeit beigetragen haben.
Ein ganz großes Dankeschön auch an meine Familie und ganz besonders meine Schwester Steffi, die mich immer unterstützt und für mich da ist.

Dieses Arbeit wurde gefördert von der Deutschen Forschungsgemeinschaft (DFG) durch das Projekt TROIA (DO1038/2-1).

Erklärung

Hiermit bestätige ich, dass ich diese Doktorarbeit selbstständig verfasst und keine anderen als die angegebenen Quellen und Hilfsmittel verwendet habe.
Ich versichere, dass diese Arbeit zur Erlangung eines Doktorgrades noch nicht an anderer Stelle eingereicht worden ist.
Ich erkläre, dass die vorliegende Arbeit gemäß der Grundsätze zur Sicherung guter wissenschaftlicher Praxis der Deutschen Forschungsgemeinschaft erstellt wurde.

Kiel, 14.10.2010

(Claudia Frauen)